Sample-based Probabilistic Estimation for Indoor Positioning and Tracking Under Ranging Uncertainty

Dissertation

zur Erlangung des akademischen Grades
der Doktorin der Naturwissenschaften
(Dr. rer. nat)

eingereicht
am Institut für Informatik
des Fachbereichs Mathematik und Informatik
der Freien Universität Berlin

Telematics
Computer Systems

von

Yuan Yang

Berlin, März 2015

Gutachter:

Prof. Dr. Marcel Kyas

Department of Computer Science

Freie Universit*ä*t Berlin

Prof. Dr. Moe Z. Win

Department of Aeronautics and Astronautics

Massachusetts Institute of Technology

Tag der Disputation: 13. März 2015

Eidesstattliche Erklärung

Ich versichere, dass ich die Diplomarbeit selbständig verfasst, und keine anderen als die angegebenen Quellen und Hilfsmittel benutzt habe. Die Arbeit hat keiner anderen Prüfungsbehörde vorgelegen.

Mir ist bekannt, dass bei Verwendung von Inhalten aus dem Internet ich diese zu kennzeichnen und einen Ausdruck mit Angabe des Datums sowie der Internet-Adresse als Anhang der Diplomarbeit anzugeben habe.

Author's Declaration

I hereby declare to have written this thesis on my own. I have used no other literature and resources than the ones referenced. All text passages that are literal or logical copies from other publications have been marked accordingly. All figures and pictures have been created by me or their sources are referenced accordingly. This thesis has not been submitted in the same or a similar version to any other examination board.

Yuan Yang, Berlin

den March 19, 2015

Abstract

The critical problem in range-based indoor positioning is the severe ranging uncertainty, which typically resorts to the probabilistic perspective. Since there is no analytical solution to the nonlinear and non-Gaussian positioning problem, the research trends have moved towards exploring sample-based approximations in the probabilistic frame. However, the sample-based methods are generally inaccessible for application not only because of the high complexity, but also for the sampling difficulty and divergence. This thesis studies the sample-based probabilistic positioning to achieve the tradeoff in performance (accuracy and robustness), cost (time and space complexity), and usability (in terms of the required number of samples and implementation difficulty).

The work of this thesis covers both the theoretical and practical sides of sample-based probabilistic algorithms positioning. The proposed algorithms are tested by extensive simulations and real-world experiments on the Nanotron platform. Specifically, the contributions of this thesis can be summarized in the following:

- Chapter 3.3 characterizes the indoor TOF ranging, i.e., the relationship of the ranging error to time, space, anchor connectivity and the ground truth of the ranging, etc. Then, intensive distribution fitting, hypothesis test, and model verification of different parametric models are carried out.
- Via the imposition of the state constraints from the most recent observation, four constrained sampling methods are developed (see Chapter 4), with the advantages including: 1) effectively reduce the sample size; 2) suppress sample degeneracy and impoverishment without resampling; 3) no requirement of keeping all samples' properties in memory.
- The NLOS mitigation proposed in Chapter 4 refines the measurement model as a positively biased and right-tail distribution.
- Both the theoretical and practical anchor deployment are suggested in Chapter 4.
- To address the estimation instability and sparsity problems, the one time-step smoothing methods are incorporated in the sample-based Bayesian estimation.

Keywords Indoors positioning, target tracking, Bayesian filtering, Bayesian smoothing, sample-based approximation, frequentist measurement modeling, NLOS mitigation, anchor deployment

Das grundlegende Problem von distanzbasierter Indoor-Lokalisierung, ist die hohe Ungenauigkeit der Distanzmessungen. Die weit verbreitetste Strategie mit diesem Problem umzugehen, ist die probalistische Schätzung. Da es für das nicht-lineare und nicht-gaussche Lokalisierungsproblem keine analytische Lösung gibt, besteht ein wachsendes Interesse in der Untersuchung von Sample-basierten Näherungen. Sample basierte Näherungen haben jedoch den Nachteil, dass sie Aufgrund ihrer hohen Komplexität und des sampling-Aufwandes im Feld kaum anwendbar sind. Daher ist es das Ziel dieser Arbeit Sample-basierte probalistische Lokalisierungsverfahren zu studieren und einen Optimum zwischen Genauigkeit und Robustheit, Kosten (zeitliche und örtliche Komplexität) und Anwendbarkeit (im Sinne der benötigten Sample-Zahl und Implementierungsaufand) zu finden.

Der wissenschaftliche Beitrag dieser Arbeit findet sich sowohl auf der anwendungs- als auch auf der theoretischen Seite von probalistischen Lokalisierungsverfahren. Die Lokalisierungsverfahren werden mittels aufwändiger Simulationen, sowie durch Experimente in realistischen Szenarien evaluiert. Als Platform für die Experimente dient das funkbasierte Entfernungsmesssystem der Firma Nanotron. Im Detail lassen sich die Beiträge wie folgt zusammenfassen:

- Kapitel 3 charakterisiert die Besonderheiten von Time-Of-Flight basierter Indoor-Distanzmessung. Beispielsweise die Abhängigkeit des Distanzehlers zu Messzeit und -ort, zu der Anzahl der Anker, zur echten Position der Messung und Einflüsse des menschlichen Körpers usw. Im Anschluss werden Fehlerverteilungsfunktionen an die Verteilung der Messdaten angepasst, ein Hypothesen-Test sowie eine Model-Verifkation für verschiedene parametrische Modelle durchgeführt.

- Durch die Einführung von Zustandsbeschränkungen auf die aktuellen Messung werden vier beschränkte Sample-Methoden entwickelt (vgl. Kapitel 4), die folgende Vorteile bieten: 1. Reduzierung der benötigten Samples. 2. Robustheit gegenüber Ausreißern oder Messlücken 3. Es ist nicht mehr nötig alle Samples im Speichern

- das NLOS Abschwächungsmodell, welches in Kapitel 4 vorgestellt wird ändern das Fehlermodell der Entfernungsmessung hin zu einer positiv verschobenen rechts auslaufenden Verteilungsfunktion

- In Kapitel 4 wird die theoretisch- sowie praktisch optimale Ankerplatzierung diskutiert

- Die vorgeschlagenen Algorithmen bieten eine allgemeine Plattform für sequentielle- und nicht sequentielle Lokalisierungsverfahren

- Um Varianz-Probleme und Sampleausfälle zu unterdrücken wird ein Glättungsverfahren vorgestellt, welches auf einem einstufigen Zustand mit Bayesianischer Schätzung beruht.

Acknowledgement

The work for this thesis has been carried out in the working group CST (Computer Systems and Telematics) at the Institute of Computer Science at the Freie Universität Berlin (FUB) in Berlin, Germany. I wish to express my sincere gratitude to the people that supported me during my years of PhD study.

First of all, I wish to sincerely thank my supervisor Prof. Dr. Marcel Kyas for his invaluable advice and encouragement. During my early days in Germany, he helped me a lot made adjusting to a new country easy-in particular. Furthermore, he provided much guidance in my research leading to this dissertation. His continued focus on the practical aspects and applications was an important factor of my research. For all time, he has been more than a perfect advisor during my life at FUB, as he has been an advisor, mentor, and a good friend. Because of his valuable feedback on the writing, theorems and technical issues of this dissertation, the quality is greatly improved.

I would like thank Prof. Dr.-Ing. Jochen H. Schiller, who let me join CST and provided a friendly working environment. When I first came to FUB, he introduced me to the working group and explained many research areas. His wide knowledge in communications and wireless networks helped me to keep things in perspective.

I also wish to thank Matthias Wählisch, Yubin Zhao, Oliver Hahm, Stephan Adler, Simon Schmitt and Zhao Liu, who were an inexhaustible source of help whenever I was in need. Their patiently discussions continued to be a great inspiration of my research. Despite my lack of knowledge in the field of programming and embedded system, Stephan and Simon made great support of the real-world experiments. I would also like to take this opportunity to thank all my colleagues for creating an ever nice atmosphere in the institute. I enjoyed working with them very much.

I am very thankful to Chinese Scholarship Council (CSC) for providing the scholarship during my four years study in Germany.

Last but not least, I am very grateful for the love, support and patience of my parents and my friends.

I dedicate this thesis to my parents who have dedicated their entire life for my education.

Yuan Yang

Contents

List of Algorithms

List of Figures

List of Tables

Chapter 1

Introduction

1.1 What Makes Indoor Positioning Attractive?

With the popularity of mobile devices (i.e., portable sensor devices, personal digital assistants (PDA), smart phones and tablets), indoor positioning and tracking have become increasingly interesting for position-related applications and emergency services. Knowledge of the position of mobile devices opens up a wide range of attractive applications as follows

- positioning and tracking of people and assets;
- emergency preparedness and response for public safety;
- intelligent transportation systems;
- resource-efficient protocols;
- location-nearby service and e-commerce;
- real-time navigation and path planning;
- location-based management;
- environment monitoring, i.e., air quality and temperature, etc.;
- other fields;

As a rule of thumb, people spend much more time in indoor scenarios than outdoors. Therefore, indoor positioning of people or devices plays a more important role than outdoor positioning in context-aware applications [32].

The most widely used positioning tools, like global positioning system (GPS) and cellular networks (GSM) positioning are the mainstream technology for outdoor positioning. However, in indoor scenarios, GPS and cellular positioning may fail due to the issues of signal availability, delay and path loss, e.g., the signals from satellite or base-station are often disturbed due to the heavy

shadowing, fading and scattering loss of building structures; and these systems often take a long processing time. Consequently, numerous dedicated indoor localization systems have explored been explored using other techniques, i.e., radio characteristics form WLAN and Wireless Sensor Networks (WSNs), Inertial Measurement Unit (IMU), computer vision and infrared (IR) devices, etc.

1.2 Indoor Positioning Systems

Various indoor positioning systems have been developed for different requirements and operating environments. Positioning systems can be classified based on the terms of 1) the measurement techniques (the technique to observe measurements); and 2) position estimation methods (the method of extracting the position information from measurements) (see Fig. 1.1). A positioning system can use a single measurement technique and estimation method, while better performance can be achieved by combining multiple methods.

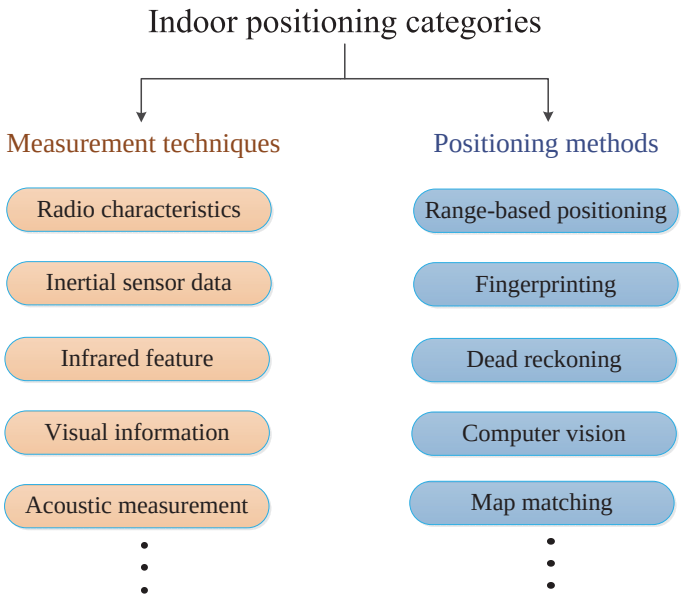

Figure 1.1: Positioning system categories according to measurement techniques and position estimation methods

1.2.1 Positioning measurement techniques

Radio characteristics

A majority of indoor positioning systems explores Radio Frequency (RF) signals to indicate the relationship between reference nodes and target [99, 167] using radio access techniques, i.e., WiFi (IEEE 802.11), Bluetooth (IEEE 802.15.1), UWB (IEEE 802.15.3) or ZigBee (IEEE 802.15.4).

The RF signals from indoor networks are convenient to extract for positioning purposes, i.e., Received Signal Strength (RSS), Time-of-Flight (TOF), Angle-of-Arrival (AOA), etc. Thus, the advantage of RF-based indoor positioning that the system can be implemented with little or no change in hardware and infrastructure. Other positioning techniques might require additional hardware or infrastructure.

The major problem of RF based positioning is that radio propagation is highly sensitive to indoor environment, which commonly observe rich multipath propagation and severe path loss. It has been reported that Ultra wideband (UWB) performs much better narrow band RF measurements, but still results in 10 meter errors [8, 151]. Unfortunately, the measurement accuracy of portable devices is difficult to improve or very expensive.

Inertial Measurement Unit (IMU)

IMU [56] is a mobile unit equipped with multiple inertial sensors (i.e., magnetometers, gyroscopes, accelerometers, compasses or odometers), which can infer the turn rate, velocity or acceleration to estimate the motion of an object. The advantage of IMU-based localization is that it does not rely on the reception of external infrastructure-free, because the inertial sensors are embedded in a single mobile device.

However, directly integrating acceleration measurements has been criticized for the error accumulation of IMU [181]. Thus, the disadvantage of IMU measurement is that it is problematic due to accumulated estimation errors. Generally, an IMU is necessary to be combined with an error correction based on wheel encoder or other measurement techniques.

Infrared (IR) measurement

Infrared-based systems [66] use IR camera to observe IR signals to indicate distance to an infrared light source (like an infrared LED). Infrared measurement accuracy is claimed to be in the magnitude of cm or even dm. Furthermore, IR light is invisible to the human eye, which is less intrusive to people's daily life compared to visible light positioning [142].

The range of IR coverage is about 10 m, which is only suitable for very limited scenarios compared to other positioning techniques. Thus, the performance of IR positioning depends on the

density of infrared light sources. More important, IR signals require Line-of-Sight (LOS) propagation (IR signal cannot travel through common indoor obstacles i.e., people or furniture). Therefore, IR systems often occur missed detection even within its coverage area.

Visual measurement

Visual measurement [148] explores visual sensors (i.e., laser-base range finder or infrared camera) for distance estimation. Optical sensors provide a tremendous amount of information about a target and the surrounding environment, which generally result in measurement accuracy in the magnitude of cm. However, visual measurement takes a high cost on communication, processing, and storage, etc. The other problem is that visual systems have a very limited coverage range [112], which is not suitable for the large scale position with sparse sensors.

Other measurement techniques

There are a variety of other measured phenomenon that can be extracted for positioning purpose, i.e., acoustic and ultrasonic measurements [112], visible light measurement, geomagnetic field measurement and hybrid systems combining multiple techniques, etc. Since these methods either require specialized and costly hardware or only work in LOS scenarios, they are suitable for some conditions but lack of generality and affordability.

1.2.2 Positioning estimation methods

Given a certain positioning measurement technique, there are various estimation methods to implement indoor positioning and tracking, to name a few as follows.

Range-based positioning

Definition 1.1. *Range-based positioning* is the methods that convert the measurements into point-to-point estimated distance (range) or angle estimations for calculating location.

Range-based positioning contains two steps [35]: first, estimate the range or angle from measurements between the target and reference nodes (know anchors or beacons) based on measurement models; then, estimate the target position from the range or angle estimate by trilateration or triangulation algorithms. Range-based positioning can provide fast, low-cost and absolute position estimation in large scale environments.

Metric ranging techniques for the distance or angle estimation include TOA, TDOA, RSS and AOA. If no metric ranging measurement is available, network connectivity (multi-hop range) can be used to approximate the range estimation [128] (also known as range-free positioning [30]).

However, the estimated range is corrupted by shadowing and obstructions of indoor scenarios, especially in NLOS conditions. Thus, range-based positioning often leads to large positioning errors

subjected to large ranging errors.

Fingerprinting positioning

Fingerprinting positioning is a mapping of the measured data (called a fingerprint or data map), which estimates position based on the pattern matching between real-time measurements and a previously stored data in the fingerprint [109]. Fingerprinting can use RSS, geomagnetic field signal and other information. Fingerprinting methods are commonly used for RSS-based positioning, because that the model of RSS measurements is difficult to obtained from indoor multipath environment. Thus, fingerprinting positioning is suitable for indoor scenarios, which is not sensitive to multipath and NLOS propagations.

In the offline step of fingerprinting system, RSS measurements from site survey of the interest area are collected, calibrated, smoothed and saved in a training database of the fingerprint. In the positioning stage, the online RSS is matched to the fingerprint; then the best matched point (e.g., probabilistic methods, k-nearest-neighbor or neural networks) is the estimated position. Fingerprinting makes use of the full knowledge of offline information. However, generating a fingerprint is time-consuming and labor-intensive in large-scale indoor environments, which can be expensive as well as dangerous in some scenarios [87].

Dead reckoning

Dead reckoning is a relative position estimation based on IMU data translated to speed, time, course and motion [95], which can only provide a relative position. Furthermore, this method is problematic for long-distance navigation because it suffers from accumulated estimation errors. As a consequence, dead reckoning is necessary to be combined with other positioning approaches, i.e., map-matching methods [124], or range-based positioning [174]. However, combining exact map or multiple sensor data generally require a centralized server, more infrastructure, a large scale database or a high cost, etc.

Image-based positioning

Image-based positioning uses the idea of image processing on positioning measurements, i.e., vision-based positioning [148], RF tomography tracking [133] and map-matching method [118], etc. The most important advantage of imaging positioning is the visualization of position data, which enable humans to perceive, read and work with invisible data. The weakness is that the data processing (i.e., image rotations, translations and feature extractions) of high resolution image is not an easy task. A variety of imaging localization algorithms have been suggested to reduce processing complexity. Popular approaches are pixel-based techniques that compute the correlation

between images or feature-based methods that exploit typical properties of environments such as linear structures [168].

1.2.3 Comparison of positioning systems

Different positioning applications have different requirements of positioning accuracy, robustness, coverage, and complexity, etc. There is no unique answer to which positioning system is the best. Table 1.1 summarizes the features of some positioning systems, showing different features, requirements and limits from recent work [8, 86, 120, 165].

Table 1.1: Comparison of positioning systems

Positioning technique	Typical accuracy /m	Major drawback
RF fingerprinting	1-10	intensive offline calibration
Geomagnetic fingerprinting	1-100	complicated Geo-referenced training
RF range-based	1-10	susceptible to NLOS conditions
Computer vision	0.01-0.1	intensive feature extractions and processing
RFID benchmarking	0.1-1	short coverage
Acoustic or ultrasonic	0.1-1	might influence animals
Dead reckoning	1-10	high accumulation errors
Infrared scan	0.01-0.2	line of sight required
Tomography tracking	0.1-1	dense infrastructure

Any individual positioning technique alone may have difficulties for indoor positioning, while integration with multiple techniques can complement to a single positioning technique. Consequently, a hybrid positioning system combining multiple techniques and estimation methods can provide higher accuracy for all scenarios.

1.3 Practical Probabilistic Positioning Algorithms

Since the infrastructure of RF systems is the most common property, this study investigates RF range-based positioning from WSNs. In order to enhance positioning performance, it can either upgrade ranging techniques or optimize positioning algorithms. The hardware updating or combining multiple positioning techniques is a costly engineering task, which is of less interest.

Instead of using the most advanced positioning technique, optimizing positioning algorithms is a more potential and affordable way. Therefore, this dissertation deals with indoor positioning in the algorithmic domain of a given ranging technique.

1.3.1 Motivation

There are a number of range-based positioning methods, which are specific for certain purposes or requirements. Generally, probabilistic positioning (such as Bayesian inference, max a posterior and M-estimators [172, 175]) captures more information than non-probabilistic positioning (like the geometric positioning: circle overlapping [125, 182]; and connectivity-based positioning, i.e., the centroid algorithm [127] and APIT [140], DV-hop [129] and weighted nearest neighbors [109, 165]). Consequently, probabilistic algorithms have been widely proposed for accurate positioning, but with the modeling, computation and implementation problems arise from real-world scenarios.

Among various probabilistic positioning algorithms, some that have careful theoretical foundations and convergence proofs but may work poorly in practice; and some with higher computation and buffer are also less considerable. Agreeing with this quote,

> *"An approximate answer to the right problem is worth a good deal more than an exact answer to an approximate problem."*
>
> *–John W. Tukey*

this dissertation aims to study the right questions of the practical indoor positioning:

1. to characterize and model the real indoor ranging, and verify the qualify the measurement model;
2. to derive the sample-based approximation for positioning purposes, providing a general framework for either non-sequential or sequential positioning;
3. to require a low cost for practical positioning rather than a mathematical optimization;
4. to adapt to the NLOS ranging errors;
5. to address the estimation instability, exploring smoothing schemes for real-time positioning.

1.3.2 Practical considerations

Non-Gaussian RF ranging error

The RF ranging measurement is the estimated distance between a target node (the position unknown node) and a reference node (the position unknown node, also called an anchor or beacon). Several anchors are scattered throughout the indoor environment, which know their own locations by GPS receivers or manual configuration.

Most work states the fact that RF ranging is always severely afflicted by non-Gaussian measurement errors [102, 162, 176], due to multipath propagations, NLOS environment or system noise, etc. Thus, the challenge of range-based positioning is to evaluate the measurement error or make online calibration. Despite the widely investigations of positioning algorithms, the studies on the features

of real RF ranging are sparse. Thus, it is necessary to characterize the non-Gaussian indoor ranging, including the model parameters, bounds and connections to the physical world.

Tradeoff between performance and cost

Complicated algorithms might enhance positioning performance, i.e., mixture models, intensive online training, a large number of iterations or memory-involved smoothing. However, they are very costly, which are out of less interest. The positioning algorithms should achieve satisfied performance on lightweight computation and implementation.

Requirement on infrastructure deployment

A dense infrastructure deployment of positioning system can improve positioning accuracy, but it is restricted to the indoor structure and system expense. On the other hand, sparse infrastructure may result in an insufficient number of ranging measurements for position estimation. Thus, the infrastructure density and deployment should be designed with the performance analysis in real indoor scenarios. Furthermore, in order to allow large scale positioning and pervasive applications, the positioning algorithms should be less dependent to the infrastructure deployment.

Additional knowledge

Additional knowledge can further refine positioning performance, i.e., map information of indoor environment, prior information of the target's position, the motion model for mobile tracking, measurement database and other data. However, using these information may cause high communication, computation, memory and implementation difficulty, which is impractical to resource-limited positioning devices. The challenge is how the information can be extracted and efficiently incorporated into the positioning framework.

1.4 Research Content

This dissertation focuses on probabilistic algorithms for range-based indoor positioning, with the performance, robustness and limits analyzed by numerous simulations and real-world indoor experiments. The following domains are primarily investigated, involving the methods proposed in our previous work [166, 176–180].

1.4.1 Modeling the uncertainty of indoor RF ranging

The measurements of indoor positioning systems suffer from a number of inherent uncertainties, i.e., the thermal noise, multi-path effect, NLOS propagations, interference, and system noise due to clock jitters, drifts and system calibration. The fundamental theorem of probabilistic estimation is

to derive the state probability from measurements, given the measurement model. Therefore, prior to developing a positioning algorithm, the properties and model of real-world ranging should be analyzed.

The ranging measurement model serves as a connection between the physical world and the positioning algorithm. This work holds that the problem of the measurement modeling is not to design a perfectly accurate model, but an appropriate model transmitting into the probabilistic frame. In the majority work of range-based positioning, the measurement model can be far too complex or not nearly well enough to represent the characteristics of indoor RF ranging. Thus, this thesis focuses on the model representativeness and efficiency rather than the model optimization.

1.4.2 From non-sequential to sequential positioning

Chapter 4 proposes algorithms for both non-sequential to sequential positioning. The distinction between non-sequential and sequential positioning are whether sequential measurements or prior are needed for each positioning request.

Non-sequential position estimation

Definition 1.2. *Non-sequential positioning* is the position estimation only involving the measurements observed at the moment of one positioning request.

Non-sequential positioning is very important, as unstable ranging often encounters situations that no history measurements are available. Another reason is that many positioning applications are event-driven services, e.g., the position is only estimated when the user demands. In these applications, it is not desirable to keep all the history measurements in memory. Thus, for non-sequential positioning, the iterative methods on the current measurements are often employed.

Sequential position estimation

Definition 1.3. *Sequential positioning* is the time-series estimation in sequence given (also known as the position filtering), making use of time-series ranging measurements.

A variety of positioning applications are able to provide time-series ranging measurements, and request to continuously tracking the target at every time step, e.g., indoor navigation and rescue systems. Given the sequential measurements and target motion model, continuous position estimation can be derived. Sequential positioning can achieve better accuracy than non-sequential positioning, as the history measurements and estimations are powerful to remove uncertainty [121].

1.4.3 NLOS mitigation and smoothing

Further, NLOS mitigation and smoothing approaches are explored to refine the position estimation.

NLOS mitigation

The performance of probabilistic estimations highly depends on the fitness of the measurement model [92]. Unfortunately, the NLOS ranging always violates the common assumed models [10, 170], which easily misleads the estimate. Thus, the NLOS problem has been extensively studied, which can be categorized into NLOS identification and NLOS mitigation.

The main weaknesses of existing NLOS identification and mitigation are: 1) there is always the possibility of false identifications of the NLOS measurements; 2) the loss of information due to the hard decision of discarding the NLOS ranges; 3) incurring additional latency, computation and memory; 4) difficulty in calculating the joint probability from the complex measurement model. More important, there is still a lack of efficient NLOS mitigation methods on the sample-based algorithms.

Smoothing

For sequential positioning, smoothing methods have been applied to reduce the variance of estimation. The definitions of the Bayesian filtering and smoothing are

- Filtering ($p(\mathbf{x}_t|\mathbf{z}_{0:t})$): is to estimate the state conditionally to the observations up to time t.
- Smoothing ($p(\mathbf{x}_t|\mathbf{z}_{0:T_{\text{smoothing}}})$): is to estimate the state conditionally to the observations up to time $T_{\text{smoothing}}$ (with $T_{\text{smoothing}} \geq t$).

The Bayesian optimal smoothing consists of a forward filtering and backward update. The complexity of the smoothing algorithm is proportional to how many time-steps of the future measurements are involved in the backward update step. Since the goal is real-time positioning, this thesis investigates the smoothing algorithms using only one time-step backward update.

1.5 Thesis Outline

The outline of this thesis is organized as follows:

Chapter 2 reviews the basic probabilistic framework, which are the mathematical foundation of the existing algorithms for range-based positioning and tracking.

Chapter 3.3 discusses one of the contributions of this thesis, the frequentist modeling of real indoor TOF ranging. It presents the idea of statistical distribution fitting, and the models are verified by hypotheses testing.

Chapter 4 presents the detailed design and implementation of seven sample-based approximation and NLOS mitigation algorithms on the probabilistic framework, and verifies them in both simulations and real-world experiments. These results are the major contribution of this thesis, which

enhance the performance and usability for sample-based probabilistic positioning.

Chapter 5 implements the smoothing scheme to suppress the estimation variance and sparsity problems, with the innovation that the one time-step smoothing imposes a low cost on real-time positioning.

Chapter 6 concludes this thesis and proposes the future perspectives. It also suggests the possible improvements and implementations for practical indoor positioning.

Chapter 2

Existing Probabilistic Approaches for Range-based Positioning

After choosing a ranging technique, the positioning problem becomes an algorithmic optimization procedure. Probabilistic estimation is the most widely-used strategy to deal with observation uncertainty. This chapter reviews literature on the typical probabilistic methods for range-based positioning.

2.1 Bayesian Range-based Positioning

There are two broad branches of the interpretations of probability: Bayesian inference and frequentist inference. Frequentist interprets the probability of an event as the relative frequency of a large number of trials. Bayesian inference provides a generalization of model-based probability, combing both a priori information and observed evidence.

Bayesian inference is widely used to deal with dynamic and non-Gaussian uncertainty, with the variations as Maximum A Posteriori (MAP) estimations, Maximum Likelihood (ML) estimations, or other M-estimators [42] (M-estimator is defined to obtain the minimum or maximum of an objective function of the data).

2.1.1 Basis of Bayesian inference

Bayesian inference is based on Bayes' theorem

$$\Pr(A|B) = \frac{\Pr(B|A)\Pr(A)}{\Pr(B)}\,, \tag{2.1}$$

where

- $\Pr(A|B)$ stands for the conditional probability of A given B;
- $\Pr(B|A)$ is the likelihood of observations based on an observation model;
- $\Pr(A)$ is the unknown variable before the evidence is seen;
- $\Pr(B)$ is a normalization factor representing evidence, which can be derived as

$$\Pr(B) = \int \Pr(B|A)\Pr(A)dA$$

.

In the context of two dimensional (2D) scenario, the positioning problem is defined:

Definition 2.1. *The state space of range-based positioning* is the target's position coordinates (a hidden state)

$$\mathbf{x} = (x, y), \tag{2.2}$$

with $\mathbf{x} \in \mathbb{R}^2$.

Definition 2.2. *The measurable space of range-based positioning* is the ranging measurement set from N_{anc} anchors

$$\mathbf{z} = \{r_l\}_{l=1}^{N_{\text{anc}}}. \tag{2.3}$$

The space-limited indoor scenario causes rich multipath signals, then, the ranging measurements observe high uncertainty.

Definition 2.3. *The ranging measurement* is the estimated distance between the lth anchor ($\mathrm{a}_l = (a_{xl}, a_{yl})$) and the target

$$r_l = \bar{r}_l + \varepsilon_r^l, \;\; l \in \{1, 2, \cdots, N_{\text{anc}}\}\,, \tag{2.4}$$

with $\bar{r}_l = \|\mathbf{x} - \mathbf{a}_l\|$ denoting the ground truth and ε_r^l for the lth ranging error.

Definition 2.4. *The object of positioning* is to derive the posterior of the state conditional to the measurements. Equation (2.1) is expressed by substituting $\mathbf{x}$ for A and $\mathbf{z}$ for B:

$$\underbrace{p(\mathbf{x}|\mathbf{z})}_{\text{Posterior}} = \frac{\overbrace{p(\mathbf{z}|\mathbf{x})}^{\text{Likelihood}} \overbrace{p(\mathbf{x})}^{\text{Prior}}}{\underbrace{p(\mathbf{z})}_{\text{Evidence}}}\,, \tag{2.5}$$

where the denominator is the evidence according to the ranging measurements

$$p(\mathbf{z}) = \int_{\mathbf{x}} p(\mathbf{x})p(\mathbf{z}|\mathbf{x})\, d\mathbf{x}\,, \tag{2.6}$$

and

- $p(\mathbf{x}|\mathbf{z})$ is the posterior of 2D position ($\mathbf{x}$) given a set of measurements ($\mathbf{z}$);
- $p(\mathbf{z}|\mathbf{x})$ denotes the likelihood of observing $\mathbf{z}$;
- $p(\mathbf{x})$ is the prior of $\mathbf{x}$ before seeing $\mathbf{z}$.

For the ranging measurements given the state value, it is often assumed that each measurement is conditionally independent. Thus, the joint likelihood is the product of the conditional density of all the measurements

$$p(\mathbf{z}|\mathbf{x}) = \prod_{l=1}^{N_{\text{anc}}} p(r_l|\mathbf{x}) \ . \tag{2.7}$$

Since the denominator of (2.5) is independent of the state and serves as the normalization factor, it does not need to be known. Then, the full Bayesian inference can be spelled out in words apart from the normalizing constant

$$\text{Posterior} \propto \text{Likelihood} \cdot \text{Prior} \ , \tag{2.8}$$

where $\propto$ means being proportional to. Equation (2.8) decomposes the posterior into two information: the prior and likelihood.

Prior $p(\mathbf{x})$ The prior allows a guess with models using subjective experience before obtaining the observation

$$\text{Prior} = \text{Belief using subjective experience before the observation} \ . \tag{2.9}$$

Likelihood $p(\mathbf{z}|\mathbf{x})$ The likelihood evaluates the guess on how well the measurements agree with the prior.

Then, the posterior combines the prior and observations, which is

$$\text{Posterior} = \text{Belief corrected by observations} \ . \tag{2.10}$$

Once the posterior distribution is available, any features of $\mathbf{x}$ can be analyzed by a particular estimation algorithm. Bayes' Theorem can also be formed in the log scale

$$log(\text{Posterior}) \propto log(\text{Prior}) + log(\text{Likelihood}) \ . \tag{2.11}$$

2.1.2 Dynamical models of Bayesian inference

Bayesian inference for range-based positioning is a model-based posterior conditionally to the known motion and ranging models. Since the real-word is dynamic in nature, Bayesian algorithms may then use dynamical models to adapt to reality instead of static models from statistics. The probability density in (2.5) is the posterior with a model parameterized of θ [157, 171]

$$\underbrace{p^{\theta}(\mathbf{x}|\mathbf{z})}_{\text{Posterior}} = \frac{\overbrace{\prod_{l=1}^{N_{\text{anc}}} p^{\theta}(r_l|\mathbf{x})}^{\text{Likelihood}} \overbrace{p(\mathbf{x}|\theta)}^{\text{Prior}}}{\underbrace{p^{\theta}(\mathbf{z})}_{\text{Evidence}}}, \tag{2.12}$$

Definition 2.5. *The hyperparameter (θ)* is the parameters of the transition or observation models, which are assumed constant or to be dynamically estimated together with the state.

In theory, learning the models is to estimate the posterior over the hyperparameters [113]. Similar to the derivation of the posterior of the state (2.6), one can obtain the posterior of the hyperparameters involving the coming observations

$$p(\mathbf{x}|\mathbf{z}) = \frac{p(\mathbf{z}|\mathbf{x})p(\mathbf{x})}{p(\mathbf{z})} = \frac{p(\mathbf{z}|\mathbf{x})p(\mathbf{x})}{\int_{\mathbf{x}} p(\mathbf{x})p(\mathbf{z}|\mathbf{x})\, d\mathbf{x}} \tag{2.13}$$

$$\Rightarrow \qquad p(\theta|\mathbf{z}) = \frac{p(\mathbf{z}|\theta)p(\theta)}{p(\mathbf{z})} = \frac{p(\mathbf{z}|\theta)p(\theta)}{\int_{\theta} p(\theta)p(\mathbf{z}|\theta)\, d\theta}. \tag{2.14}$$

This is for the purpose of adapting the model after obtaining the observations, i.e., the values of the parameters or the models depending on the posterior of the hidden state.

Once the hyperparameters θ are learned, the Bayesian frame can accurately represent the dynamic process. Similar to (2.13), the posterior of $\mathbf{x}$ given the observations and the learning models can be extracted

$$p^{\theta}(\mathbf{x}|\mathbf{z}) = \frac{p^{\theta}(\mathbf{z}|\mathbf{x})p^{\theta}(\mathbf{x})}{p^{\theta}(\mathbf{z})} = \frac{p^{\theta}(\mathbf{z}|\mathbf{x})p^{\theta}(\mathbf{x})}{\int_{\mathbf{x}} p^{\theta}(\mathbf{x})p^{\theta}(\mathbf{z}|\mathbf{x})\, d\mathbf{x}}. \tag{2.15}$$

If the model (θ) is static, then Eq.(2.15) is equal to Eq.(2.13).

Given the Bayesian inference of $\mathbf{x}$ and $\mathbf{z}$, we can refine the model parameter θ [14]

$$p(\theta|\mathbf{z}, \mathbf{x}) = \frac{p^{\theta}(\mathbf{z}|\mathbf{x})p(\theta|\mathbf{x})}{p(\mathbf{z}|\mathbf{x})} = \frac{p^{\theta}(\mathbf{z}|\mathbf{x})p(\theta|\mathbf{x})}{\int_{\theta} p(\theta|\mathbf{x})p^{\theta}(\mathbf{z}|\mathbf{x})\, d\theta}. \tag{2.16}$$

Numerous work offers a comparative review of the possible choices available for parameter estimation, such as the expectation maximization (EM) algorithms used to learn the model parameters by maximizing the log likelihood function [58, 90].

Dynamical models from (2.14) to (2.16) consists of working out three Bayesian estimations

- $p(\theta|\mathbf{z})$: calculate the posterior over the model parameters given the observations (2.14);
- $p^{\theta}(\mathbf{x}|\mathbf{z})$: calculate the posterior over the state given the current model parameters (2.15);
- $p(\theta|\mathbf{z}, \mathbf{x})$: calculate the posterior over the hyperparameters given the state posterior (2.16).

Refining the Bayesian estimation of both the state density and hyperparameters is an iterative procedure until reaching convergence, which falls into a chicken-and-egg problem: a good state estimation can refine the hyperparameters; and good hyperparameters result in a good state estimation. The on-line estimation of the model parameters is formulated as an iterative procedure, whereas, its high computation and long processing time are critical issues for practical applications.

2.2 Approximation to Bayesian Positioning

Applying the full Bayesian frame may arise difficulties, such as specifying rigorous state propagation and measurement models. Therefore, approximations to Bayesian inference are studied [37], aiming for less requirements on the modeling procedure and computation. The simplest approximation is a point estimation from the posterior to find a solution with the maximum possibility, i.e., the posterior mean (MMSE estimation), the MAP estimation, ML estimation and Least Square estimation (LS estimation).

2.2.1 Minimum Mean Square Error (MMSE) estimation

Better estimate in mean squared sense is the posterior expectation, known as an estimate of Minimum Mean Square Error (MMSE estimator) [145]

$$\widehat{\mathbf{x}}_{\text{MMSE}} = \mathrm{E}[\mathbf{x}|\mathbf{z}, \theta] = \int_{\mathbf{x}} \mathbf{x} p^{\theta}(\mathbf{x}|\mathbf{z})\, d\mathbf{x} \tag{2.17}$$

$$= \frac{\int_{\mathbf{x}} \mathbf{x} p^{\theta}(\mathbf{z}|\mathbf{x}) p^{\theta}(\mathbf{x})\, d\mathbf{x}}{p^{\theta}(\mathbf{z})}$$

$$= \frac{\int_{\mathbf{x}} \mathbf{x} p^{\theta}(\mathbf{z}|\mathbf{x}) p^{\theta}(\mathbf{x})\, d\mathbf{x}}{\int_{\mathbf{x}} p^{\theta}(\mathbf{x}) p^{\theta}(\mathbf{z}|\mathbf{x})\, d\mathbf{x}}\,. \tag{2.18}$$

The generalization of MMSE estimators (2.18) can be succinctly expressed as the expectation of a function of interest $g(\mathbf{x})$ over the posterior [139]:

$$\widehat{g(\mathbf{x})}_{\text{MMSE}} = \text{E}[g(\mathbf{x})|\mathbf{z}, \theta] = \int_{\mathbf{x}} g(\mathbf{x}) p^{\theta}(\mathbf{x}|\mathbf{z})\, d\mathbf{x} \tag{2.19}$$

$$= \frac{\int_{\mathbf{x}} g(\mathbf{x}) p^{\theta}(\mathbf{z}|\mathbf{x}) p^{\theta}(\mathbf{x})\, d\mathbf{x}}{\int_{\mathbf{x}} p^{\theta}(\mathbf{x}) p^{\theta}(\mathbf{z}|\mathbf{x})\, d\mathbf{x}} \,. \tag{2.20}$$

The MMSE estimator of Eq. (2.20) is the estimator of the function $g(\mathbf{x})$ resulting in minimum mean square error

$$\text{E}[\| \varepsilon \left(\widehat{g(\mathbf{x})}_{\text{MMSE}} \right) \|^2] = \int_{\mathbf{x}} \| g(\mathbf{x}) - \widehat{g(\mathbf{x})}_{\text{MMSE}} \|^2 \; p(\mathbf{x})\, d\mathbf{x} \,. \tag{2.21}$$

The mean square error of the estimation $\widehat{g(\mathbf{x})}$ is

$$\text{E}[\| \varepsilon \left(\widehat{g(\mathbf{x})} \right) \|^2] = \text{E}[\left(g(\mathbf{x}) - \widehat{g(\mathbf{x})} \right)^{\text{T}} \left(g(\mathbf{x}) - \widehat{g(\mathbf{x})} \right)] \tag{2.22}$$

$$= \text{E}[g(\mathbf{x})^T g(\mathbf{x}) - 2\widehat{g(\mathbf{x})}^{\text{T}} g(\mathbf{x}) + \widehat{g(\mathbf{x})}^{\text{T}} \widehat{g(\mathbf{x})}]$$

$$= \text{E} \parallel g(\mathbf{x}) \parallel^2 - 2\widehat{g(\mathbf{x})}^{\text{T}} \text{E} g(\mathbf{x}) + \widehat{g(\mathbf{x})}^{\text{T}} \widehat{g(\mathbf{x})} \,. \tag{2.23}$$

Differentiate (2.23), we get $\widehat{g(\mathbf{x})}_{\text{MMSE}} = \text{E}[g(\mathbf{x})]$. The MMSE estimation procedure is most naturally expressed in terms of statistical decision theory [16], as it is easy to handle in the case of analytical posterior distribution.

2.2.2 Maximum A Posteriori (MAP) estimation

Given the posterior distribution, the most probable point value is given by the maximum of the posterior distribution (MAP estimation). As $\mathbf{x}$ is a random point in the state-space, the MAP estimate is defined as the maximum of the posterior distribution.

$$\hat{\mathbf{x}}_{\text{MAP}} = \arg\max_{\mathbf{x}} \frac{p^{\theta}(\mathbf{z}|\mathbf{x}) p^{\theta}(\mathbf{x})}{p^{\theta}(\mathbf{z})} \,. \tag{2.24}$$

Since the denominator of (2.5) is independent of the state, the MAP estimate can be

$$\hat{\mathbf{x}}_{\text{MAP}} = \arg\max_{\mathbf{x}} p^{\theta}(\mathbf{z}|\mathbf{x}) p^{\theta}(\mathbf{x}) \,. \tag{2.25}$$

For a convex posterior, the MAP estimation approximates the MMSE estimation. The posterior median may also be used as an estimate minimizing the expected absolute error. But MAP estimation can be very difficult because the posterior density is not expressible in terms of a fixed number of

parameters and cannot be maximized easily. Furthermore, MAP cuts out all the benefits of learning other possibilities.

2.2.3 Maximum Likelihood (ML) estimation

When the priori density of $p(\mathbf{x}|\theta)$ is unknown, one can use a non-informative prior or a uniform prior. With a uniform prior, the MAP estimate is called the maximum likelihood (ML) estimate [5]

$$\hat{\mathbf{x}}_{\mathrm{ML}} = \arg\max_{\mathbf{x}} p^{\theta}(\mathbf{z}|\mathbf{x}) \, . \tag{2.26}$$

Because the ML estimation does not consider a proper prior; the posterior may be improper.

To seek the value of the state which maximizes the likelihood or log-likelihood, the ML solution can be obtained by setting

$$\frac{\partial L}{\partial \mathbf{x}} = 0 \, . \tag{2.27}$$

where

$$L = \log p^{\theta}(\mathbf{z}|\mathbf{x}) \, . \tag{2.28}$$

Although the method of finding the most likely point estimation is the conceptually simplest, it is the most brutal approximation to Bayesian inference. The lack of the prior precludes the opportunity for smoothing and converging the object function of L. Hence, the likelihood estimation often sticks to the local maxima. In particular, ML estimation is sensitive to NLOS ranging measurements as the large measurement error plays a crucial effect in the object function of MLE.

2.2.4 Least-square (LS) estimation

By assuming a Gaussian measurement error and unknown prior, the MAP turns to be the least squares (LS) estimation. With a set of measured ranges ($\mathbf{z}$) between the target ($\mathbf{x} = (x, y)$) and anchors ($\mathbf{a} = \bigcup_{l=1}^{N_{\mathrm{anc}}} a_l = \bigcup_{l=1}^{N_{\mathrm{anc}}} (a_{xl}, a_{yl})$), the target's position satisfies a set of circles:

$$(x - a_{xl})^2 + (y - a_{yl})^2 = (r_l)^2, \;\; l \in \{1, 2, \cdots, N_{\mathrm{anc}}\}. \tag{2.29}$$

The nonlinear least-squares (NLS) estimation of the target's position is the point minimizing the object function of the sum of squared residuals (SSR) [26]

$$\hat{\mathbf{x}}_{\mathrm{NLS}} = \arg\min_{\mathbf{x}} \left\{ \sum_{l=1}^{N_{\mathrm{anc}}} Res^{l2}(\mathbf{x}) \right\} \tag{2.30}$$

$$= \arg\min_{\mathbf{x}} \left\{ \sum_{l=1}^{N_{\mathrm{anc}}} (r_l - \|\mathbf{x} - \mathbf{a}_l\|)^2 \right\} , \tag{2.31}$$

where $Res^l(\mathbf{x})$ is the residual between r_l and $\|\mathbf{x} - \mathbf{a}_l\|$.

Minimizing SSR can be achieved by exhausted searching or iteration methods [67]. To reduce the computation of searching the minimum values of the object function (2.30), a linearization can be used, known as the linear least-squares (LLS) estimation [177] by subtracting the fth measurement equation (2.29), with $j \in \{1, 2, \cdots, N_{\mathrm{anc}}\}$ and $j \neq f$:

$$\hat{\mathbf{x}}_{\mathrm{LLS}} = \frac{1}{2}(\mathbf{A}^{\mathrm{T}}\mathbf{A})^{-1}\mathbf{A}^{\mathrm{T}}\mathbf{P} , \tag{2.32}$$

where

$$\mathbf{A} = \begin{bmatrix} (a_{x1} - a_{xf}) & (a_{y1} - a_{yf}) \\ (a_{x2} - a_{xf}) & (a_{y2} - a_{yf}) \\ \vdots & \vdots \\ (a_{xN_{\mathrm{anc}}} - a_{xf}) & (a_{yN_{\mathrm{anc}}} - a_{yf}) \end{bmatrix} , \tag{2.33}$$

and

$$\mathbf{P} = \begin{bmatrix} a_{x1}^2 - a_{xf}^2 + a_{y1}^2 - a_{yf}^2 - r_1^2 + r_f^2 \\ a_{x2}^2 - a_{xf}^2 + a_{y2}^2 - a_{yf}^2 - r_2^2 + r_f^2 \\ \vdots \\ a_{xN_{\mathrm{anc}}}^2 - a_{xf}^2 + a_{yN_{\mathrm{anc}}}^2 - a_{yf}^2 - r_{N_{\mathrm{anc}}}^2 + r_f^2 \end{bmatrix} . \tag{2.34}$$

Both NLS and LLS assume a Gaussian measurement error and treat all the measurements equally as in (2.30) and (2.32), with the larger ranging error takes a stronger role in the minimization of SSR. Thus, LS estimation behaves badly when the error is biased and non-Gaussian. Unfortunately, the real-world ranging error is non-normal distributed, biased and heavily right-tailed as in [164]. In the case that indoor ranging measurement observes a severe NLOS error, the performance of LS

estimation is significantly degraded.

2.3 Sample-based Probabilistic Positioning

In principle, the full Bayesian inference provides the optimal probabilistic solution from the posterior. The computation of the integrals involved in the Bayesian equations (2.20) can only be tractable in linear Gaussian conditions. However, the closed form expression of (2.53) turns out to be impossible in the case of nonlinearity and non-Gaussian of indoor range-based positioning, as it can be NP-hard [40]. An approximate alternative to Bayesian inference is numerical Bayesian methods, including sample-based methods and interpolatory methods [135]. Among different numerical strategies, the most straightforward method is a sample-based approximation using grid-based interpretation, Monte Carlo sampling or importance sampling (IS). Rapid development in computing technologies gradually makes these computation-intensive numerical approximations feasible.

2.3.1 Gaussian-sum approximation

The non-Gaussian posterior can be approximated by a Gaussian-sum approximation [152], where each Gaussian component represents one hypothesis of the state. The positioning problem is expressed by M single Gaussian components

Samples

$$p(\mathbf{x}) \approx p_{\mathcal{N}}(\mathbf{x}) = \sum_{i=1}^{M} \alpha_i \mathcal{N}(\mathbf{x}; m_i, P_i) \,, \tag{2.35}$$

where α_i is the mixing weight of the ith Gaussian component ($\mathcal{N}(\mathbf{x}; m_i, P_i)$).

Posterior

$$p(\mathbf{x}|\mathbf{z}) = \frac{\sum_{i=1}^{M} \alpha_i \, \mathcal{N}(\mathbf{x}; m_i, P_i) \, p^{\theta}(\mathbf{z}|\mathbf{x})}{\lambda} \,, \tag{2.36}$$

with λ as a normalizing constant.

From the additivity property of integrals, the MMSE of the density $p(\mathbf{x})$ (2.20) is

$$\begin{aligned} \widehat{g(\mathbf{x})}_{\text{MMSE}} &\approx \widehat{g(\mathcal{N}_M)}_{\text{MMSE}} \\ &= \int_{\mathbf{x}} \frac{\sum_{i=1}^{M} \alpha_i \, g(\mathbf{x}) \, \mathcal{N}(\mathbf{x}; m_i, P_i) \, p^{\theta}(\mathbf{z}|\mathbf{x})}{\lambda} \, d\mathbf{x} \,, \end{aligned} \tag{2.37}$$

where λ is the denominator of the posterior.

The Gaussian-sum approximation can represent any density $p(\mathbf{x})$ by a few Gaussian components [82]. However, the computation cost increases exponentially with the number of the state dimension [9, 94].

2.3.2 Grid-based approximation

The grid-based representation of the position probability is developed as [24]. The grid-based method, also known the point-mass method, divides the state-space into equally spaced grid-cells with a small side length. The weight of each cell refers to the probability of the cell for the target to locate in. With a fine enough resolution of the grid cells, a good approximation accuracy can be achieved.

The posterior can be numerically approximated by grid cells associated with weights [19]

$$p^{\theta}(\mathbf{x}|\mathbf{z}) \approx \sum_{i=1}^{N_{\mathrm{g}}} w^i \delta(\mathbf{x} - \mathbf{x}^i) \,, \tag{2.38}$$

where w^i denotes the weight associated with ith cell center ($\mathbf{x}^i$), and $\delta(\cdot)$ is the Dirac delta measure; N_{g} is the number of grid cells. In the most basic version of grid-based positioning algorithms, the grid space and N_{g} are time-invariant; thus, each grid cell is of the same size [155].

The grid-based estimation is expressed as

Prior The prior probability $p(\mathbf{x}^i|\theta)$ on the set of grid cells $\mathbf{G} = \{\mathbf{x}^i\}_{i=1:N_{\mathrm{g}}}$.

Posterior The weight vector $\mathbf{w} = \{w^i\}_{i=1:N_{\mathrm{g}}}$ is formed

$$w^i = \frac{p^{\theta}(\mathbf{z}|\mathbf{x}^i)p^{\theta}(\mathbf{x}^i)}{\lambda}, \; i \in \{i\}_{i=1:N_{\mathrm{g}}} \,. \tag{2.39}$$

Letting $N_{\mathrm{g}} \to \infty$, the grid-based interpretation (2.38) can approximate the continuous density arbitrarily well.

The MMSE of the density $g(\mathbf{x})$ of interest is derived as

$$\begin{aligned} \widehat{g(\mathbf{x})}_{\mathrm{MMSE}} &\approx \widehat{g(\mathbf{G})}_{\mathrm{MMSE}} \\ &= \sum_{\mathbf{x} \in \mathbf{G}} g(\mathbf{x}) p^{\theta}(\mathbf{x}|\mathbf{z}) \\ &= \sum_{i=1}^{N_{\mathrm{g}}} g(\mathbf{x}^i) w^i \,. \end{aligned} \tag{2.40}$$

However, a number of issues arise when implementing grid localization. The grid state space and the grid resolution (the size of grid cells) need to be predefined: a finer grid resolution can result in a

better numerical approximation, but the computation and memory complexity grows exponentially with the dimension of the integration over all grid cells [46].

2.3.3 Markov chain Monte Carlo methods

Markov Chain Monte Carlo (MCMC) methods [72] provide a numerical solution of calculating the integrals in form of Eq. (2.18), which are especially useful when dealing with high dimensional integrals. Monte Carlo sampling refers to a general class of methods, where the continuous state-space is represented by discrete samples drawn by inversion sampling, rejection sampling or MCMC methods (Gibbs sampling and Metropolis-Hastings sampling) [60]. In (perfect) Monte Carlo approximation, independent random samples can be drawn from the posterior density:

Samples

$$\mathbf{x}^i \sim p^\theta(\mathbf{x}|\mathbf{z}) \;,\; i \in \{i\}_{i=1:N_\mathrm{s}} \;, \tag{2.41}$$

where N_s is the number of samples.

Posterior Differing from the grid-based representation, the MCMC method is described by a set of equally weighted samples

$$p^\theta(\mathbf{x}|\mathbf{z}) \approx \sum_{i=1}^{N_\mathrm{s}} \delta(\mathbf{x} - \mathbf{x}^i) \;, \tag{2.42}$$

where $\mathbf{x}^i$ is the ith sample drawn from $p^\theta(\mathbf{x}|\mathbf{z})$.

By the strong law of large numbers, the MMSE is estimated

$$\begin{aligned} \widehat{g(\mathbf{x})}_\mathrm{MMSE} &= \int_\mathbf{x} g(\mathbf{x}) p^\theta(\mathbf{x}|\mathbf{z})\, d\mathbf{x} \\ &\approx \frac{1}{N_\mathrm{s}} \sum_\mathbf{x} g(\mathbf{x}) \qquad (2.43) \\ &= \frac{1}{N_\mathrm{s}} \sum_{i=1}^{N_\mathrm{s}} g(\mathbf{x}^i) \;, \quad \mathbf{x}^i \sim p^\theta(\mathbf{x}|\mathbf{z}) \;, \qquad (2.44) \end{aligned}$$

with N_g denoting the number of grid cells.

Monte Carlo methods are superior when the dimensionality of the state is high. The convergence of Monte Carlo approximation is guaranteed by the central limit theorem as discussed in [114]. Dellaert *et al.* introduced the Monte Carlo method into the field of mobile localization in [46], namely, Monte Carlo Localization (MCL). However, the state sampling arises difficulties. The amount of samples needed to adequately explore the state is exponential of the state dimensionality [37].

2.3.4 Importance sampling

In most applications, it is impossible to directly sample from the posterior. Importance sampling [61] is an alternative method of estimating the target distribution with samples from a proposed density, namely, the importance density ($q(\mathbf{x})$).

The difference to the direct Monte Carlo sampling is that the state samples are drawn from the proposed density ($q(\mathbf{x})$), then the posterior is

$$\begin{aligned} p^{\theta}(\mathbf{x}|\mathbf{z}) &= p^{\theta}(\mathbf{x}|\mathbf{z})\frac{q(\mathbf{x})}{q(\mathbf{x})} \\ &= q(\mathbf{x})\frac{p^{\theta}(\mathbf{x}|\mathbf{z})}{q(\mathbf{x})} \\ &\approx \sum_{i=1}^{N_s} \frac{p^{\theta}(\mathbf{x}^i|\mathbf{z})}{q(\mathbf{x}^i)}\delta(\mathbf{x}-\mathbf{x}^i),\ \mathbf{x}^i \sim q(\mathbf{x})\ . \end{aligned} \tag{2.45}$$

with N_s denoting the number of samples. The weight assigned to each sample is called importance weight

$$w^i = \frac{p^{\theta}(\mathbf{x}^i|\mathbf{z})}{q(\mathbf{x}^i)}\ . \tag{2.46}$$

Thus, we can describe the state as

Samples

$$\mathbf{x}^i \sim q(\mathbf{x})\ ,\ i \in \{i\}_{i=1:N_s}\ , \tag{2.47}$$

Posterior The state-space is described by a set of weighted samples

$$p^{\theta}(\mathbf{x}|\mathbf{z}) \approx \sum_{i=1}^{N_s} w^i \delta(\mathbf{x}-\mathbf{x}^i)\ , \tag{2.48}$$

where $\mathbf{x}^i$ is the ith sample drawn from $p^{\theta}(\mathbf{x}|\mathbf{z})$.

Since the samples are not from the true posterior, each particle uses a weight to correct the difference between the true posterior and the importance density. Then, the MMSE is the estimate expectation

$$\begin{aligned} \widehat{g(\mathbf{x})}_{\text{MMSE}} &= \int_{\mathbf{x}} g(\mathbf{x})p^{\theta}(\mathbf{x}|\mathbf{z})\,d\mathbf{x} \\ &= \int_{\mathbf{x}} q(\mathbf{x})\frac{g(\mathbf{x})p^{\theta}(\mathbf{x}|\mathbf{z})}{q(\mathbf{x})}\,d\mathbf{x}\ . \end{aligned} \tag{2.49}$$

According to (2.43) and (2.49), we can obtain the MMSE estimate based on Monte Carlo sampling using the importance density

$$\widehat{g(\mathbf{x})}_{\mathrm{MMSE}} \approx \frac{1}{N_{\mathrm{s}}} \sum_{\mathbf{x}} \frac{g(\mathbf{x}) p^{\theta}(\mathbf{x}|\mathbf{z})}{q(\mathbf{x})} \tag{2.50}$$

$$= \frac{1}{N_{\mathrm{s}}} \sum_{i=1}^{N_{\mathrm{s}}} g(\mathbf{x}^i) \, \frac{p^{\theta}(\mathbf{x}^i|\mathbf{z})}{q(\mathbf{x})} \, , \quad \mathbf{x}^i \sim q(\mathbf{x}) \, . \tag{2.51}$$

Importance sampling is the basis of a wide variety of sample-based algorithms. The importance density can differ from the shape and location of the true posterior, usually has a very simple form for easy sampling. If the importance density fails to concentrate the true state, the sample distribution can diverge from to the true state. Thus, the main difficulty of importance sampling is in the selection of the importance density.

2.4 Sequential position estimation

For most positioning applications, time-series ranging measurements are available, such as object tracking and navigation, etc. This positioning problem is to sequentially estimate the target's position at each discrete instance of time given all the available observations, namely sequential position estimation.

Let $p(\mathbf{z}_t|\mathbf{x}_t, \mathbf{z}_{1:t-1})$ be the dynamical observation model conditional on the current state and the history observations (the following uses the subscript $\{\cdot\}_{1:t}$ to refer to all events up to time t). The vector of the current observations ($\mathbf{z}_t$) from N^t_{anc} reachable anchors ($\{\mathbf{a}^t_l = (a^t_{xl}, a^t_{yl})\}_{l=1:N^t_{\mathrm{anc}}}$) is

$$\mathbf{z}_t = \{r^t_l\}_{l=1:N^t_{\mathrm{anc}}}, \tag{2.52}$$

with r^t_l the ranging measurement from the lth anchor at t. Then, the posterior ($p^{\theta_t}(\mathbf{x}_t|\mathbf{z}_{1:t})$) is sequentially calculated

$$p^{\theta_t}(\mathbf{x}_t|\mathbf{z}_{1:t}) = \frac{p^{\theta_t}(\mathbf{z}_t|\mathbf{x}_t, \mathbf{z}_{1:t-1}) p^{\theta_{t-1}}(\mathbf{x}_t|\mathbf{z}_{1:t-1})}{p^{\theta_t}(\mathbf{z}_t|\mathbf{z}_{1:t-1})} \, , \tag{2.53}$$

where the denominator $p(\mathbf{z}_t|\mathbf{z}_{1:t-1})$ is a normalization constant (the following denoted by λ)

$$p^{\theta_t}(\mathbf{z}_t|\mathbf{z}_{1:t-1}) = \int p^{\theta_t}(\mathbf{z}_t|\mathbf{x}_t) p^{\theta_{t-1}}(\mathbf{x}_t|\mathbf{z}_{1:t-1}) d\mathbf{x}_t \, . \tag{2.54}$$

The prediction density (the prior $p(\mathrm{x}_t|\mathbf{z}_{1:t-1})$) of the Bayesian frame in (2.53) can be accomplished

by applying the Chapman-Kolmogorov equation [11]

$$p^{\theta_{t-1}}(\mathbf{x}_t|\mathbf{z}_{1:t-1}) = \int p^{\theta_{t-1}}(\mathbf{x}_t|\mathbf{x}_{t-1}, \mathbf{z}_{1:t-1}) p^{\theta_{t-1}}(\mathbf{x}_{t-1}|\mathbf{z}_{1:t-1}) d\mathbf{x}_{t-1} \ . \tag{2.55}$$

where $p^{\theta_{t-1}}(\mathbf{x}_t|\mathbf{x}_{t-1}, \mathbf{z}_{1:t-1})$ is the density of the current state given the previous state and history observations.

The Eq. (2.53), (2.54) and (2.55) form the complete sequential Bayesian solution of the position tracking problem. The main weakness is that the state transition model ($p^{\theta_{t-1}}(\mathbf{x}_t|\mathbf{x}_{t-1}, \mathbf{z}_{1:t-1})$) and the measurement model ($p^{\theta_t}(\mathbf{z}_t|\mathbf{x}_t, \mathbf{z}_{1:t-1})$) require to store the full history observations ($\mathbf{z}_{1:t-1}$). To improve the efficiency of the sequential estimation, certain approximations are described in the following subsections.

2.4.1 Bayesian frame of hidden Markov model

To perform on-line filtering of the Bayesian frame (2.53), it essentially applies a hidden Markov model (HMM) [155]. Thus, the prior is able to recur at each time step.

Definition 2.6. *The positioning models assuming Markov process of order one*

Transition model

$$\mathbf{x}_t = f^{\theta_{t-1}}(\mathbf{x}_{t-1}, \mathbf{q}_t) \ , \tag{2.56}$$

where $\mathbf{q}_t$ denoting the measurement noise. It is the state propagation from time $t-1$ to t as $p^{\theta_{t-1}}(\mathbf{x}_t|\mathbf{x}_{t-1}, \mathbf{z}_{1:t-1}) \approx p^{\theta_{t-1}}(\mathbf{x}_t|\mathbf{x}_{t-1})$, assuming the state at time t is stochastically dependent on the state at time $t-1$.

Measurement model

$$\mathbf{z}_t = g^{\theta_t}(\mathbf{x}_t, \mathbf{n}_t) \ , \tag{2.57}$$

with $\mathbf{n}_t$ being the measurement noise. It assumes the observation at t is conditionally independent given the state at t as $p^{\theta_t}(\mathbf{z}_t|\mathbf{x}_t, \mathbf{z}_{1:t-1}) \approx p^{\theta_t}(\mathbf{z}_t|\mathbf{x}_t)$.

Hidden Markov model is a widespread assumption for recursive positioning, which is visualized in Fig. 2.1. Then, the sequential position estimation can be proceed into the classic *two-steps filtering*: the iterative prediction and update structure

Prediction Compute the prior $p^{\theta_{t-1}}(\mathbf{x}_t|\mathbf{z}_{1:t-1})$ by the Chapman-Kolmogorov equation knowing $p^{\theta_{t-1}}(\mathbf{x}_{t-1}|\mathbf{z}_{1:t-1})$.

$$p^{\theta_{t-1}}(\mathbf{x}_t|\mathbf{z}_{1:t-1}) \overset{\text{Markov}}{=} \int p^{\theta_{t-1}}(\mathbf{x}_t|\mathbf{x}_{t-1}) p^{\theta_{t-1}}(\mathbf{x}_{t-1}|\mathbf{z}_{1:t-1}) \, d\mathbf{x}_{t-1} \ . \tag{2.58}$$

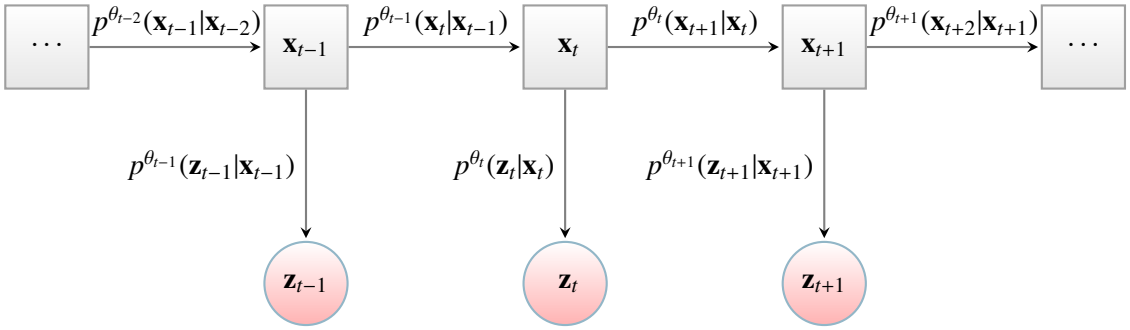

Figure 2.1: Hidden Markov Model (HMM) of the hidden state ($\mathbf{x}$) given the observations ($\mathbf{z}$)
$\mathbf{x}_t$ denotes the unobserved state;
$\mathbf{z}_t$ is the observation;
$P^{\theta_{t-1}}(\mathbf{x}_t|\mathbf{x}_{t-1})$ is the state propagation model of the Markov chain, with $t \geq 1$;
$p^{\theta_t}(\mathbf{z}_t|\mathbf{x}_t)$ is the conditional probability of $\mathbf{z}_t$ given $\mathbf{x}_t$

Update Obtain the posterior $p^{\theta_t}(\mathbf{x}_t|\mathbf{z}_{1:t})$ knowing $p^{\theta_t}(\mathbf{z}_t|\mathbf{x}_t)$ by the Bayes' rule

$$p^{\theta_t}(\mathbf{x}_t|\mathbf{z}_{1:t}) \overset{\text{Markov}}{=} \frac{p^{\theta_t}(\mathbf{z}_t|\mathbf{x}_t)p^{\theta_{t-1}}(\mathbf{x}_t|\mathbf{z}_{1:t-1})}{p^{\theta_t}(\mathbf{z}_t|\mathbf{z}_{1:t-1})} \,. \tag{2.59}$$

This two-steps framework (2.58) and (2.59) are known as a Bayesian filter, which is illustrated in Fig. 2.2: the prediction step guesses the new state given the old observations, with the initial density state as $p(\mathbf{x}_0)$; then, the update step corrects the guess by the new observation. An integrated version of the prediction and update recursion is formulated as

$$\begin{aligned} p^{\theta_t}(\mathbf{x}_t|\mathbf{z}_{1:t}) &= \int p^{\theta_t}(\mathbf{x}_{0:t}|\mathbf{z}_{1:t})\, d\mathbf{x}_{0:t-1} \\ &= \frac{p^{\theta_t}(\mathbf{z}_t|\mathbf{x}_t) \int p^{\theta_{t-1}}(\mathbf{x}_t|\mathbf{x}_{t-1})p^{\theta_{t-1}}(\mathbf{x}_{t-1}|\mathbf{z}_{1:t-1})\, d\mathbf{x}_{t-1}}{\int p^{\theta_t}(\mathbf{z}_t|\mathbf{x}_t)p^{\theta_{t-1}}(\mathbf{x}_t|\mathbf{z}_{1:t-1})d\mathbf{x}_t} \qquad (2.60) \\ &\propto \underbrace{p^{\theta_t}(\mathbf{z}_t|\mathbf{x}_t)}_{\text{Likelihood}} \underbrace{\int \underbrace{p^{\theta_{t-1}}(\mathbf{x}_t|\mathbf{x}_{t-1})}_{\text{State transition density}} \underbrace{p^{\theta_{t-1}}(\mathbf{x}_{t-1}|\mathbf{z}_{1:t-1})}_{\text{Old posterior}}\, d\mathbf{x}_{t-1}}_{Prior} \,. \qquad (2.61) \end{aligned}$$

This recursion of the posterior in (2.60) is a conceptual solution, but it only has analytical solutions in a restrictive set of cases. In the other cases, numerical methods are needed to solve the complete prior and likelihood. The key concern in implementing this probabilistic recursion is the continuous nature of the states $\mathbf{x}$, and the noisy measurements $\mathbf{z}$. The algorithms described in the following

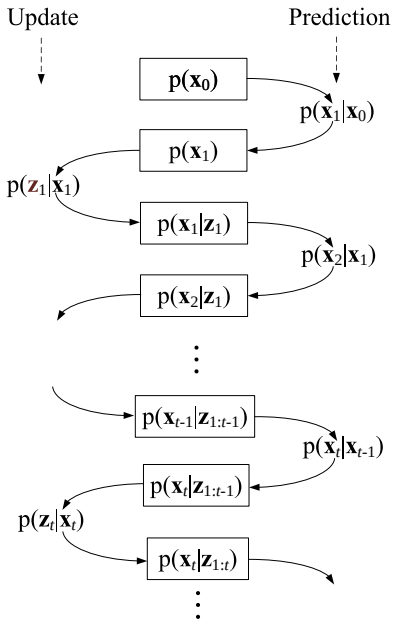

Figure 2.2: Classic two-steps Bayesian filtering with Markov models and constant θ: the iterative prediction-update structure

subsections are based on the two-steps filtering, including the Kalman filter, grid-based filter and particle filter.

2.4.2 Kalman Filter (KF)

The recursion (2.60) can be solved analytically in the case of linear and Gaussian models, as the Kalman filters [88].

Standard Kalman filter

The standard Kalman filter assumes the posterior at any time step is Gaussian variable. It has been proved that if $p^{\theta_{t-1}}(\mathbf{x}_{t-1}|\mathbf{z}_{1:t-1})$ in (2.58) is Gaussian, then $p^{\theta_t}(\mathbf{x}_t|\mathbf{z}_{1:t})$ in (2.59) can be also Gaussian under certain assumptions [75]:

- the model noise $\mathbf{q}$ in (5.3) and $\mathbf{n}$ in (5.4) are Gaussian with known parameters;
- $f(\mathbf{x}_t, \mathbf{n}_t)$ in (5.3) and $g(\mathbf{x}_t, \mathbf{n}_t)$ in (5.4) are known linear functions.

Thus, to obtain $p^{\theta_t}(\mathbf{x}_t|\mathbf{z}_{1:t})$ we only need to characterize its mean and variance. The linear Gaussian state-space can be solved explicitly using the standard Kalman filter, but for the 2D positioning, the state is a nonlinear and non-Gaussian process. Alternative ways are to use the ranging measurements to estimate another variable which is linearly related to the target's position, such as a temporary

position estimation or the target's velocity.

Let **y** denote the observation linear to the state; **x** is the state vector. Then the tracking models of (5.3) and (5.4) are expressed as

State transition model

$$\mathbf{x}_t = F\mathbf{x}_{t-1} + \mathbf{q}_{t-1} \quad \text{with } \mathbf{q}_{t-1} \sim \mathcal{N}^{\theta_{t-1}}(0, Q_{t-1}) \tag{2.62}$$

Measurement model

$$\mathbf{y}_t = H\mathbf{x}_t + \mathbf{n}_t \quad \text{with } \mathbf{n}_t \sim \mathcal{N}^{\theta_t}(0, R_t) \tag{2.63}$$

where

- the matrices $F,\ H$ are the system and measurement matrices respectively;
- $\mathbf{q}$ and $\mathbf{n}$ are the covariance matrix of the process and measurement noise;
- the matrices $F,\ H,\ \mathbf{q},\ \mathbf{n}$ are called the state-space matrices. The state-space model is said to be time-variant when the state-space matrices are time varying;
- the initial condition is

$$\mathbf{x}_0 \sim \mathcal{N}(\mu_0, P_0)\ . \tag{2.64}$$

Since $x_{t|\cdot}$ is a Gaussian random variable, it is sufficient to keep the prediction and update stages of (5.26)-(2.64) by the following computations at each time t:

Prediction

$$\mathbf{x}_{t|t-1} = F\mathbf{x}_{t-1|t-1} \tag{2.65}$$

$$P_{t|t-1} = FP_{t-1|t-1}F^{\mathrm{T}} + Q_{t-1} \tag{2.66}$$

Update

$$K_t = P_{t|t-1}H^{\mathrm{T}}\left(HP_{t|t-1}H^{\mathrm{T}} + R_t\right)^{-1} \tag{2.67}$$

$$\mathbf{x}_{t|t} = \mathbf{x}_{t|t-1} + K_t\left(\mathbf{y}_t - H\mathbf{x}_{t|t-1}\right) \tag{2.68}$$

$$P_{t|t} = P_{t|t-1} - P_{t|t-1}H^{\mathrm{T}}\left(HP_{t|t-1}H^{\mathrm{T}} + R_t\right)^{-1}HP_{t|t-1} \tag{2.69}$$

with the matrix K called Kalman gain matrix, and the following notation:

$$\begin{aligned}
\mathbf{x}_{t|t} &= E\left[\mathbf{x}_t|\mathbf{y}_{0:\,t}\right] \\
P_{t|t} &= E\left[\left(\mathbf{x}_t - \mathbf{x}_{t|t}\right)\left(\mathbf{x}_t - \mathbf{x}_{t|t}\right)^{\mathrm{T}}|\mathbf{y}_{0:\,t}\right] \\
\mathbf{x}_{t|t-1} &= E\left[\mathbf{x}_t|\mathbf{y}_{0:\,t-1}\right] \\
P_{t|t-1} &= E\left[\left(\mathbf{x}_t - \mathbf{x}_{t|t-1}\right)\left(\mathbf{x}_t - \mathbf{x}_{t|t-1}\right)^{\mathrm{T}}|\mathbf{y}_{0:\,t-1}\right]
\end{aligned}$$

The Kalman filter can address the state estimation of linear models. But the function of the ranging measurement to the 2D positioning process is non-linear.

Extended Kalman Filter (EKF)

In the nonlinear conditions, the Extended Kalman filter is often used, which expresses the transition model (5.3) and measurement model (5.4) as

State transition model

$$\mathbf{x}_t = f(\mathbf{x}_{t-1}) + \mathbf{q}_{t-1} \quad \text{with } \mathbf{q}_{t-1} \sim \mathcal{N}^{\theta_{t-1}}(0, Q_{t-1}) \tag{2.70}$$

Measurement model

$$\mathbf{z}_t = h(\mathbf{x}_t) + \mathbf{n}_t \quad \text{with } \mathbf{n}_t \sim \mathcal{N}^{\theta_t}(0, R_t) \tag{2.71}$$

where the non-linear function $h(\cdot)$ in (2.71) relates the target's position to the ranging measurements.

Extended Kalman filter represents the distribution of the state given the observations by a Gaussian approximation

$$p^{\theta_t}(\mathbf{x}_t|\mathbf{z}_{1:t}) \approx \mathcal{N}(\mathbf{x}_{t|t}, P_t)\ . \tag{2.72}$$

Similar to Kalman filter, EKF propagate the state density in two steps

Prediction

$$\mathbf{x}_{t|t-1} = f(\mathbf{x}_{t-1|t-1}) \tag{2.73}$$

$$P_{t|t-1} = F_{\mathbf{x}}(\mathbf{x}_{t-1|t-1})P_{t-1|t-1}F_{\mathbf{x}}(\mathbf{x}_{t-1|t-1})^{\mathrm{T}} + Q_{t-1} \tag{2.74}$$

Update

$$\begin{aligned}
\mathbf{v}_t &= \mathbf{z}_t - h(\mathbf{x}_{t|t-1}) \\
S_t &= H_{\mathbf{x}}(\mathbf{x}_{t|t-1}) P_{t|t-1} H_{\mathbf{x}}(\mathbf{x}_{t|t-1})^{\mathrm{T}} + R_t \\
K_t &= P_{t|t-1} H_{\mathbf{x}}^{\mathrm{T}}(\mathbf{x}_{t|t-1}) S_t^{-1} \qquad (2.75) \\
\mathbf{x}_{t|t} &= \mathbf{x}_{t|t-1} + K_t \mathbf{v}_t \qquad (2.76) \\
P_{t|t} &= P_{t|t-1} - K_t S_t K_t^{\mathrm{T}} , \qquad (2.77)
\end{aligned}$$

where the matrices $F_{\mathbf{x}}(\mathbf{x}_{t-1|t-1})$ and $H_{\mathbf{x}}^{\mathrm{T}}(\mathbf{x}_{t|t-1})$ are the Jacobins of f and h with the elements [85]

$$[F_{\mathbf{x}}(\mathbf{x}_{t-1|t-1})]_{j,j'} = \frac{\partial f_j(\mathbf{x}_{t-1|t-1})}{\partial \mathbf{x}'_j} , |_{\mathbf{x}=\mathbf{x}_{t-1|t-1}} \qquad (2.78)$$

$$[H_{\mathbf{x}}(\mathbf{x}_{t|t})]_{j,j'} = \frac{\partial h_j(\mathbf{x}_{t|t-1})}{\partial \mathbf{x}'_j} |_{\mathbf{x}=\mathbf{x}_{t|t-1}} . \qquad (2.79)$$

The EKF formally requires the measurement model and state model functions to be differentiable. Another KF variation called Unscented Kalman Filter (UKF) makes use of the unscented transformation to deal with the nonlinearity of the system, with more theoretical details in [159].

2.4.3 Grid-based Filter (GF)

Grid-based Bayesian filter (GF), also known as the point-mass filter [20], allows the inference of the full posterior via Bayesian filtering in nonlinear and non-Gaussian conditions.

The GFs have been demonstrated to yield accurate positioning with easy implementations [55]. It performs numerical integration by uniformly discretizing the continuous state-space into a finite number (N_{g}) of evenly spaced grid of points (grid cells or a piecewise function). Let $\mathbf{G}_t$ denote the grid cells at t

$$\mathbf{G}_t = \{\mathbf{x}_t^i\}_{i=1:N_{\mathrm{g}}} . \qquad (2.80)$$

Based on a Markov process of order one, the density of (2.61) is solved by

$$p^{\theta_t}(\mathbf{x}_t|\mathbf{z}_{1:t}) \propto p^{\theta_t}(\mathbf{z}_t|\mathbf{x}_t) \sum_{j=1}^{N_{\mathrm{g}}} p^{\theta_{t-1}}(\mathbf{x}_t|\mathbf{x}_{t-1}^j) p^{\theta_{t-1}}(\mathbf{x}_{t-1}^j|\mathbf{z}_{1:t-1}) . \qquad (2.81)$$

The state posterior ($p^{\theta_t}(\mathbf{x}_t|\mathbf{z}_{1:t})$) is represented by the weighted grid cells [19]

$$p^{\theta_t}(\mathbf{x}_t|\mathbf{z}_{1:t}) \approx \sum_{i=1}^{N_g} w_{t|t}^i \delta(\mathbf{x}_t - \mathbf{x}_t^i), \tag{2.82}$$

where $\delta(\cdot)$ is the Dirac delta measure and $w_{t|t}^i$ for the weight associated with the ith cell center. The prediction and update steps of the GF are defined as [11]

Prediction

$$w_{t|t-1}^i \triangleq \sum_{j=1}^{N_g} p^{\theta_{t-1}}(\mathbf{x}_t^i|\mathbf{x}_{t-1}^j) w_{t-1|t-1}^j,\ i \in \{i\}_{i=1:N_g} \tag{2.83}$$

Update

$$w_{t|t}^i \approx \frac{p^{\theta_t}(\mathbf{z}_t|\mathbf{x}_t^i) w_{t|t-1}^i}{\sum_{j=1}^{N_g} p^{\theta_t}(\mathbf{z}_t|\mathbf{x}_t^j) w_{t|t-1}^j} = \frac{p^{\theta_t}(\mathbf{z}_t|\mathbf{x}_t^i) w_{t|t-1}^i}{\lambda},\ i \in \{i\}_{i=1:N_g}\ , \tag{2.84}$$

where the denominator denoted by λ is for normalization.

In the Bayesian framework, Eq.(2.83) specifies the prior on the state, and the likelihood is updated in (2.84). Similar to (2.40), the MMSE of the GF at each time step can be approximated by

$$\widehat{g(\mathbf{x})}_{\text{MMSE}} \approx \sum_{i=1}^{N_g} g(\mathbf{x}_t^i) w_{t|t}^i\ . \tag{2.85}$$

The GF is very simple and powerful, which can approximate arbitrary density. However, it strongly relies on dense grid cells over the complete state-space. The computational overhead grows exponentially as the grid number increases, thus, the GF is prohibitive in fast positioning.

2.4.4 Particle Filter (PF)

The particle filter (PF), also known as a sequential Monte Carlo (SMC)) approach, bootstrap filter and condensation algorithm [68, 91], is a popular alternative to the Bayesian estimation of dynamic models. The main idea of PF is to generate more particles in the region with a high probability but less in low probable region.

Sequential Importance sampling (SIS)

The sequential importance sampling (SIS) algorithm [12] is the basis of most particle filters, and other improved versions of PFs are based on the SIS proposing better importance sampling. Particle filters discretely approximate the joint posterior by a set of random samples (particles)

$$p^{\theta_t}(\mathbf{x}_{0:t}|\mathbf{z}_{1:t}) \approx \sum_{i=1:N_s} w_t^i \delta(\mathbf{x}_{0:t} - \mathbf{x}_{0:t}^i), \tag{2.86}$$

where w_t^i is the normalized weight associated with the ith particle at t. According to Eq. (2.46), the importance weight of the ith particle is assigned

$$w_t^i \propto \frac{p^{\theta_{0:t}}(\mathbf{x}_{0:t}^i|\mathbf{z}_{1:t})}{q(\mathbf{x}_{0:t}^i|\mathbf{z}_{1:t})} \,. \tag{2.87}$$

The joint posterior given the observations up to t is derived

$$\begin{aligned}
p^{\theta_{0:t}}(\mathbf{x}_{0:t}|\mathbf{z}_{1:t}) &= \frac{p^{\theta_{0:t}}(\mathbf{z}_{1:t}|\mathbf{x}_{0:t})p^{\theta_{0:t}}(\mathbf{x}_{0:t})}{p^{\theta_{1:t}}(\mathbf{z}_{1:t})} \\
&= \frac{p^{\theta_{0:t}}(\mathbf{z}_t|\mathbf{z}_{0:t-1}, \mathbf{x}_{0:t})p^{\theta_{0:t-1}}(\mathbf{z}_{1:t-1}|\mathbf{x}_{0:t})p^{\theta_{0:t}}(\mathbf{x}_{0:t})}{p^{\theta_t}(\mathbf{z}_t|\mathbf{z}_{1:t-1})p^{\theta_{1:t-1}}(\mathbf{z}_{1:t-1})} \\
&= \frac{p^{\theta_{0:t}}(\mathbf{z}_t|\mathbf{z}_{1:t-1}, \mathbf{x}_{0:t})p^{\theta_{0:t-1}}(\mathbf{x}_{0:t}|\mathbf{z}_{1:t-1})p^{\theta_{1:t-1}}(\mathbf{z}_{1:t-1})p^{\theta_{0:t}}(\mathbf{x}_{0:t})}{p^{\theta_t}(\mathbf{z}_t|\mathbf{z}_{1:t-1})p^{\theta_{1:t-1}}(\mathbf{z}_{1:t-1})p^{\theta_{0:t}}(\mathbf{x}_{0:t})} \\
&= \frac{p^{\theta_{1:t}}(\mathbf{z}_t|\mathbf{x}_{0:t})p^{\theta_{0:t-1}}(\mathbf{x}_t|\mathbf{x}_{0:t-1}, \mathbf{z}_{0:t-1})}{p^{\theta_t}(\mathbf{z}_t|\mathbf{z}_{1:t-1})} p^{\theta_{0:t-1}}(\mathbf{x}_{0:t-1}|\mathbf{z}_{1:t-1}) \qquad (2.88) \\
&\propto p^{\theta_{0:t-1}}(\mathbf{z}_t|\mathbf{x}_{0:t})p^{\theta_{0:t-1}}(\mathbf{x}_t|\mathbf{x}_{0:t-1}, \mathbf{z}_{1:t-1})p^{\theta_{0:t-1}}(\mathbf{x}_{0:t-1}|\mathbf{z}_{1:t-1}) \,. \qquad (2.89)
\end{aligned}$$

Applying Markov process of order one, the joint posterior is

$$\begin{aligned}
p^{\theta_{0:t}}(\mathbf{x}_{0:t}|\mathbf{z}_{1:t}) &= \frac{p^{\theta_t}(\mathbf{z}_t|\mathbf{x}_t)p^{\theta_{t-1}}(\mathbf{x}_t|\mathbf{x}_{t-1})}{p^{\theta_{0:t-1}}(\mathbf{z}_t|\mathbf{z}_{1:t-1})} p^{\theta_t}(\mathbf{x}_{0:t-1}|\mathbf{z}_{1:t-1}) \qquad (2.90) \\
&\propto p^{\theta_t}(\mathbf{z}_t|\mathbf{x}_t)p^{\theta_{t-1}}(\mathbf{x}_t|\mathbf{x}_{t-1})p^{\theta_{0:t-1}}(\mathbf{x}_{0:t-1}|\mathbf{z}_{1:t-1}) \,. \qquad (2.91)
\end{aligned}$$

The importance density $q(x_{0:t}|y_{0:t})$ (introduced in Subsection 2.3.4) is defined as

$$q(\mathbf{x}_{0:t}|\mathbf{z}_{1:t}) = q(\mathbf{x}_t|\mathbf{x}_{0:t-1}, \mathbf{z}_{1:t})q(\mathbf{x}_{0:t-1}|\mathbf{z}_{1:t-1}) \,. \tag{2.92}$$

Then, the weight is formulated by substituting (2.92) and (2.90) to (2.87) [11]

$$\begin{aligned}
w_t^i &= \frac{p^{\theta_t}(\mathbf{z}_t|\mathbf{x}_t^i)p^{\theta_t}(\mathbf{x}_t^i|\mathbf{x}_{t-1}^i)p^{\theta_{0:t-1}}(\mathbf{x}_{0:t-1}^i|\mathbf{z}_{1:t-1})}{p^{\theta_t}(\mathbf{z}_t|\mathbf{z}_{1:t-1})q(\mathbf{x}_t^i|\mathbf{x}_{0:t-1}^i, \mathbf{z}_{1:t})q(\mathbf{x}_{0:t-1}^i|\mathbf{z}_{1:t-1})} \\
&= w_{t-1}^i \frac{p^{\theta_t}(\mathbf{z}_t|\mathbf{x}_t^i)p^{\theta_{t-1}}(\mathbf{x}_t^i|\mathbf{x}_{t-1}^i)}{p^{\theta_t}(\mathbf{z}_t|\mathbf{z}_{1:t-1})q(\mathbf{x}_t^i|\mathbf{x}_{0:t-1}^i, \mathbf{z}_{1:t})} \,.
\end{aligned} \tag{2.93}$$

Since the $p^{\theta_t}(\mathbf{z}_t|\mathbf{z}_{1:t-1})$ in (2.93) does not depend on the state, the weight is

$$w_t^i \propto w_{t-1}^i \frac{p^{\theta_t}(\mathbf{z}_t|\mathbf{x}_t^i)p^{\theta_{t-1}}(\mathbf{x}_t^i|\mathbf{x}_{t-1}^i)}{q(\mathbf{x}_t^i|\mathbf{x}_{0:t-1}^i, \mathbf{z}_{1:t})} . \tag{2.94}$$

Note that w_t^i in (2.94) needs to be normalized at each time step. And the filtered density ($p^{\theta_t}(\mathbf{x}_t|\mathbf{z}_{1:t})$) can be approximated by the finite mixture of weighted Dirac masses given measurements ($\mathbf{z}^{1:t}$) up to time t

$$p^{\theta_t}(\mathbf{x}_t|\mathbf{z}_{1:t}) \approx \sum_{i=1:N_\mathrm{p}} w_t^i \delta(\mathbf{x}_t - \mathbf{x}_t^i) . \tag{2.95}$$

The two-step filter framework of SIS filtering is

Prediction The new particles ($\{\mathbf{x}_t^i\}_{i=1:N_\mathrm{p}}$) is generated from $q(\mathbf{x}_t|\mathbf{z}_{0:t-1})$ by propagating the previous sampling density $q(\mathbf{x}_{t-1}|\mathbf{z}_{0:t-1})$.

Update the weights with the new observations as (2.94).

The MMSE of the function $g(\mathbf{x}_t)$ at each time step can be calculated by

$$\widehat{g(\mathbf{x})}_{\mathrm{MMSE}} \approx \sum_{i=1}^{N_\mathrm{p}} g(\mathbf{x}_t^i) w_t^i . \tag{2.96}$$

Equation (2.94) provides the very core of SIS updating the weights of particles from the importance density at each time step. However, the SIS practically appears particle degeneracy after a few iterations, which is often solved by a resampling step to remove the particles with very low weights [52, 100] and replicate the particles with large weights.

Resampling

Particle filters have been criticized of the particle degeneracy problem, hence, a resampling procedure is most often employed. Resampling enables the particles to distribute naturally in areas of high posterior, nevertheless, the problem is the sample impoverishment [27] due to the loss of diversity in the particle population.

1) Resampling schemes

The idea of the resampling is to depress the samples with very small weights and duplicate particles with large weights, i.e., multinomial resampling, residual resampling, residual systematic resampling, stratified resampling and systematic resampling [52].

Systematic resampling is the most favorable both in resampling quality and computational complexity [76], with the details given in **Algorithm** 1. Used on the SIS filter, it leads to the well-known Sampling Importance Resampling (SIR) filter. A trivial implementation for such simulations re-

quires first to draw u_t^1 from a uniform distribution and then compare the CDF to find the resampling particles. Other resampling schemes also appear to be popular.

Algorithm 1 Resampling

Output and input: $\left[\{\mathbf{x}_t^{j*},\ w_t^j\}_{j=1}^{N_\mathrm{p}}\right] = \mathrm{Resampling}\left[\{\mathbf{x}_t^i,\ w_t^i\}_{i=1}^{N_\mathrm{p}}\right]$
Setting: Construct CDF of the sample weights $\{c_i\}_{i=1}^{N_\mathrm{p}}$
Initialization: $u_1 \sim \frac{1}{N_\mathrm{p}} U[0,1]$, $i = 1$

```
FOR j = 1 : N_p
    WHILE u_1 + (1/N_p)(j − 1) > c_i
        i = i + 1
    END WHILE
    Update new samples x_t^{j*} = x_t^i
    Assign weights w_t^j = 1/N_p
END FOR
```

2) Selective resampling

Resampling brings extra random variance to the state estimation and causes a high computation [51,51]. Instead of executing resampling at every time step, a solution is to perform resampling unless it reaches a given threshold [115], known as selective resampling or adaptive resampling [65].

A popular measure of the sample degeneracy is the so-called effective sample size (N_eff) [97]

$$N_\mathrm{eff} = \frac{N_\mathrm{p}}{1 + \mathrm{Cov}[w_t(\mathbf{x}_t)]} = \frac{N_\mathrm{p}}{\mathrm{E}[w_t^2(\mathbf{x}_t)]}\ . \tag{2.97}$$

This quantity is usually numerically approximated by the following estimate

$$\widehat{N_\mathrm{eff}} = \frac{1}{\sum_{i=1}^{N_\mathrm{p}} (w_t^i)^2}. \tag{2.98}$$

It ranges from N_p (reached when all the particles share equal weights of value 1) to 1 (reached when only a single particle is given the whole probability mass as a weight of 1).

The Shannon entropy of the importance weights, ranging from $\log N_\mathrm{p}$ to 0, is sometimes also used to estimate the effective sample size. The measure of one (or more) of these criteria is evaluated at each time-step, with the sampling procedures taking place if and only if the criterion reaches a certain threshold. The most common threshold found in literature is ${N_\mathrm{eff}}^{threshold} = 0.5N_\mathrm{p}$.

2.5 Summary

This chapter reviews the basic probabilistic methods appearing in literature for range-based positioning, which differ in the model requirements, performance and cost. The fundamental stumbling block of applying these Bayesian inference methods to real applications can be either a prohibitive-complexity, inappropriate measurement models or poor adaption ability to reality. e.g., the Kalman filter and its variation methods do not work for the non-Gaussian problems; the Grid-based methods need to predetermine the grid cells; the particle based methods may lead to particle divergence and particle degeneracy problems.

Aiming at practical Bayesian estimations on range-based positioning, sample-based methods are potential. Furthermore, the positioning accuracy can be related to multiple factors, i.e., the measurement model, prior, estimation approximation and anchor deployment, etc. The following chapters will discuss the two most important aspects: the measurement model of indoor TOF ranging and the estimation approximation in the probabilistic perspective.

Chapter 3

Characteristics and Frequentist Modeling of Indoor Ranging Uncertainty

The problem of range-based indoor positioning has long been regarded as the imprecise ranging measurements. Characterizing and modeling the ranging error are crucial for understanding positioning behaviors and optimizing positioning algorithms. The time-of-arrival (TOA) ranging error differs from the commonly used signal-to-distance propagation models. On the other hand, frequentist modeling offers simplicity as needing only incomplete statistical information from a small experimental dataset. However, the existing statistical TOA models have less attention to the ranging characteristics and their effect on positioning performance. In this chapter, we present the statistics of TOA ranging measurements from indoor sensor testbed (with six ranging experiments carried out in classrooms and corridors), and model the ranging errors by distribution fitting. This chapter reports extensive statistics of indoor TOA ranging errors, with the contributions in threefold.

1. Summarize the characteristics of indoor TOA ranging errors and remark that the TOA error follows a biased and right tailed distribution.
2. Perform frequentist modeling of both single-distribution and mixture-distribution models by distribution fitting from real-world indoor experiments.
3. Validate the modeling results by KS test [119], the maximum entropy principle [80] and the performance difference between simulations and real positioning.

The results reveal that the statistical modeling is capable to describe the multipath and the non-line-of-sight (NLOS) errors of indoor-specific TOA ranging; moreover, its simplicity allows computationally efficient positioning.

3.1 TOA Ranging Uncertainty

The ranging techniques typically explore Radio Frequency (RF) properties to measure distance or angle (either narrow band or UWB), which can also be implemented by other kinds of signals such as acoustic, ultrasound, laser and infrared, etc. There are four main ranging techniques: time-of-arrival (TOA), received-signal-strength (RSS), time-difference-of-arrival (TDOA) and angle-of-arrival (AOA). Since our system employs TOA ranging, other ranging techniques will not be discussed.

Wireless environment is a fading channel with intrinsic temporal and frequency variations, thus, the radio ranging error is a common and non-negligible phenomenon. Modeling the ranging uncertainty provides foundations in several aspects of range-based positioning:

- *Components of positioning algorithms*, i.e., likelihood-based estimations and Bayesian methods.
- *Simulation setup*: the better the model imitates the real ranging, the more reasonable the simulation representing for practices.
- *Derivations of valuation criteria*, i.e., Cramér-Rao Lower Bound (CRLB) [156] and geometric dilution of precision (GDOP) [29].
- *System configuration*: a useful model helps to refine system deployments and calibrations.

3.1.1 Related work

Radio ranging of indoor positioning systems always suffer from a number of inherent uncertainties, arising from thermal noise, multi-path effects, NLOS propagations, wireless interference, and system noise [63, 101]. Since positioning performance highly depends on ranging accuracy, it is crucial to characterize and model the ranging error.

Range-based positioning resorts to the statistical models from existing expertise or experimental data, including the parametric models of a single probability density (a single-distribution model) [4, 5,62,161,162], a mixture of multiple probability density (a mixture-distribution model) [6,8,71,157] and empirical models [48, 84, 166]. Mostly, TOA-based positioning assumes the ranging model as a Normal distribution [4, 7, 161, 162]. However, a non-negligible proportion of TOA errors violate the Normal distribution, as indoor scenarios (especially NLOS conditions) lead to a high failure rate of detecting direct path (DP) signal. There are also other probability distributions claimed for indoor TOA models, i.e., the Uniform distribution [4], the negative Exponential distribution [7, 8, 62, 71], the Weibull distribution [138] and the Lognormal distribution [5, 7, 8], etc.

Several theoretical analysis, simulations and experiments have analyzed that radio ranging measurements are pretty noisy in indoor radio channels [8, 43, 71]. TOA ranging not only tolerates the

attenuation of the signal amplitude by the effect of path loss, but also depends on the shape of the received multipath signals according to the limited bandwidth [4, 6, 122]. However, the existing radio models for telecommunication systems [7] cannot be used for the TOA uncertainty, as they mainly focus on the path loss and packet delivery rate but not the time delay for ranging. The ray tracing (RT) method has been used to analyze indoor radio propagations, nevertheless, it requires complete knowledge of wireless channel and is site-specific [73]. Also, the TOA error differs from the commonly used signal-to-distance propagation models [43, 163]. Modeling based on the relationship between multipath signal and bandwidth [6, 43] is impracticable for ability-limited sensor networks in large scale environments. We consider that no model can fully represent indoor ranging errors, whereas some are adequate for certain applications. For meter-level indoor network positioning, we prefer an efficient statistical model over a complicated analytical model.

3.1.2 Error sources of TOA ranging

The major sources of ranging noises are listed in Table 3.1. Radio interference affects on whether a packet can be successfully received rather than the delay of the signal; thus, it is ignored for the TOA ranging error. Propagation error depends on the ability of detecting the direct path (DP) signal. System error is caused by processing delay, inaccuracy of the time-estimating algorithm, clock drift and jitter, and device diversity, etc. Thermal noise is random errors, varying with temperature and humidity, etc.

Table 3.1: Main error sources of indoor TOA ranging noise

Error source	Model
Radio interference	ignored
Propagation error	non-normal noise with large variance
Calibrated system error	normal noise with unknown mean and variance
Thermal noise	normal noise with zero mean and small variance

System errors and thermal noises are caused by a variety of unknown factors; according to the central limit theorem, they can be approximated as a Gaussian error with the magnitude relatively steady in a given scenario. Then, the entire ranging error (ε_r) is expressed as

$$\varepsilon_r = r - \bar{r} = n_r + \varepsilon_{\text{propagation}}(r), \tag{3.1}$$

where the propagation error ($\varepsilon_{\text{propagation}}(r)$) is the dominant component in ε_r.

3.1.3 Analytical form of TOA ranging error

The multipath signal at the receiver of indoor limited space is usually formulated as [8]

$$h(\tau) = \sum_{k=1}^{K} \beta_k \exp(j\phi_k)\delta(\tau - \tau_k), \tag{3.2}$$

where K denotes the number of multipath signals; β_k, ϕ_k, and τ_k are the amplitude, phase and propagation delay of the kth signal, respectively. The actual ranging is the propagation time of the DP signal (τ_1). Then, the ranging error depends on which path in (3.2) is chosen to be estimated as the DP, with the chosen path denoted by $\widehat{\text{DP}}$.

There are three main methods to estimate the DP signal [8, 44]: 1) the time of the first peak (FP) of the channel profile above a detection threshold; 2) the first trigger time (FT) over a threshold; 3) the time of the strongest path (SP) above a threshold. The module of our test-bed uses the FP method, thus, the measured range is r_{FP}. Then, the ranging error ε_r is expressed as

$$\varepsilon_{\text{propagation}}(r) = \varepsilon_{\text{DP}}^{\text{FP}}(r) = r_{\text{FP}} - r_{\text{DP}} \, . \tag{3.3}$$

Based on the time-distance relationship and wave propagation speed, the range is proportional to the signal travel time. Thus, modeling ranging error becomes to model the delay between DP and FP, which converts (3.1) to

$$\varepsilon_r \propto \varepsilon(\tau) = n_\tau + \varepsilon_{\text{DP}}^{\text{FP}}(\tau) \, , \tag{3.4}$$

where the propagation delay is

$$\varepsilon_{\text{DP}}^{\text{FP}}(\tau) = \hat{\tau}_1 - \tau_1 = \tau_{\text{FP}} - \tau_{\text{DP}} \, , \tag{3.5}$$

with $\hat{\tau}_1$ denoting the estimated propagation time of DP. The delay $\varepsilon_{\text{DP}}^{\text{FP}}(\tau)$ depends on the quality of $\hat{\tau}_1$, which is affected by the mean square delay spread, the capability of detecting FP (according to path loss and detection threshold), and etc.

The IEEE indoor channel model summarizes a clustering phenomenon [123]: signals arrive at the receiver in groups. The clustered model is similar to the SV (Saleh-Valenzuela) multipath model [28, 122],

$$h_{cluster}(\tau) = \sum_{c=1}^{L} \sum_{k=1}^{K_c} P_{k,c}\delta(\tau - T_c - \tau_{k,c}) \, , \tag{3.6}$$

where L denotes the number of all observed signal clusters; K_c is the number of signals in the cth

cluster; $P_{k,c}$ is the power of the kth signal in the cth cluster; T_c is the arrival time of the peak of the cth cluster; $\tau_{k,c}$ represents the delay of the kth signal in the cth cluster.

The first cluster (FC) is the cluster containing the main power of the DP signal; T_1 is the delay of FC, which is very close to the DP delay (τ_1). If the cth cluster is detected as FC, Eq. (3.4) is rewritten as

$$\begin{aligned}\varepsilon(\tau) &= n_\tau + \varepsilon_{\tau_{1,c}}^{\tau_{k,c}}(\tau) + \varepsilon_{\mathrm{FC}}^{T_c}(T) \\ &= n_T + \varepsilon_{\mathrm{FC}}^{T_c}(T)\,,\end{aligned} \tag{3.7}$$

where $\varepsilon_{\tau_{1,c}}^{\tau_{k,c}}(\tau)$ denotes the delay of taking the kth signal as the first signal in the cth cluster; $\varepsilon_{\mathrm{FC}}^{T_c}(T)$ is the delay between the cth cluster and the FC; n_T measures the sum of n_τ and $\varepsilon_{\tau_{1,c}}^{\tau_{k,c}}(\tau)$. Compared with the delay of losing FC, $\varepsilon_{\tau_{1,c}}^{\tau_{k,c}}(\tau)$ is relatively small. Therefore, n_T is deemed as a Gaussian variable

$$n_T \sim \mathcal{N}(n_T; 0, \sigma_T). \tag{3.8}$$

The cluster arrival model is commonly defined as a Poisson arrival process model [122]. The interval between two neighbored clusters is expressed as

$$\Delta T_c = T_c - T_{c-1}\,, \quad c = 2, 3, \cdots, C, \tag{3.9}$$

with $\Delta T_1 = T_1 - \tau_{\mathrm{DP}}$ being the delay of FC. Thus, the waiting time ΔT_c between a pair of neighborhood clusters is an exponential variable $\Delta T_c \sim \mathrm{EXP}(\Delta T_c; \mu_c)$ with the density function

$$\mathrm{EXP}(\Delta T_c; \mu_c) = \frac{1}{\mu_c} \exp\left(-\tfrac{\Delta T_c}{\mu_c}\right), \quad c = 1, 2, \cdots, C. \tag{3.10}$$

Then $\varepsilon_{\mathrm{FC}}^{T_c}(T)$ is written in the form of ΔT_c:

$$\begin{aligned}\varepsilon_{\mathrm{FC}}^{T_c}(T) &= T_C - T_1 \\ &\approx \sum_{c=2}^{C} (T_c - T_{c-1}) = \sum_{c=2}^{C} \Delta T_c\,.\end{aligned} \tag{3.11}$$

The multipath signals compose several clusters and each cluster peaks depending on the main signals in that cluster. The clustering phenomenon is stochastic due to the complex indoor environment, thus, all ΔT_c can be considered independent. The difference among the clusters is the power

decaying by the path loss of all member signals, which has a small effect on the peaking time. Thus, ΔT_c can be deemed as identically distributed. Since ΔT_c is an i.i.d exponential variable, $\varepsilon_{\mathrm{FC}}^{T_c}(T)$ follows a Gamma distribution $\varepsilon_{\mathrm{FC}}^{T_c}(T) \sim \Gamma(\varepsilon_{\mathrm{FC}}^{T_c}(T); C, \theta_{T_1})$:

$$\Gamma(\varepsilon_{\mathrm{FC}}^{T_c}(T); C, \theta_{T_1}) = \frac{1}{\theta_{T_1}^{C}\,\Gamma(C)}(\varepsilon_{\mathrm{FC}}^{T_c}(T))^{C-1}\exp\left(-\frac{\varepsilon_{\mathrm{FC}}^{T_c}(T)}{\theta_{T_1}}\right), \tag{3.12}$$

where $\Gamma(C)$ is the gamma function with C, and θ_{T_1} for the shape and scale parameters, respectively.

Since n_T and $\varepsilon_{\mathrm{FC}}^{T_c}(T)$ are independent, $\varepsilon(\tau)$ in (3.7) obeys the convolution of the normal PDF and Gamma PDF

$$\varepsilon(\tau) \sim \mathcal{N}(n_T; 0, \sigma_T) * \Gamma(\varepsilon_{\mathrm{FC}}^{T_c}(T); C, \theta_{T_1}). \tag{3.13}$$

The model of (3.13) is an analytical form of the TOA error, nevertheless, it still requires a comprehensive knowledge of the channel for the multi-parameter configuration and the clustering phenomenon related to channel frequency and bandwidth. Consequently, we resort to statistical modeling for the TOA ranging error.

3.2 Testbed Description and Experiment Setup

Six TOA ranging experiments are carried out, considering two typical indoor scenarios: a classroom and a corridor in our Computer Science building during daytime. The experiment platform uses nanoPAN 5375 RF module and Microcontroller LPC 2387 [1, 2], with the reported ranging accuracy of 2 meters indoors (see more details in [146, 177]). Four stationary experiments (with the target node placed at fixed test-sites) and two mobile experiments (with the target node carried by a mobile robot) are described as follows.

- *F1*: the stationary experiment in the classroom, ranging between one target and one anchor at 25 fixed test sites
- *F2*: the stationary experiment in the classroom, ranging from one target to 5 anchors at 25 fixed test sites
- *F3*: the stationary experiment in the corridor, ranging between one target and one anchor at 28 fixed test sites
- *F4*: the stationary experiment in the corridor, ranging from one target to 10 anchors at 28 fixed test sites
- *M1*: the mobile experiment in the corridor, ranging from one target to 17 anchors along 100 meters trajectory

- *M2*: the mobile experiment in the corridor, ranging from one target to 17 anchors along 80 meters trajectory

Figure 3.1 depicts the indoor scenario and experiment device; Figure 3.2 shows the setup of each experiment, with the area size, anchor deployment and test sites or mobile trajectories.

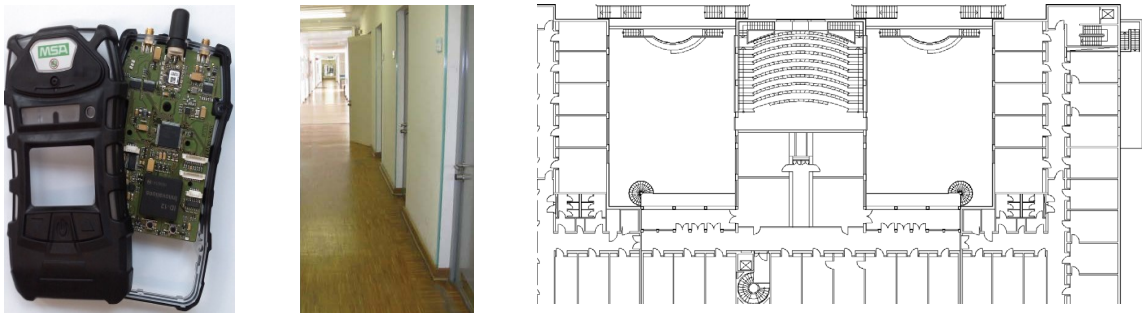

(a) Test-bed device (b) Indoor scenario (c) Floor plan of the experiment area (40×70 meter^2)

Figure 3.1: Experiment device and indoor scenarios

3.3 Characteristics of Indoor Ranging Uncertainty

The TOA error is a stochastic process, whereas it exhibits certain characteristics related to the measuring time and space, the geometric relation between the target and anchors, the ground truth of the range, etc. To characterize the indoor TOA error, the basic statistics of real experiments are explored.

3.3.1 Typical statistics

The typical statistics of the ranging error are analyzed in Table 3.2. The ranging error is denoted by ε_r; μ_{ε_r}, σ_{ε_r}, $\text{Min}_{\varepsilon_r}$ and $\text{Max}_{\varepsilon_r}$ are the mean, standard deviation, minimum and maximum of the ranging error, respectively; Avg_r is the average range; N_{smp} is the sample size of each experiment.

The multipath effect of indoor environments causes a remarkable positive bias [13, 39, 164] to time-based ranging. Specifically, the ranging error in the NLOS condition is severely larger than the one in a line-of-sight (LOS) condition. Hence, the skewness (S) is also evaluated. If S gets a positive value, the distribution observes a tail on the right side; otherwise, it presents a left-side tail.

$$S_{\varepsilon_r} = \frac{\text{E}((\varepsilon_r - \mu_{\varepsilon_r})^3)}{\sigma^3_{\varepsilon_r}} . \tag{3.14}$$

Table 3.2 summaries as follows.

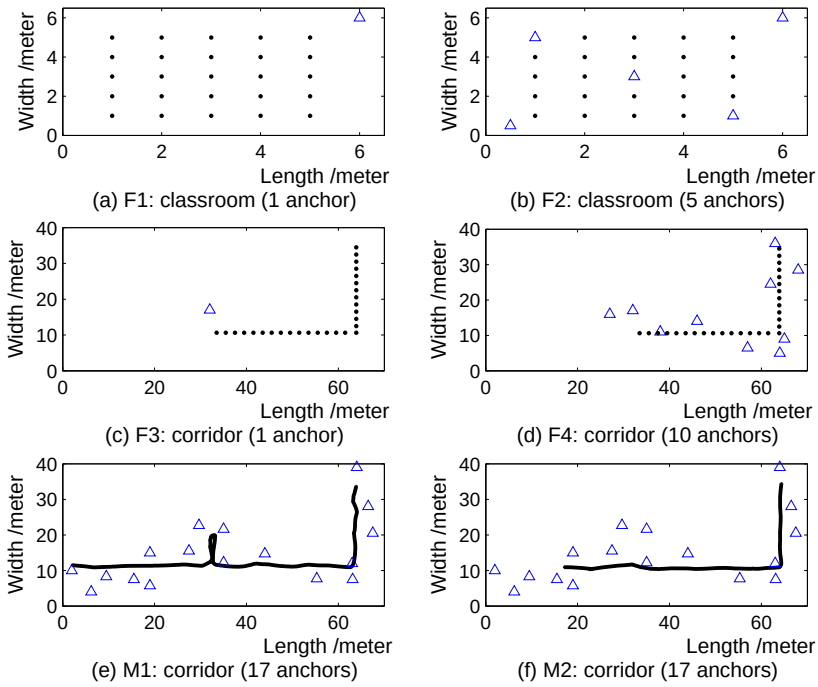

Figure 3.2: Experiment setup: the experiment area (the length and the width of each sub-figure), and the anchor deployment (denoted by △). (a)-(d) describe the stationary experiments with the target fixed at each test site (•). (e)-(f) are the mobile experiments carrying the target by a mobile robot, with the true trajectory depicted by the solid line.

Table 3.2: Typical values of the ranging error (ε_r) in real-world experiments (/meter)

Experiment	μ_{ε_r}	σ_{ε_r}	$\text{Min}_{\varepsilon_r}$	$\text{Max}_{\varepsilon_r}$	Avg_r	S_{ε_r}	N_{smp}
F1	3.04	2.56	-1.56	10.83	7.52	0.60	49495
F2	2.58	2.97	-1.80	14.08	5.99	0.84	234923
F3	2.27	2.76	-1.97	17.12	16.10	1.22	1803
F4	2.47	7.26*	-2.57	116.97*	15.97	9.85*	154270
M1	2.42	3.57	-3.31	74.18	18.16	3.37	22901
M2	2.20	3.71	-3.70	63.39	18.18	5.11	17277

1. The indoor TOA ranging obtain severe uncertainty, as the large values of μ_{ε_r} and σ_{ε_r}.
2. All the experiments get a positive skewness S_{ε_r}, confirming a right tail of the error distribution. Consequently, a skew model is more reasonable.
3. All the experiments obtain a positive bias as the positive μ_{ε_r}, which is introduced by the multipath and NLOS effect.
4. The experiment F4 obtains a much larger value of σ_{ε_r}, $\text{Max}_{\varepsilon_r}$ and S_{ε_r} marked by $*$ of F4 in Table 3.2. The reason is that: 1) the experiment is carried out by a human, whose motion and the way of holding the device cause a larger variance than a robot; 2) the human body has a great influence on the signal strength and propagation time of RF signals, which is confirmed as the body shadowing effect [54, 130].
5. There are a few negative ranging errors due to thermal noise, clock jitter and system calibrations.
6. It seems that the device diversity enlarges the ranging uncertainties, e.g., the experiments with one anchor obtain smaller σ_{ε_r} than the ones with multiple anchors.

Overall, Table 3.2 gives an impression that the ranging error of the same scenario observes similar statistics. Therefore, the ranging error of a given scenario can be interpreted by a statistical model. Additionally, the model should be able to represent the positive bias, right-tail, and a few negative values of the ranging error.

3.3.2 Non-Gaussianity

The TOA error is commonly assumed as a Gaussian error, untruly, extensive evidences have interpreted a strong non-Gaussian and non-linearities of the ranging errors. Figure 3.3 depicts the Normal Probability Plot: from 0 to 5 meters on x-axis, the sample distribution is close to the Normal fitting line (the dashed line), revealing that most ranging observes Gaussian errors; the samples in the upper-right side extremely deviates from the fitting line, which is often referred to the NLOS error. Thus, it confirms that the indoor TOA error violates the Gaussian model.

3.3.3 Ranging variation with time and space

The ranging variation over time and space are plotted in Fig. 3.4 and Fig. 3.5.

The scatter plot in Fig. 3.4 illustrates the wide variation of the indoor TOA error. The mixture Gaussian fitting demonstrates that the ranging error severely varies with time, even from one anchor and the same test-site at close time. This is because that the channel is influenced by time-varying noise, such as a short-term or a long-term interference.

Figure 3.5 interprets the high variation of TOA ranging over space, by reason that the reflections, refractions, diffractions and scattering vary with the indoor environment. Additionally, the ranging

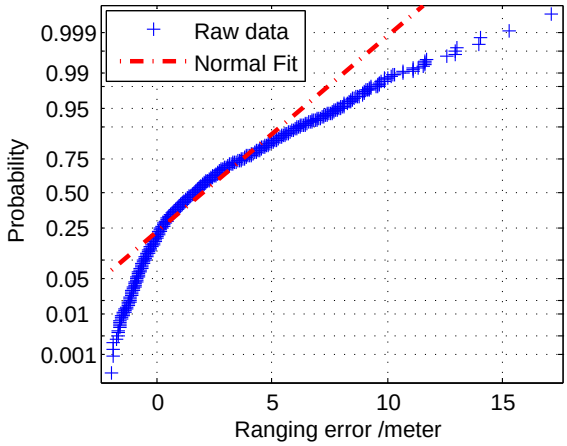

Figure 3.3: Normal Probability Plots of the TOA ranging error of F3. The dashed line represents the Normal fitting, and the marker '+' denotes one sample of the ranging error. Deviations of samples from the fitting line represent the difference of the ranging error to the Normal distribution.

error is related to the antenna irregularity in different directions, which is verified by the field studies on Berkeley mote platform [59].

3.3.4 Ranging error versus distance

Generally, RSS decreases proportionally with the distance. Unfortunately, the relationship of TOA errors versus the true range is hard to know. Figure 3.6 presents two points: 1) with the increase of the true distance between the anchors and the target, the number of successfully obtained ranging measurement decreases; most of the obtained ranging measurements are within the distance of 30 meters; 2) the linear fitting implies the ranging error is not proportional to the true distance; as one can see, except the few outliers, the ranging error with a larger distance is not necessarily larger than the one with a small distance.

Table 3.3: Correlation ($\rho_{\varepsilon_r,\bar{r}}$) between the ranging error and the ground truth distance

Experiments	F1	F2	F3	F4	M1	M2
$\rho_{\varepsilon_r,\bar{r}}$	0.32	0.46	0.20	0.18	0.13	0.22

Table 3.3 lists the correlation between the ranging error and the true distance in the six experiments: F1 and F2 obtain a little bit higher correlation, while there is no significant relevance in the other experiments. The reason is that the true ranges are very short in F1 and F2 (the classroom

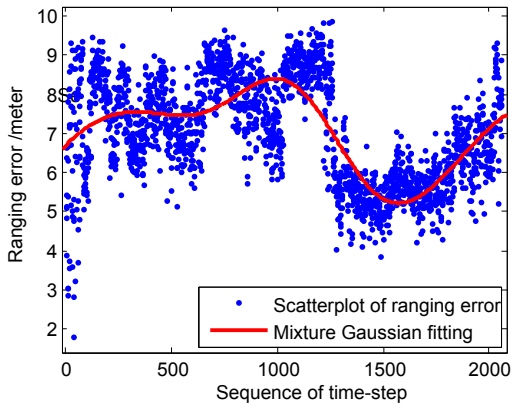

Figure 3.4: TOA ranging error varying over time at one test-site, with the measurements between one anchor and the target fixed at one test-site in F1

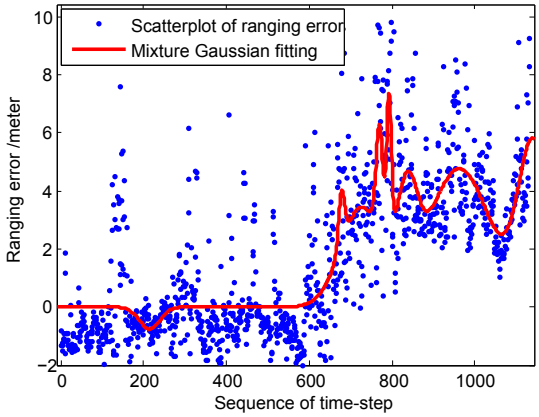

Figure 3.5: TOA ranging error varying with space, with the ranging between one anchor and the mobile target from M1

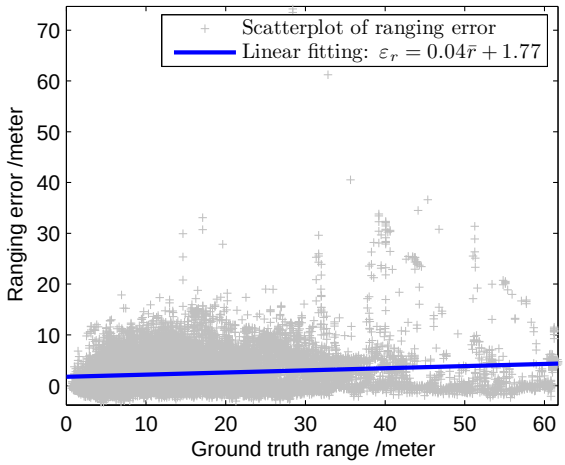

Figure 3.6: TOA ranging error (ε_r) versus the true distance ($\bar{r}$), with the ranging of multiple anchors and the moving target from M1.

scenario); thus, the very large measurements are more likely to have a large error. It can be concluded that if the anchors are spread widely, the correlation between the TOA error and the true distance is very low, which differs from the assumption that the ranging error is proportional to the distance [7, 8].

3.3.5 Ranging variation of device diversity

Device diversity is a common problem in such low-cost sensor systems, which can lead to inconsistent ranging measurements. Figure 3.7 depicts the boxplot of the ranging error from eight anchors, with the anchors placed at the same position.

Through Fig. 3.7, the dispersion of the ranging errors from eight anchors is not the same. The ranging from some devices observes larger median errors than the others. In this case, an online/offline calibration is feasible, e.g., the work [131, 132] explores the device diversity to enhance positioning, which corrects the device diversity via a dissimilarity function like Kullback-Leibler divergence.

3.3.6 Positive and negative ranging errors

Real TOA ranging observes an asymmetric distribution of the negative and positive errors. In our indoor TOA experiments, about 80%-90% measurements observe positive errors, similar to the studies [8, 164]. The scatter plot of Fig. 3.8 demonstrates this negative and positive ranging errors.

From Fig. 3.8, most of the ranging errors are positive, whereas the negative errors are around

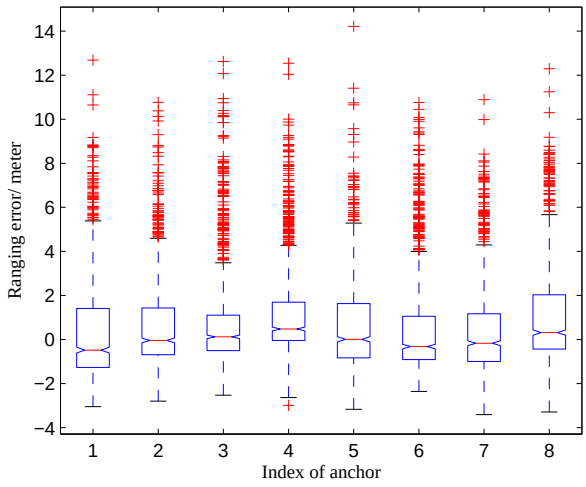

Figure 3.7: TOA ranging error of device diversity, with the ranging between one mobile target and eight anchors (placed at the same site).

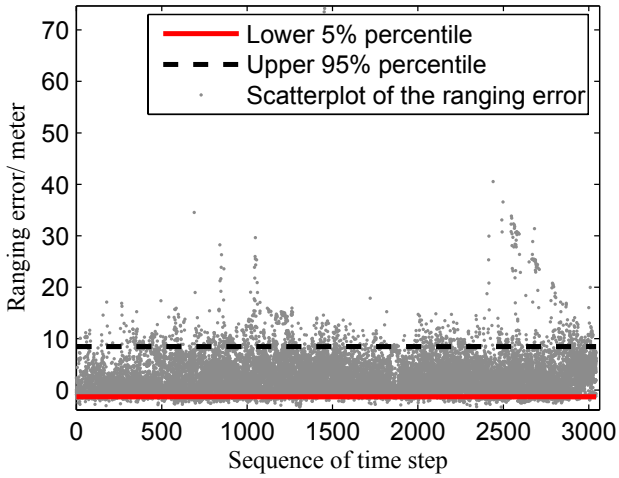

Figure 3.8: Lower bound (the 5% percentile) and upper bound (the 95% percentile) of the TOA ranging errors, with the ranging between mobile target and multiple anchors in M1

10% of all the samples. The positive error is mainly introduced by multipath effect and NLOS propagations, whereas the negative error can be caused by calibration, system errors and thermal noise. Hence, the ranging model needs to represent both the positive and negative errors.

3.3.7 NLOS errors

Indoor TOA ranging inherently has a high occurrence of NLOS errors. Figure 3.9 illustrates the NLOS errors can be present at any test-site, indicating that the NLOS error is not strongly spatially correlated. Additionally, the minimum error at each test-site is always small, implying that accurate positioning is possible by these ranging with small errors.

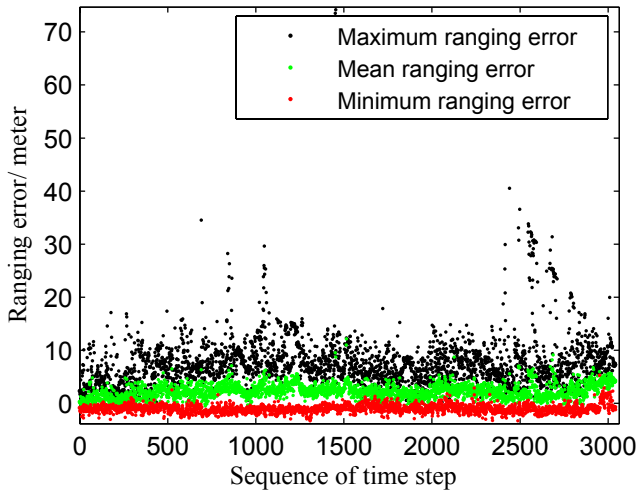

Figure 3.9: Maximum, mean and minimum of the ranging error, with the ranging between one mobile target and multiple anchors in M1

Figure 3.10 describes that the variance of the ranging error is large around the 820th sequence, but small around the 860th sequence. It demonstrates that the variance of the ranging errors varies significantly, even at the neighborhood time and space. Consequently, the variance weighted algorithms [69] cannot indicate the quality of the TOA ranging.

3.4 Frequentist Modeling

The above statistics present that the TOA ranging is highly affected by multiple factors. Unfortunately, it is difficult to know the contribution of each factor on the timing-based ranging error. On the other hand, it is feasible to use a frequentist modeling by distribution fitting on a small sample

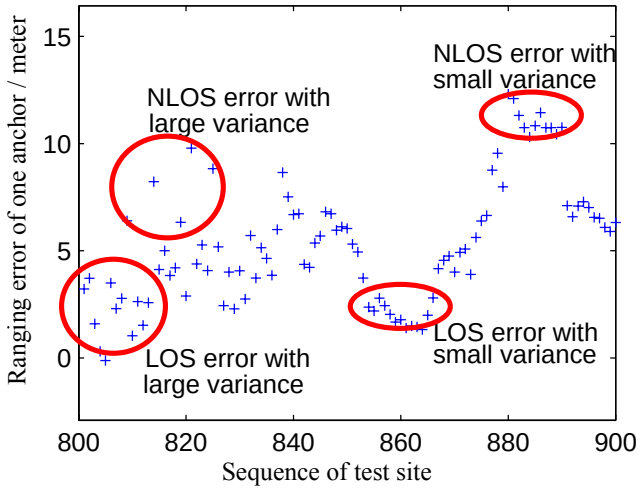

Figure 3.10: Moving variance of the ranging error, with the ranging between one mobile target and one anchor in M1

set of experimental data.

3.4.1 Statistical models

Most current work of indoor positioning refers the ranging error to a rich class of statistical models through existing expertise or an experimental data set. These models are often simplified into two categories: a single-distribution model and a mixture-distribution model.

Single-distribution models

To simplify the TOA error model, it is commonly assumed as a single probability distribution, such as

- *Gaussian* $\mathcal{N}$: the Normal distribution
- *Lognormal*: the Lognormal distribution
- *Exponential EXP*: the negative Exponential distribution
- *Rayleigh*: the Rayleigh distribution
- *Gamma*: the Gamma distribution

Most research assume the TOA error as a Gaussian distribution. As a matter of fact, the Gaussian model is insufficient to represent the positively skewed distribution [81]. Some studies explore the possibilities of skewed models, i.e., the Negative Exponential distribution, Lognormal distribution, Weibull and Gamma distribution, which have not been intensively compared with experimental data.

Mixture-distribution models

Besides the single-distribution models, the models combining multiple probability distributions (a mixture model) are also proposed.

The ranging error is separated into the LOS error ($\varepsilon_{\mathrm{LOS}}$) and the NLOS error ($\varepsilon_{\mathrm{NLOS}}$). The NLOS part is controlled by a random variable ξ, such as a Bernoulli variable taking the value of one when an NLOS condition is present and zero otherwise:

$$\varepsilon_r = \varepsilon_{\mathrm{LOS}}(r) + \xi\varepsilon_{\mathrm{NLOS}}(r) \, . \tag{3.15}$$

The $\varepsilon_{\mathrm{LOS}}(r)$ and $\varepsilon_{\mathrm{NLOS}}(r)$ can be modeled in different ways [49, 71, 157], e.g., a weighting method of the LOS and NLOS components

$$\varepsilon_r = W_{\mathcal{N}}\mathcal{N}_{\mathrm{LOS}}(r) + W_{\mathrm{EXP}}\mathrm{EXP}_{\mathrm{NLOS}}(r) \, . \tag{3.16}$$

With an appropriate setting of $W_{\mathcal{N}}$ and W_{EXP}, this model can fit the real ranging error well.

Differing from the models of (3.15) and (3.16) generating the NLOS component through a random variable or constant weights, Alavi in [6] uses a function ($\xi_W(r)$) as

$$\varepsilon_r = \log(1 + r)\mathcal{N}_{\mathrm{LOS}} + \xi_W(r)\mathcal{N}_{\mathrm{NLOS}}, \tag{3.17}$$

where $\xi_W(r)$ depends on the distance. However, it is difficult to form $\xi_W(r)$ if without enough knowledge of the multipath propagation and the limited bandwidth effect [160]. Therefore, the mixture models are less applicable than the single-distribution models due to the problems of the multi-parameter configuration and requiring a complete knowledge of the channel.

3.4.2 Distribution fitting

The aforementioned single-distribution models are fitted to the experimental data by the parameter estimation tool of Matlab. We add two probability distributions because of their abilities to appear a skew and a right-tailed distribution, which have not been considered by the current studies of TOA modeling: the Gamma distribution and the Rayleigh distribution. Note that these probability distributions, which only provide positive values, need a translation based on the $\mathrm{Min}_{\varepsilon_r}$ in Table 3.2, i.e., the Exponential distribution, Gamma distribution, Lognormal distribution and etc. Additionally, two mixture models are also compared: $\mathcal{N}_{\mathrm{LOS}} + \xi\mathrm{EXP}_{\mathrm{NLOS}}$ [6] and $\mathcal{N}_{\mathrm{LOS}} + \xi\mathcal{N}_{\mathrm{NLOS}}$ [157] of (3.15) with ξ being a Bernoulli random variable.

Table 3.4 gives the distribution fitting results, with the meaning of the parameters explained in

Table 3.4: Distribution fitting results of the ranging error in the real-world experiments

Scenario	Gaussian		Exponential	Lognormal		Gamma		Rayleigh	$\mathcal{N}+\xi$EXP		$\mathcal{N}+\xi\mathcal{N}$	
	$\mu_{\mathcal{N}}$	$\sigma_{\mathcal{N}}$	μ_{EXP}	μ_{LOGN}	σ_{LOGN}	α_Γ	θ_Γ	*phat*	$(\mu_{\mathcal{N}},\sigma_{\mathcal{N}})$	μ_{EXP}	(μ,σ)	$(\mu_{\mathcal{N}},\sigma_{\mathcal{N}})$
F1	3.04	2.56	4.61	1.31	0.74	2.51	1.83	3.73	(0,0.83)	6.09	(0,0.83)	(6.09,2.87)
F2	2.58	2.97	4.38	1.20	0.79	2.00	2.18	3.74	(0,0.73)	5.16	(0,0.73)	(5.16,4.26)
F3	2.75	2.61	5.42	1.57	0.50	4.44	1.22	4.25	(0,0.74)	5.50	(0,0.74)	(5.50,3.35)
F4 raw data	2.47	7.26	13.37	2.53	0.27	9.45	1.41	10.76	(0,0.98)	4.94	(0,0.98)	(4.94,12.21)
F4 discard outliers	2.05	3.55	12.95	2.53	0.23	16.67	0.77	9.50	(0,0.94)	4.94	(0,0.94)	(4.94,5.40)
M1	2.42	3.57	5.73	1.58	0.56	3.30	1.73	4.78	(0,0.96)	4.85	(0,0.96)	(4.85,5.44)
M2	2.20	3.71	5.90	1.63	0.51	3.82	1.54	4.93	(0,1.09)	4.40	(0,1.09)	(4.40,5.74)

Matlab Statistics Toolbox. As one can see, the fitting results of the six experiments obtain similar results, except F4 with the raw data. By removing outliers in F4, the result of F4 is similar to that of the others. It implies that, without severe outliers, the statistical model has a good generality in the similar scenarios.

Fig. 3.11 plots the normalized histogram regarding the ranging error from M1. The histogram depicts a positive biased and heavily right-tail distribution. The positive bias is because of the delay spread of multipath signals of indoor scenarios. The right-hand tail is mostly due to the NLOS propagations, which cannot be handled by a Gaussian model. Then, it also plots the statistical models by distribution fitting. For the single-distribution models, the two best results from distribution fitting are drawn: the Lognormal distribution and the Gamma distribution. It is found that the Lognormal distribution, the Gamma distribution and $\mathcal{N} + \xi\mathcal{N}$ tend to fit to the histogram well.

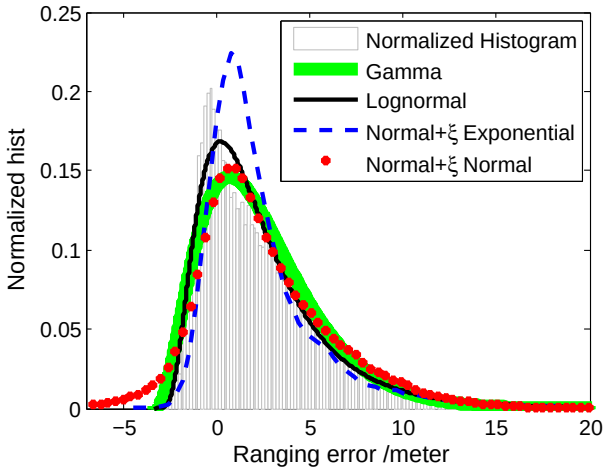

Figure 3.11: Normalized histogram and distribution fitting models on the real TOA error, with data from the experiment M1 (17 anchors).

Overall, the observations from the statistical models give us an expression that a skewed model has the ability to imitate the ranging features (the biased and tailed appearance).

3.5 Model Validation

The distribution fitting results do not reveal insights about the model quality, thus, further verifications are investigated.

3.5.1 Kolmogorov-Smirnov (KS) test

How well each statistical model matches the real ranging is evaluated by Kolmogorov-Smirnov (KS) goodness-of-fit hypothesis test. Let $CDF(\varepsilon)$ be Cumulative Distribution Function (CDF) of the experimental ranging error and $\widehat{CDF}(\varepsilon)$ for the hypothesized model. Then, the KS statistic is the distance between the real CDF and the modeled CDF:

$$KS(\varepsilon) = |\widehat{CDF}(\varepsilon) - CDF(\varepsilon)|. \tag{3.18}$$

The smaller $KS(\varepsilon)$, the better the model is. If the experimental samples exactly follow the hypothesized model, then $\sum_{\varepsilon=0}^{\infty} KS(\varepsilon)$ converges to zero. Table 3.5 gives the average KS statistic $\text{Avg}_{\text{KS}} = \text{mean}(KS(\varepsilon))$ and the maximum $\max_{\text{KS}} = \max(KS(\varepsilon))$ of the models in Table 3.4.

The top two goodness-of-fit of Avg_{KS} in each experiment is marked by '*'. The KS statistics of six experiments almost agree that the Lognormal distribution and the Gamma distribution (with a translation of the $\text{Min}_{\varepsilon_r}$ in Table 3.2) fit well the measurements. The Exponential distribution is the worst, and the Gaussian distribution also obtains a low goodness-of-fit. In addition, the KS statistics of F4 differ much by removing the outliers. Thus, a preprocessing is necessary for mitigating the influence of the outliers but needs careful consideration.

3.5.2 Maximum entropy principle

The maximum entropy principle has been exploited to model wireless propagations [45] but not for the TOA ranging. The maximum entropy principle chooses the distribution ($p \subseteq \mathbf{P}$) that maximizes the entropy (H) given a set of constraints [79]

$$\mathbf{P}_{\max(H)} = \arg\max_{p \subseteq \mathbf{P}} H \ . \tag{3.19}$$

The distribution with the maximum entropy ($\mathbf{P}_{max(H)}$) is derived by Lagrange multipliers as (3.20)-(3.27), which is a constrained optimization of the objective function

$$H = -\int_{-\infty}^{\infty} p(\varepsilon_r) \ln(p(\varepsilon_r))\, d\varepsilon_r \ , \tag{3.20}$$

on the basis of the fact that the integral of a PDF is one

$$\int_{-\infty}^{\infty} p(\varepsilon_r)\, d\varepsilon_r = 1 \ . \tag{3.21}$$

Table 3.5: Maximum ($\max_{KS}$) and average (Avg_{KS}) of KS test statistic (%) between the real CDF and the modeled CDF of the TOA ranging error

Scenario		Gaussian		Exponential		Lognormal		Gamma		Rayleigh		$\mathcal{N}+\xi$EXP		$\mathcal{N}+\xi\mathcal{N}$	
		$\max_{KS}$	Avg_{KS}	$\max_{KS}$	Avg_{KS}	$\max_{KS}$	Avg_{KS}	$\max_{KS}$	Avg_{KS}	$\max_{KS}$	Avg_{KS}	$\max_{KS}$	Avg_{KS}	$\max_{KS}$	Avg_{KS}
F1		10.31	4.12	26.15	8.70	16.12	5.43	11.45	3.16*	7.74	2.91*	20.60	8.71	8.35	3.21
F2		9.02	3.49	12.90	5.69	8.59	3.81	5.54	2.07*	16.13	4.94	11.73	6.52	9.23	2.94*
F3		8.94	3.57	27.66	11.78	3.89	1.55	3.12	0.85*	6.69	2.54	13.09	5.90	2.92	1.16*
F4	raw data	25.65	13.86	47.27	16.55	10.13	5.48*	13.94	7.98	27.92	12.57	19.76	7.75*	19.24	8.62
	discard outliers	12.34	6.87	48.84	16.64	10.78	4.20*	11.32	5.00*	35.21	10.22	19.87	7.79	14.81	6.86
M1		10.55	5.83	24.92	10.92	2.38	1.22*	4.51	1.81*	8.74	4.85	10.31	4.95	5.51	2.29
M2		11.71	7.09	27.45	12.55	1.76	0.77*	3.82	2.16*	8.99	5.45	6.59	3.38	6.98	2.91

To get the constraints on the ranging error distribution (p), we investigate the ranging stability by a simple moving average method. Figure 3.12 displays the moving average, Moving Geometric Mean (M-GeoM) and Moving Standard Deviation (M-STD) of the ranging error of M1, with two window sizes for the moving subset $N_{\text{mov}} = 11$ and $N_{\text{mov}} = 101$. It demonstrates that, by averaging a few samples (more than ten samples), the moving average, M-GeoM and M-STD of the ranging error almost maintain at a stable level. At some points, the moving average and the M-STD display a fluctuation. These statistical behaviors are used to construct the constraints on p as follows.

Constraint of a lower bound ($\text{LB}_{\varepsilon_r}$) and a upper bound ($\text{UB}_{\varepsilon_r}$)

It sets the limits on the ranging error

$$\text{LB}_{\varepsilon_r} \leq \varepsilon_r \leq \text{UB}_{\varepsilon_r}, \tag{3.22}$$

The $\text{LB}_{\varepsilon_r}$ is often a negative value, while $\text{UB}_{\varepsilon_r}$ is positive due to the fact that the ranging measurements of losing the DP signal are always larger than the actual range.

Constraint of a stable value of the expectation

Figure 3.12(a) illustrates that the TOA error obtains approximately a stable moving average of a certain scenario, because the main reflectors like the walls and ceilings are the same. Thus, we make the constraint of a constant expectation

$$\mu_{\varepsilon_r} = \int_{-\infty}^{\infty} \varepsilon_r p(\varepsilon_r)\, d\varepsilon_r \,. \tag{3.23}$$

Constraint of a stable geometric mean

Figure 3.12(b) describes a stable M-GeoM, posing another constraint

$$\nu_{\varepsilon_r} = \int_{-\infty}^{\infty} ln(\varepsilon_r) p(\varepsilon_r)\, d\varepsilon_r \,. \tag{3.24}$$

Based on the constraints of (3.21)-(3.24), the Lagrangian L is

$$\begin{aligned} L = &- \int_{\text{LB}_{\varepsilon_r}}^{\text{UB}_{\varepsilon_r}} p(\varepsilon_r) \ln p(\varepsilon_r)\, d\varepsilon_r + \text{C}_1 \left(\int_{\text{LB}_{\varepsilon_r}}^{\text{UB}_{\varepsilon_r}} p(\varepsilon_r)\, d\varepsilon_r - 1 \right) \\ &+ \text{C}_2 \left(\int_{\text{LB}_{\varepsilon_r}}^{\text{UB}_{\varepsilon_r}} \varepsilon_r p(\varepsilon_r)\, d\varepsilon_r - \mu_{\varepsilon_r} \right) + \text{C}_3 \left(\int_{\text{LB}_{\varepsilon_r}}^{\text{UB}_{\varepsilon_r}} ln(\varepsilon_r) p(\varepsilon_r)\, d\varepsilon_r - \nu_{\varepsilon_r} \right). \end{aligned} \tag{3.25}$$

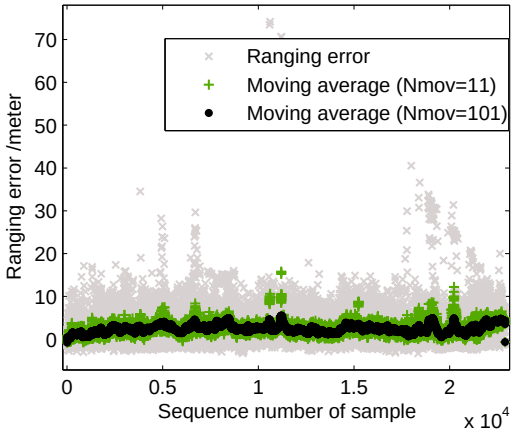

(a) Moving average

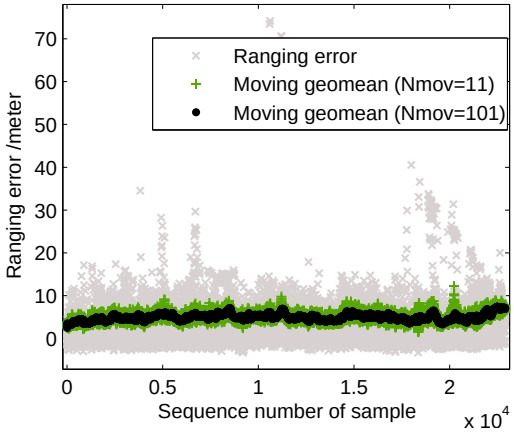

(b) Moving geometric mean (M-GeoM)

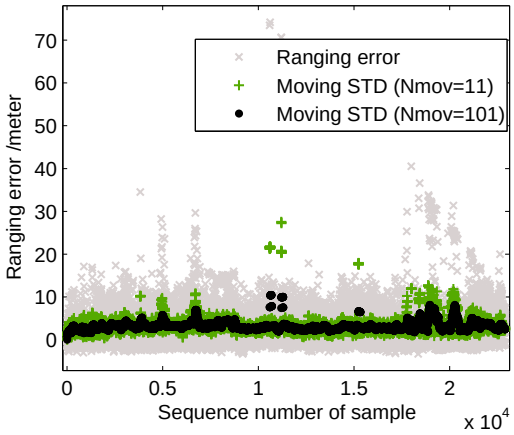

(c) Moving standard deviation (M-STD)

Figure 3.12: Scatter plot of the ranging error with about 22901 samples of M1. The moving average, moving geometric mean (M-GeoM) and moving standard deviation (M-STD) are averaged by a moving window of N_{mov} measurement samples.

Differentiate L with respect to p, one can get

$$\ln p(\varepsilon_r) = -1 + \mathrm{C}_1 + \mathrm{C}_2\varepsilon_r + \mathrm{C}_3 ln(\varepsilon_r). \tag{3.26}$$

As a result, the ranging error distribution with $\max(H)$ subject to the constraints (3.21)-(3.24) is

$$p(\varepsilon_r) = \exp(\mathrm{C}_1 - 1)\exp(\mathrm{C}_2\varepsilon_r)\varepsilon_r^{\mathrm{C}_3}. \tag{3.27}$$

which turns out to be PDF of the Gamma distribution with unknown constants. Therefore, the distribution of the maximum entropy and constraints (3.21)-(3.24) is a Gamma distribution.

Alternatively, one can assume other reasonable constraints, e.g., the most likely distribution, satisfying (3.21)-(3.23) and a stable M-STD as Fig. 3.12(c), is a Lognormal distribution.

The proof of entropy enhances the distribution fitting results of Table 3.5, e.g., it explains why the Gamma distribution and Lognormal distribution fit well in the KS test, according to the fact that the TOA error is finite and statistically stability of the moving average and M-GeoM/ M-STD.

3.5.3 Influence of ranging models on positioning

To examine how the error model influences positioning performance, a nonlinear least-squares (NLS) positioning algorithm [69] is implemented in the experiment M1 and the simulations using the above models. The simulations employ the same setup as M1 (i.e., the anchor deployment and the received ranging rate, etc.).

Table 3.6 shows the basic statistics of positioning of the experiment and simulations, where μ_p, $\max_\mathrm{p}$ and PCT_{95} denotes the mean, the maximum and the 95th percentile of the positioning error, respectively. The positioning error of the experiment serves as a benchmark for the simulations. In other words, the higher similarity of the simulated positioning performance to the experiment, the more similar the model is to represent the real ranging. Figure 3.13 plots CDF of the experimental and simulated positioning errors.

Table 3.6 and Fig. 3.13 demonstrate the difference between the experiment and the simulations of different ranging error models. The results are mostly consistent with the KS statistics in Table 3.5. The worst fitting model in the KS test (the Exponential distribution) leads to the largest difference to the experimental positioning; on the other hand, the better fitting models (the Lognormal and the Gamma distribution) obtain more similar positioning errors to the experiment results. It also finds that the model $\mathcal{N}$+ξEXP also gets a high positioning similarity, indicating that the mixture model can also represent the ranging error. Note the highest difference between the simulated and experimental positioning CDF in Fig. 3.13 is more than 20%, which implies that an improper ranging model can

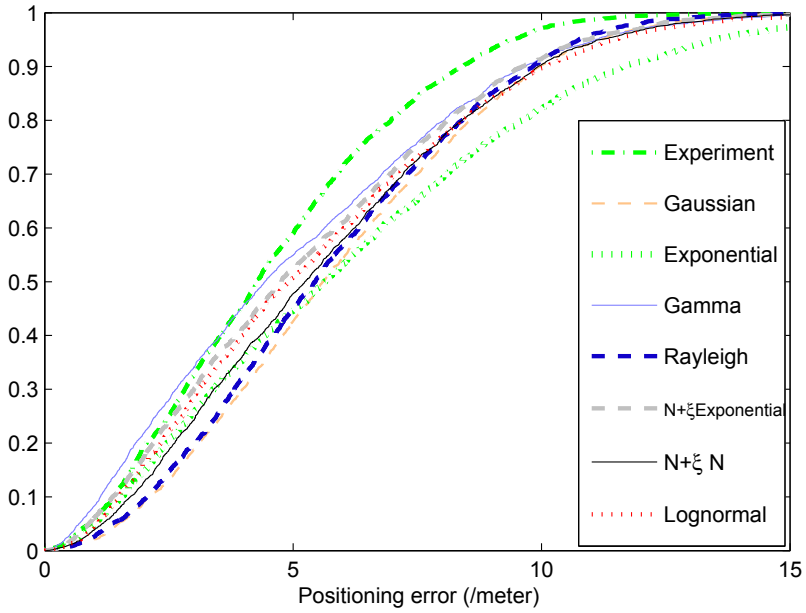

Figure 3.13: CDF of the positioning error of M1 and the simulations (with the same setup to M1) using different models

Table 3.6: Positioning error (/meter) of M1 and the simulations (with the same setup to M1) using different models

Ranging method	Ranging error model	μ_p	$\max_p$	PCT_{95}
M1	\	4.61	23.42	9.40
Simulations of M1	Gaussian	5.59	15.78	10.66
	EXP	6.02	26.11	12.98
	Lognormal	4.96	17.18	11.04
	Gamma	4.65	17.21	11.14
	Rayleigh	5.50	13.51	10.57
	$\mathcal{N} + \xi$EXP	4.45	14.58	10.53
	$\mathcal{N} + \xi\mathcal{N}$	5.22	15.47	10.69

definitely lead to a wrong simulated evaluation of positioning.

3.6 Summary

Based on the exhaustive TOA ranging measurements, we present the mathematical analysis, characteristics and statistical models of indoor ranging error. The frequentist modeling procedure indicates that the TOA error can be fitted well by a statistical model, either the single-distribution models or the mixture-distribution models. Considering the limits faced by portable devices, a positively skewed single-distribution is preferable, e.g., the refined Gamma distribution or Lognormal distribution is rational, as they satisfactorily imitate the positive bias and right-side tail of the TOA error distribution in the mixed LOS and NLOS conditions; on the other hand, the mixture models are less flexible due to the multi-parameter configuration problem. Then, the KS test, maximum entropy principle and simulations validate the efficiency of a proper statistical model to reality. Furthermore, modeling via distribution fitting does not require the complete information of wireless channel. Overall, we recommend frequentist modeling for TOA range-based positioning. As future work, we will consider introducing the ranging characteristics and modeling results to optimize positioning algorithms.

Chapter 4

Sample-based Probabilistic Estimation for Indoor Positioning

The nonlinear and non-Gaussian positioning problem does not exist an analytical solution, thus, sample-based approximations are generally employed. The two key questions about applying sample-based Bayesian methods are:

- how to generate appropriate samples for the nonlinear and non-convex state;
- how to alleviate the effect of ranging uncertainty.

The majority of recent papers of the sampling of Bayesian frame solely rely on the prediction density [153]. From a practical point of view, the sampling from a prediction density suffers from the assumption of the correctly known prior. There is effort in resampling methods to alleviate the sample degeneracy, which have been criticized for losing sample diversity and high complexity [18]. The Bayesian filters in [17,19] suggest to use noninformative prior or flat-tailed measurement model, unfortunately, they are ineffective if the likelihood is also vague. Machine learning approaches (i.e, clustering, splitting and merging) are possible to cope with estimation divergence [106], but they face implementation difficulty.

Specific for indoor scenarios, the NLOS ranging is too arbitrary to be modeled or to be removed (see Chapter 3.3). Some effort has been made to introduce NLOS identification and mitigation, which increases the complexity and may lead to an overfitting problem.

This chapter focuses on three terms: 1) positioning error analysis 2) constrained sampling; 3) NLOS mitigation. Seven sampling and NLOS mitigation algorithms are proposed, which are compared with grid-based estimations, Gaussian filters and particle filters.

4.1 Aspects of Range-based Positioning

4.1.1 Error propagation from ranging to positioning

An analytical description of the positioning uncertainty under the noise ranging can be elaborated by the error propagation analysis [110]. The function of the position estimation with regard to the ranging measurements is denoted as f. Let $\mathbf{x}$ be the actual target's position and $\mathbf{z}$ for the ranging observations, and the ground truth of the position with the ideal ranging measurements is

$$\mathbf{x} = f(\mathbf{z}) \, . \tag{4.1}$$

Given the noise ranging measurements, the estimated position is $\hat{\mathbf{x}} = f(\mathbf{z})$. Then, the positioning uncertainty ($\sigma_{\mathbf{x}}$) is determined by the ranging uncertainty (σ_l)

$$\sigma_{\mathbf{x}}^2 = \sum_{l=1}^{N_{\text{anc}}} \left(\frac{\partial \mathbf{x}}{\partial r_l} \right)^2 \sigma_l^2 \, . \tag{4.2}$$

Here, the positioning uncertainty is analyzed in two cases: the one dimensional (1D) and two dimensional (2D) positioning as follows.

One dimension case

If f is an unbiased estimation, the 1D position function is

$$x = f(\mathbf{z}) = \frac{1}{N_{\text{anc}}} \sum_{l=1}^{N_{\text{anc}}} (a_{xl} \pm r_l) \, . \tag{4.3}$$

According to (4.2), the uncertainty of 1D positioning is derived with

$$\sigma_{\text{x-1D}}^2 = \sum_{l=1}^{N_{\text{anc}}} \left(\pm \frac{1}{N_{\text{anc}}} \right)^2 \sigma_l^2 = \frac{1}{N_{\text{anc}}^2} \sum_{l=1}^{N_{\text{anc}}} \sigma_l^2 \, . \tag{4.4}$$

Assuming that the ranging uncertainty of all anchors is equally deviated $\sigma_{\varepsilon_r}^2 = \frac{1}{N_{\text{anc}}} \sum_{l=1}^{N_{\text{anc}}} \sigma_l^2$, then, we can obtain

$$\sigma_{\text{x-1D}}^2 = \frac{1}{N_{\text{anc}}} \sigma_{\varepsilon_r}^2 \, , \tag{4.5}$$

with $\sigma_{\varepsilon_r}^2$ being the average variance of the ranging errors from all anchors.

Two dimension case

The 2D range-based positioning is defined

$$(x, y) = \Big(f_x(\mathbf{z}), f_y(\mathbf{z})\Big) \ . \tag{4.6}$$

Similarly, the uncertainty of x-axis and y-axis state estimation is

$$(\sigma_x^2, \sigma_y^2) = \left(\sum_{l=1}^{N_{\text{anc}}} \left(\frac{\partial f_x}{\partial r_l}\right)^2 \sigma_l^2, \ \sum_{l=1}^{N_{\text{anc}}} \left(\frac{\partial f_y}{\partial r_l}\right)^2 \sigma_l^2\right) . \tag{4.7}$$

The 2D positioning error is derived from the x-axis and y-axis estimation errors as

$$\varepsilon_{\text{p}-2D} = \sqrt{\varepsilon_x^2 + \varepsilon_y^2} \ . \tag{4.8}$$

Equation (4.2) of 2D positioning is expressed as

$$\begin{aligned}
\sigma_{\mathbf{x}-2D}^2 =& \left(\frac{\varepsilon_x}{\sqrt{\varepsilon_x^2 + \varepsilon_y^2}}\right)^2 \sigma_x^2 + \left(\frac{\varepsilon_y}{\sqrt{\varepsilon_x^2 + \varepsilon_y^2}}\right)^2 \sigma_y^2 \\
=& \left(\frac{\varepsilon_x^2}{\varepsilon_x^2 + \varepsilon_y^2}\right) \sum_{l=1}^{N_{\text{anc}}} \left(\frac{\partial f_x}{\partial r_l}\right)^2 \sigma_l^2 + \left(\frac{\varepsilon_y^2}{\varepsilon_x^2 + \varepsilon_y^2}\right) \sum_{l=1}^{N_{\text{anc}}} \left(\frac{\partial f_y}{\partial r_l}\right)^2 \sigma_l^2 \\
\approx& \sigma_{\varepsilon_r}^2 \sum_{l=1}^{N_{\text{anc}}} \left(\frac{\varepsilon_x^2}{(\varepsilon_x^2 + \varepsilon_y^2)} \left(\frac{\partial f_x}{\partial r_l}\right)^2 + \frac{\varepsilon_y^2}{(\varepsilon_x^2 + \varepsilon_y^2)} \left(\frac{\partial f_y}{\partial r_l}\right)^2 \right) .
\end{aligned} \tag{4.9}$$

In comparison with the 1D positioning, the uncertainty of the 2D positioning is a complex non-linear problem:

- the variance of 1D positioning simply depends on the ranging uncertainty ($\sigma_{\varepsilon_r}^2$) and the number of ranging measurements (N_{anc});
- the uncertainty of the 2D positioning is related to the ranging uncertainty ($\sigma_{\varepsilon_r}^2$), the number of observed measurements (N_{anc}), the positioning function (f_x, f_y) and the value of positioning error ($\varepsilon_x, \varepsilon_y$). The function ($f_x, f_y$) and positioning error ($\varepsilon_x, \varepsilon_y$) are depending to the relative relation between the target to each anchor ($x - a_{xl}, y - a_{yl}$).

These factors of the 2D positioning error are depicted in Fig. 4.1. As a consequence, to enhance the probabilistic positioning, one needs to refine the model of the ranging uncertainty, the anchor placement and the positioning algorithm.

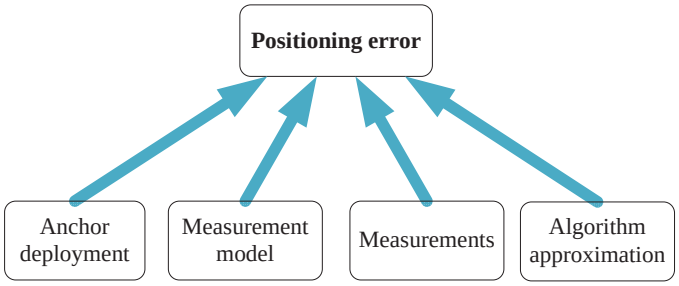

Figure 4.1: Factors of positioning error derived from the error propagation analysis

4.1.2 Anchor placement

The error propagation analysis has concluded that an appropriate anchor placement is essential for the potential performance of range-based positioning. The anchor placement of indoor positioning is constrained by several practical factors, i.e., sensing coverage, system cost, existing infrastructure and environment characteristics (such as the perimeter and corner of the floor). Therefore, the anchor deployment is an engineering problem, whereas, the mathematical optimization of the anchor placement provides a suggestion for practice

Cramér-Rao Lower Bound (CRLB) has been used to study the anchor placement [21, 69, 116] and the anchor selection [111] for optimizing the positioning performance. Thus, the geometry influence of the anchor deployment on the positioning error is described by a 2D distribution of the best achievable MMSE according to CRLB, namely CRLB-2D.

Cramér-Rao Lower Bound (GRLB)

The Cramér-Rao Lower Bound (CRLB) is known as a lower limit for the variance of an unbiased estimate. The CRLB for 2D position estimation requires the following factors:

- the anchors' position $\{\mathbf{a}^l = (a_{xl}, a_{yl})\}_{l=1}^{N_{\text{anc}}}$;
- the ground truth of the target's position $\mathbf{x} = (x, y)$;
- the model of lth ranging measurement, such as a Gaussian model $\mathcal{N}(0, \sigma_l^2)$.

The CRLB matrix is defined as the inverse of the Fisher information matrix ($\mathrm{J}_{\mathbf{x}}$), then an unbiased position satisfies

$$\mathrm{Cov}(\hat{\mathbf{x}}) = \mathrm{E}[(\hat{\mathbf{x}} - \mathbf{x})(\hat{\mathbf{x}} - \mathbf{x})^{\mathrm{T}}] \geq [\mathrm{J}_{\mathbf{x}}]^{-1} . \tag{4.10}$$

where E stands for the expectation and $^{\mathrm{T}}$ denotes the transpose of a matrix. The element of $[\mathrm{J}_{\mathbf{x}}]$ is defined as

$$[\mathrm{J}_{\mathbf{x}}]_{ij} = -\mathrm{E}[\frac{\partial^2 \log p(\mathbf{x}, \mathbf{z})}{\partial \mathbf{x}_i \partial \mathbf{x}_j}] \,, \tag{4.11}$$

where i and j is the index of the state dimension. If the prior of the state is unknown, then Eq. (4.11) can be rewritten into

$$[\mathrm{J}_{\mathbf{x}}]_{ij} \approx -\mathrm{E}[\frac{\partial^2 \log p(\mathbf{z}|\mathbf{x})}{\partial \mathbf{x}_i \partial \mathbf{x}_j}] \,, \tag{4.12}$$

Then, the Fisher matrix can be calculated [69]

$$\mathrm{J}_{\mathbf{x}} = \begin{pmatrix} \sum_{l=1}^{N_{\mathrm{anc}}} (\sigma_l^2)^{-1} \frac{(x_l - a_{xl})^2}{(x_l - a_{xl})^2 + (y_l - a_{yl})^2} & \sum_{l=1}^{N_{\mathrm{anc}}} (\sigma_l^2)^{-1} \frac{(x_l - a_{xl})(y_l - a_{yl})}{(x_l - a_{xl})^2 + (y_l - a_{yl})^2} \\ \sum_{l=1}^{N_{\mathrm{anc}}} (\sigma_l^2)^{-1} \frac{(x_l - a_{xl})(y_l - a_{yl})}{(x_l - a_{xl})^2 + (y_l - a_{yl})^2} & \sum_{l=1}^{N_{\mathrm{anc}}} (\sigma_l^2)^{-1} \frac{(y_l - a_{yl})^2}{(x_l - a_{xl})^2 + (y_l - a_{yl})^2} \,. \end{pmatrix} \tag{4.13}$$

In 2D positioning, the MMSE of the position estimation is indicated by the diagonal terms of the CRLB matrix

$$\mathrm{E}[(\hat{\mathbf{x}}_b - \mathbf{x})^2] \geq [\mathrm{J}_{\mathbf{x}}]_{bb}^{-1}, \; b = x, y \,. \tag{4.14}$$

with

$$[\mathrm{J}_{\mathbf{x}}]_{xx} = -\mathrm{E}[\frac{\partial^2 \log p(\mathbf{z}|\mathbf{x})}{\partial x \partial x}] \tag{4.15}$$

and

$$[\mathrm{J}_{\mathbf{x}}]_{yy} = -\mathrm{E}[\frac{\partial^2 \log p(\mathbf{z}|\mathbf{x})}{\partial y \partial y}] \,. \tag{4.16}$$

Thus, the best achievable MMSE of positioning errors is the 2CRLB

$$\mathrm{CRLB} - 2\mathrm{D} = trace[\mathrm{J}_{\mathbf{x}}^{-1}] \,. \tag{4.17}$$

2D distribution of GRLB

The geometry influence of the anchor deployment is characterized by the distribution of CRLB-2D (4.17) in Fig. 4.2. There are six constellations of the anchor deployment being considered:

1. Sparse interior case[1] (Fig. 4.2(a)): four anchors lie in the interior part of the playing field;
2. Sparse borderline case (Fig. 4.2(b)): four anchors are located on the borderline of the field;
3. Sufficient entire-field case (Fig. 4.2(c)): eight anchors are spread all over the playing field, with comparable density as the experiments;

[1]The average number of reachable anchors in our experiments is 7.5; the anchor density lower than the experiment density is defined as the sparse anchor deployment; otherwise, it is defined as the sufficient anchor deployment

4. Sufficient borderline case (Fig. 4.2(d)): eight anchors are placed on the borderline of the field;
5. Sufficient irregular case (Fig. 4.2(e)): the anchor placement is an irregular constellation;
6. Sufficient even case (Fig. 4.2(f)): the anchors are deployed evenly in the field.

Figure 4.2 illustrates that

- from the sparse and sufficient cases: the denser anchor placement, the better performance of a positioning algorithm can theoretically approach to, e.g., the CRLB is considerably reduced with the anchor number increasing from four to nine;
- from the interior and borderline case: the borderline case deployment is superior than placing anchors in the interior region, as Fig. 4.2(b) almost outperforms Fig. 4.2(a) all over the field;
- from the entire and borderline case: the borderline case is better than the entire-field case, as Fig. 4.2(d) almost outperforms Fig. 4.2(c) everywhere of the playing filed;
- from the irregular and even case: the irregular anchor placement achieves the similar performance as the even placement, as the small difference of the GRLB values between Fig. 4.2(e) and Fig. 4.2(f).
- through Fig 4.2(d) to Fig. 4.2(f), the CRLB values of the even case and the irregular case is smaller than the borderline case (averagely 0.2 unit), because of involving one more ranging measurements.

Summarily, the 2D GRLB infers that the better anchor deployment is to place sufficient anchors on the borderline of the positioning field, rather than the even style or interior style deployment.

Practical anchor placement

Although the distribution of CRLB-2D demonstrates the guideline of the anchor placement for the best positioning performance, the anchor deployment is an engine problem rather than a theoretical optimization. According to our field experience, the following suggestions are made for a practical anchor placement:

- to ensure that there are sufficient anchors placed on the borderline of the positioning field;
- to be aware of the NLOS region, such as corners or blind areas (such as behind a metal door) of indoor environments;
- the anchors should not cluster in parts of the positioning field;
- it is also necessary to place anchors in the interior field, in case that the borderline anchors may be out of the communication range or fail to sense measurements.

4.1.3 Probabilistic positioning methods

Given the anchor deployment and ranging measurements, the positioning problem turns to an algorithmic optimization. This chapter aims to derive sample-based approximation about the position

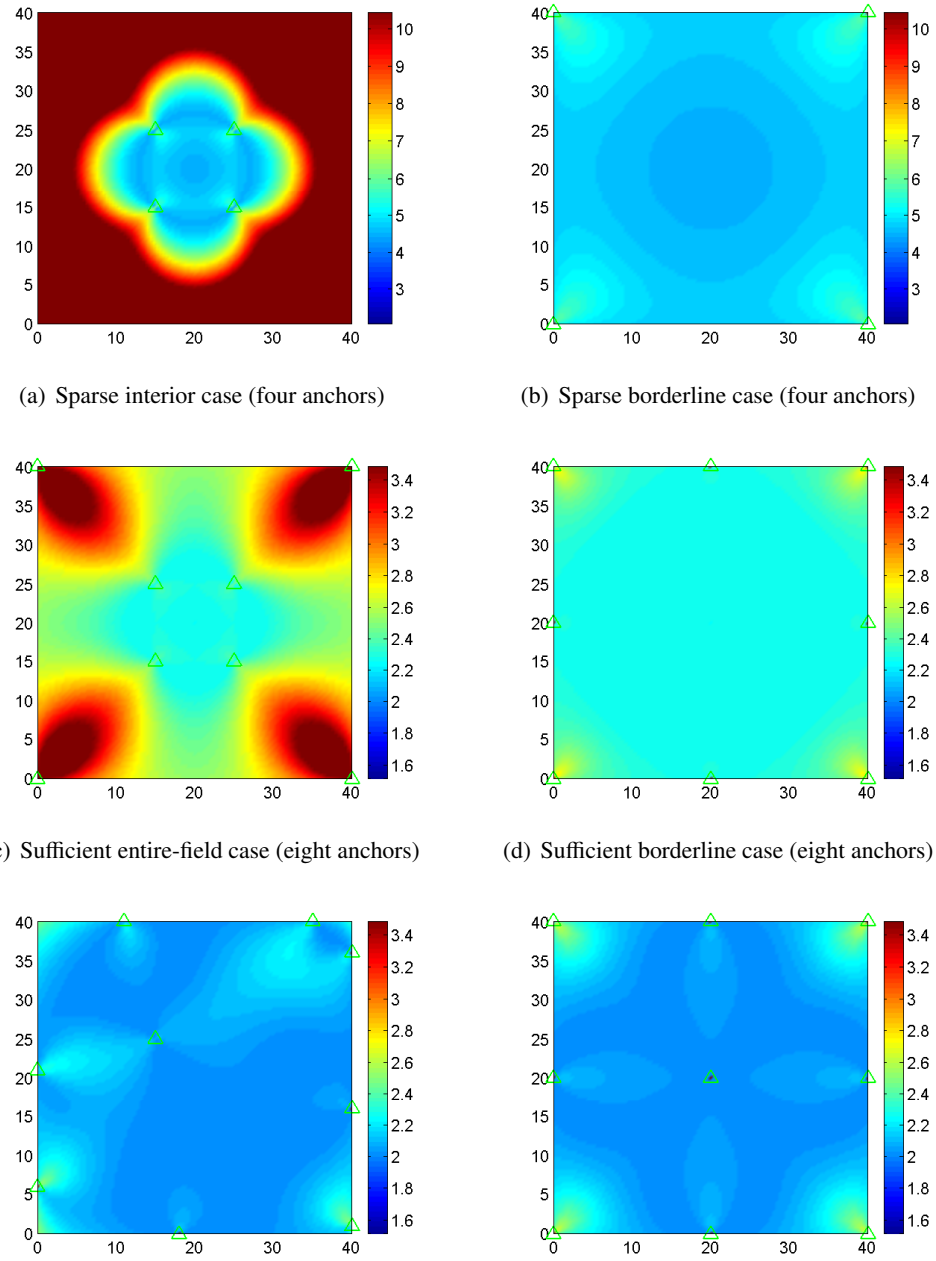

(a) Sparse interior case (four anchors)

(b) Sparse borderline case (four anchors)

(c) Sufficient entire-field case (eight anchors)

(d) Sufficient borderline case (eight anchors)

(e) Sufficient irregular case (nine anchors)

(f) Sufficient even case (nine anchors)

Figure 4.2: Geometric illustration of CRLB-2D with six anchor constellations: the size of the playing field is 40×40 units^2 represented by 100×100 discrete points; the CRLB-based MMSE at every discrete point is calculated, with the values being read from the color bar; the anchors are denoted by $\triangle$; the ranging error follows a Gaussian model $\mathcal{N}(0, 3^2)$.

estimation given the noisy ranging data, either through a non-sequential estimator ($p(\mathbf{x}_t|\mathbf{z}_t)$) or a sequential estimator ($p(\mathbf{x}_t|\mathbf{z}_{1:t})$). Seven sample-based positioning and NLOS mitigation algorithms are proposed, which are compared with six popular algorithms.

The proposed algorithms

Equation (2.5) of the posterior position estimation is formulated as

$$p^{\theta}(\mathbf{x}|\mathbf{z}) \propto \underbrace{p^{\theta}(\mathbf{z}|\mathbf{x})}_{\text{Likelihood of ranging}} \cdot \underbrace{p^{\theta}(\mathbf{x})}_{\text{Prior of 2D position}}, \tag{4.18}$$

indicating that, both the prior and the likelihood interchangeably determine the posterior. Therefore, for the success of the sample-based probabilistic positioning, this chapter proposes enhancements in both the prior and the likelihood:

Prior For non-sequential estimation, the prior depends on the distribution of the state samples; for sequential estimation, the prior is conjointly determined by a motion model and the previous state. The high-dimension motion model (i.e., velocity, acceleration, orientation, and angular velocity) [150, 155] are particularly troublesome, thus, the following simplify the motion model as a random Gaussian walk with fixed mean and variance. To enhance the prior, Section 4.2 proposes four sampling methods.

Likelihood Model-based likelihood is sensitive to the measurement model, especially when state samples are insufficient to interpret the complete state-space [17]. The classical ranging model uses a Gaussian model, which is not suited for the NLOS ranging. The complex ranging models mentioned in Chapter 3.3 are inconvenient due to the requirements of exhausted experiments and careful data training, multi-parameter configuration, limitations to a particular scenario and etc. Concerning the NLOS errors, Section 4.3 develops nonparametric bias models and an adaptive measurement model.

The compared algorithms

For performance comparison, six popular positioning algorithms are chosen.

1) Grid-based Filter (GF)

The straightforward approach to nonlinear and non-Gaussian Bayesian filtering is a Grid-based Filter, as introduced in Subsection 2.3.2. The pseudo-code of Grid-based Bayesian Filter is in **Algorithm** 2.

Algorithm 2 Grid-based filter (GF)

Output and input: $\left[\hat{\mathbf{x}}_t, \mathbf{G}_t, \{w_t^i\}_{i=1:N_\mathrm{p}}\right] = \mathrm{GF}\left[\mathbf{z}_t, \mathbf{A}_t, \hat{\mathbf{x}}_{t-1}, \mathbf{G}_{t-1}, \{w_{t-1}^i\}_{i=1:N_\mathrm{p}}\right]$
Setting: N_g, $p(\mathbf{x}_t|\hat{\mathbf{x}}_{t-1})$, $p(r|\,\|\mathbf{x}-\mathbf{a}\|)$
Initialization: $\hat{\mathbf{x}}^0$, $\left\{w_{0|0}^i = \frac{1}{N_\mathrm{g}}\right\}_{i=1:N_\mathrm{g}}$, $\mathbf{G}_0$ and $t = 1$

1: Predefine grid samples $\mathbf{G}_t = \mathbf{G}_{t-1}$
2: Assign weights $\{w_t^i\}_{i=1:N_\mathrm{g}}$ (4.39)
3: Position estimation $\hat{\mathbf{x}}_t$ (4.33)
4: Set $t = t + 1$ and iterate to item 1.

2) Sampling Importance Resampling (SIR) filter

The first particle filter is sampling importance resampling (SIR) filter (also know as bootstrap filter) proposed by Gordon *et al.* in 1993 [64]. There are variations of PFs be applied to sequential positioning in both simulations [11] and real-world experiments [38]. The pseudo-code of SIR filter is in **Algorithm** 3. Simply note that in all of our simulations of PFs, the systematic resampling method in **Algorithm** 1 is used.

Algorithm 3 Sampling Importance Resampling (SIR) for filtering

Output and input: $\left[\hat{\mathbf{x}}_t, \{\mathbf{x}_t^i\}_{i=1:N_\mathrm{p}}, \{w_t^i\}_{i=1:N_\mathrm{p}}\right] = \mathrm{SIR}\left[\mathbf{z}_t, \mathbf{A}_t, \{\mathbf{x}_{t-1}^i\}_{i=1:N_\mathrm{p}}, \{w_{t-1}^i\}_{i=1:N_\mathrm{p}}\right]$
Setting: N_p, $p(\mathbf{x}_t|\mathbf{x}_{t-1})$, $p(r|\,\|\mathbf{x}-\mathbf{a}\|)$
Initialization:

- $p(\mathbf{x}_0)$
- Importance sampling $\left\{\mathbf{x}_0^i \sim p(\mathbf{x}_0)\right\}_{i=1:N_\mathrm{p}}$
- Assign weights $\left\{w_0^i = \frac{1}{N_\mathrm{p}}\right\}_{i=1:N_\mathrm{p}}$
- $t = 1$

1: Importance sampling $\left\{\mathbf{x}_t^i \sim p(\mathbf{x}_t|\mathbf{x}_{t-1}^i)\right\}_{i=1:N_\mathrm{p}}$
2: Assign weights $\left\{w_t^i = w_{t-1}^i p(\mathbf{z}_t^i|\mathbf{x}_t^i)\right\}_{i=1:N_\mathrm{p}}$ and normalization $\left\{w_t^i = \frac{w_t^i}{\sum_{j=1}^{N_\mathrm{p}} w_t^j}\right\}_{i=1:N_\mathrm{p}}$
3: Resampling using **Algorithm** 1

$$\left[\{\mathbf{x}_t^i\}_{i=1:N_\mathrm{p}}, \{w_t^i\}_{i=1:N_\mathrm{p}}\right] = \mathrm{Resampling}\left[\{\mathbf{x}_t^i\}_{i=1:N_\mathrm{p}}, \{w_t^i\}_{i=1:N_\mathrm{p}}\right]$$

4: Estimate position $\hat{\mathbf{x}}_t$ (4.19)
5: Set $t = t + 1$ and iterate to item 1.

3) Generic Particle Filter (Generic-PF)

Differing from the SIR filter sampling from the motion model, Generic-PF algorithm suffices to sample from arbitrary proposed density. Furthermore, it employs selective resampling (also known as adaptive resampling), which only executes resampling when the particle weights get too degenerated. The particle degeneracy is simply evaluated by the effective sample size (N_{eff}) [154]. The estimated position is the MMSE of the sample-based density.

$$\hat{\mathbf{x}}_t = \mathrm{E}(p(\mathbf{x}_t|\mathbf{z}_{1:t})) = \sum_{i=1}^{N_\text{p}} \mathbf{x}_t^i w_t^i \,. \tag{4.19}$$

The pseudo-code of the Generic Particle Filter is in **Algorithm** 4.

Algorithm 4 Generic Particle Filter (Generic-PF)

Output and input: $\left[\hat{\mathbf{x}}_t, \{\mathbf{x}_t^i\}_{i=1:N_\text{p}}, \{w_t^i\}_{i=1:N_\text{p}}\right] = \text{Generic} - \text{PF}\left[\mathbf{z}_t, \mathbf{A}_t, \{\mathbf{x}_{t-1}^i\}_{i=1:N_\text{p}}, \{w_{t-1}^i\}_{i=1:N_\text{p}}\right]$
Setting: N_p, $p(\mathbf{x}_t|\mathbf{x}_{t-1})$, $p(r|\,\|\mathbf{x}-\mathbf{a}\|)$, $q(\mathbf{x}_t|\mathbf{x}_{t-1}, \mathbf{z}_t)$ and ${N_\text{eff}}^{threshold} = 0.5N_\text{p}$
Initialization:

- $p(\mathbf{x}_0)$ and $q(\mathbf{x}_0)$
- Importance sampling $\left\{\mathbf{x}_0^i \sim q(\mathbf{x}_0)\right\}_{i=1:N_\text{p}}$
- Assign weights $\left\{w_0^i = \frac{p(\mathbf{x}_0)}{q(\mathbf{x}_0)}\right\}_{i=1:N_\text{p}}$ and normalization $\left\{w_0^i = \frac{w_0^i}{\sum_{j=1}^{N_\text{p}} w_0^j}\right\}_{i=1:N_\text{p}}$
- $t = 1$

1: Importance sampling $\left\{\mathbf{x}_t^i \sim q(\mathbf{x}_t|\mathbf{x}_{t-1}^i, \mathbf{z}_t)\right\}_{i=1:N_\text{p}}$

2: Assign weights $\left\{w_t^i = w_{t-1}^i \frac{p(\mathbf{z}_t|\mathbf{x}_t^i)p(\mathbf{x}_t^i|\mathbf{x}_{t-1}^i)}{q(\mathbf{x}_t^i|\mathbf{x}_{t-1}^i, \mathbf{z}_t)}\right\}_{i=1:N_\text{p}}$ and normalization $\left\{w_t^i = \frac{w_t^i}{\sum_{j=1}^{N_\text{p}} w_t^j}\right\}_{i=1:N_\text{p}}$

3: Estimate $\widehat{N_\text{eff}}$ (2.98)

4: If $\widehat{N_\text{eff}} < {N_\text{eff}}^{threshold}$, then Resampling using **Algorithm** 1

$$\left[\{\mathbf{x}_t^i\}_{i=1:N_\text{p}}, \{w_t^i\}_{i=1:N_\text{p}}\right] = \text{Resampling}\left[\{\mathbf{x}_t^i\}_{i=1:N_\text{p}}, \{w_t^i\}_{i=1:N_\text{p}}\right]$$

5: Estimate position $\hat{\mathbf{x}}_t$ (4.19)

6: Set $t = t + 1$ and iterate to item 1.

4) Auxiliary Particle Filter (Auxiliary-PF)

The weakness of SIR and Generic-PF is that the importance sampling does not take the current observations into account, leading to filter divergence. Pitt and Shephard propose the Auxiliary-PF to involve the latest observations via an auxiliary sampling procedure [137]. However, the auxiliary

sampling increases complexity. The pseudo-code of the Auxiliary Particle Filter is in **Algorithm** 5.

Algorithm 5 Auxiliary Particle Filter (Auxiliary-PF)

Output and input: $\left[\hat{\mathbf{x}}_t, \{\mathbf{x}_t^i\}_{i=1:N_\mathrm{p}}, \{w_t^i\}_{i=1:N_\mathrm{p}}\right] = \mathrm{Auxiliary-PF}\left[\mathbf{z}_t, \mathbf{A}_t, \{\mathbf{x}_{t-1}^i\}_{i=1:N_\mathrm{p}}, \{w_{t-1}^i\}_{i=1:N_\mathrm{p}}\right]$
Setting: N_p, $p(\mathbf{x}_t|\mathbf{x}_{t-1})$, $p(r|\,\|\mathbf{x}-\mathbf{a}\|)$
Initialization:

- $p(\mathbf{x}_0)$
- Importance sampling $\left\{\mathbf{x}_0^i \sim p(\mathbf{x}_0)\right\}_{i=1:N_\mathrm{p}}$
- Assign weights $\left\{w_0^i = \frac{1}{N_\mathrm{p}}\right\}_{i=1:N_\mathrm{p}}$
- $t = 1$

1: Deterministically predict the particles $\left\{\mu_t^j = f(\mathbf{x}_{t-1}^j) \approx \mathrm{E}(\mathbf{x}_t|\mathbf{x}_{t-1}^j)\right\}_{j=1:N_\mathrm{p}}$

2: Assign weights $\left\{v_t^j = w_{t-1}^j p(\mathbf{z}_t^j|\mu_t^j)\right\}_{j=1:N_\mathrm{p}}$ and normalization $\left\{v_t^j = \frac{v_t^j}{\sum_{k=1}^{N_\mathrm{p}} v_t^k}\right\}_{j=1:N_\mathrm{p}}$

3: Resampling using **Algorithm** 1

$$\left[\{\mu_t^j\}_{j=1:N_\mathrm{p}}, \{v_t^j\}_{j=1:N_\mathrm{p}}, i^j\}_{j=1:N_\mathrm{p}}\right] = \mathrm{Resampling}\left[\{\mu_t^j\}_{j=1:N_\mathrm{p}}, \{v_t^j\}_{j=1:N_\mathrm{p}},\ \{\mathbf{x}_{t-1}^j\}_{j=1:N_\mathrm{p}}\right]$$

4: Importance sampling $\left\{\mathbf{x}_t^j \sim p(\mathbf{x}_t|\mathbf{x}_{t-1}^{i^j})\right\}_{j=1:N_\mathrm{p}}$

5: Assign weights $\left\{w_t^j = \frac{p(\mathbf{z}_t^j|\mathbf{x}_t^j)}{p(\mathbf{z}_t^j|\mu_t^{i_j})}\right\}_{j=1:N_\mathrm{p}}$ and normalization $\left\{w_t^j = \frac{w_t^j}{\sum_{k=1}^{N_\mathrm{p}} w_t^k}\right\}_{j=1:N_\mathrm{p}}$

6: Estimate position $\hat{\mathbf{x}}_t$ (4.19)

7: Set $t = t + 1$ and iterate to item 1.

5) Gaussian Particle Filter (Gaussian-PF)

Even though the resampling procedure can efficiently concentrate the state samples, it consumes much computation. It is usually interesting to avoid the resampling step, such as the Gaussian Particle Filter [98]. The Gaussian Particle Filter approximates the prior by a single Gaussian density

$$p(\mathbf{x}_t|\mathbf{z}_{1:t}) = \frac{p(\mathbf{z}_t|\mathbf{x}_t)p(\mathbf{x}_t|\mathbf{z}_{1:t-1})}{\gamma} \tag{4.20}$$

$$\approx \frac{p(\mathbf{z}_t|\mathbf{x}_t)\mathcal{N}(\mathbf{x}_t^i;\mu_t,\Sigma_t)}{\gamma}\,. \tag{4.21}$$

The Gaussian Particle Filter skips the resampling, which significantly reduces the complexity. On

the other hand, Gaussian-PF loses the advantage of PFs representing arbitrary sample density. The pseudo-code of Gaussian-PF is in **Algorithm** 6.

Algorithm 6 Gaussian Particle Filter (Gaussian-PF)

Output and input: $t[\hat{\mathbf{x}}_t] = \text{Gaussian} - \text{PF}\left[\mathbf{z}_t, \mathbf{A}_t, \mu_{t-1}, \Sigma_{t-1}\right]$
Setting: N_p, $p(\mathbf{x}_t|\mathbf{x}_{t-1})$, $p(r|\,\|\mathbf{x}-\mathbf{a}\|)$
Initialization:

- μ_0, Σ_0
- Sampling $\left\{\mathbf{x}_0^i \sim \mathcal{N}(\mathbf{x}_0^i; \mu_0, \Sigma_0)\right\}_{i=1:N_\text{p}}$
- Assign weights $\left\{w_0^i = \frac{1}{N_\text{p}}\right\}_{i=1:N_\text{p}}$
- $t = 1$

1: Sampling $\left\{\mathbf{x}_{t-1}^i \sim \mathcal{N}(\mathbf{x}_{t-1}^i; \mu_{t-1}, \Sigma_{t-1})\right\}_{i=1:N_\text{p}}$
2: Prediction $\left\{\mathbf{x}_t^i \sim p(\mathbf{x}_t|\mathbf{x}_{t-1}^i)\right\}_{i=1:N_\text{p}}$
3: Assign weights $\left\{w_t^i = p(\mathbf{z}_t^i|\mathbf{x}_t^i)\right\}_{i=1:N_\text{p}}$ and normalization $\left\{w_t^i = \frac{w_t^i}{\sum_{j=1}^{N_\text{p}} w_t^j}\right\}_{i=1:N_\text{p}}$
4: Estimate position $\hat{\mathbf{x}}_t$ (4.19)
5: Gaussian approximation

$$\mu_t = \sum_{i=1}^{N_\text{p}} \mathbf{x}_t^i w_t^i$$

$$\Sigma_t = \sum_{i=1}^{N_\text{p}} (\mathbf{x}_t^i - \mu_t)(\mathbf{x}_t^i - \mu_t)^\text{T} w_t^i$$

6: Set $t = t + 1$ and iterate to item 1.

An alternate version of the Gaussian Particle Filter is also given in the work [98], namely Gaussian Particle Filter Alternate (Gaussian-PF2). The pseudo-code of Gaussian-PF2 is described in **Algorithm** 7, differing from Gaussian-PF in the way of propagating the state samples to the next iteration. The Gaussian-PF is more efficient than Gaussian-PF2 in space complexity.

5) Annealed Particle Filter (Annealed-PF)

The Annealed Particle Filter proposed by Neal [126] modifies the sample weights through an anneal function (also referred to a cooling schedule). The effect annealed sampling is to avoid samples cluster to a single point.

There are various annealing schemes differing in the annealing rate, and the annealing function (β_k) can be variational [34]. For simplicity, we use a deterministic annealing as a negative exponen-

Algorithm 7 Gaussian Particle Filter Alternate (Gaussian-PF2)

Output and input: $\left[\hat{\mathbf{x}}_t, \{\mathbf{x}_t^i\}_{i=1:N_\mathrm{p}}, \{w_t^i\}_{i=1:N_\mathrm{p}}\right] = \mathrm{Gaussian-PF2}\left[\mathbf{z}_t, \mathbf{A}_t, \{\mathbf{x}_{t-1}^i\}_{i=1:N_\mathrm{p}}, \{w_{t-1}^i\}_{i=1:N_\mathrm{p}}\right]$
Setting: N_p, $p(\mathbf{x}_t|\mathbf{x}_{t-1})$, $p(r|\,\|\mathbf{x}-\mathbf{a}\|)$
Initialization:

- μ_0, Σ_0
- Sampling $\left\{\mathbf{x}_0^i \sim \mathcal{N}(\mathbf{x}_0^i; \mu_0, \Sigma_0)\right\}_{i=1:N_\mathrm{p}}$
- Assign weights $\left\{w_0^i = \frac{1}{N_\mathrm{p}}\right\}_{i=1:N_\mathrm{p}}$
- $t = 1$

1: Prediction $\left\{\mathbf{x}_t^i \sim p(\mathbf{x}_t|\mathbf{x}_{t-1}^i)\right\}_{i=1:N_\mathrm{p}}$
2: Estimate position $\hat{\mathbf{x}}_t$ (4.19)
3: Gaussian approximation

$$\mu_t = \sum_{i=1}^{N_\mathrm{p}} \mathbf{x}_t^i w_t^i$$

$$\Sigma_t = \sum_{i=1}^{N_\mathrm{p}} (\mathbf{x}_t^i - \mu_t)(\mathbf{x}_t^i - \mu_t)^\mathrm{T} w_t^i$$

4: Sampling $\left\{\mathbf{x}_t^i \sim \mathcal{N}(\mathbf{x}_t^i; \mu_t, \Sigma_t)\right\}_{i=1:N_\mathrm{p}}$
5: Assign weights $\left\{w_t^i = p(\mathbf{z}_t^i|\mathbf{x}_t^i)\right\}_{i=1:N_\mathrm{p}}$ and normalization $\left\{w_t^i = \frac{w_t^i}{\sum_{j=1}^{N_\mathrm{p}} w_t^j}\right\}_{i=1:N_\mathrm{p}}$
6: Set $t = t + 1$ and iterate to item 1.

tial function

$$\beta_k = e^{-k} \,, \tag{4.22}$$

with k being the index of the annealing runs ($k = \{K_{\text{Ann}}, \cdots, 0\}$), and the scalar $0 < \beta_{K_{\text{Ann}}} < \cdots < \beta_0 = 1$). The pseudo-code of Annealed-PF [104] is in **Algorithm** 8.

4.1.4 Evaluation criteria

This chapter evaluates the positioning algorithms by multiple evaluation criteria, i,e., are the positioning performance, cost and positioning behavior.

Performance

Positioning performance is investigated in terms of accuracy, precision and robustness.

1) Accuracy

The most important evaluation criterion of a positioning system is accuracy, indicating the nearness of the estimated position to the true position. It is commonly measured by Mean Absolute Error (MAE_p)

$$\text{MAE}_\text{p} = \frac{1}{N_\text{T}} \sum_{t=1}^{N_\text{T}} \|\mathbf{x}_t - \hat{\mathbf{x}}_t\| \,, \tag{4.23}$$

and the Root Mean Square Error (RMSE_p) of positioning

$$\text{RMSE}_\text{p} = \sqrt{\frac{1}{N_\text{T}} \sum_{t=1}^{N_\text{T}} \|\mathbf{x}_t - \mathbf{x}_t\|^2} \,. \tag{4.24}$$

2) Precision

The estimation precision is indicated by the inverse standard deviation

$$\text{Precise}_\text{p} = \frac{1}{\sqrt{\frac{1}{N_\text{T}} \sum\limits_{t=1}^{N_\text{T}} \left\|\mathbf{x}_t - \text{MAE}_\text{p}\right\|^2}} = \frac{1}{\sigma_\text{p}} \,. \tag{4.25}$$

Furthermore, σ_p also interprets the estimation variability.

3) Robustness

Robustness is an crucial aspect in the practical estimation process. If the robustness is too low, the estimation indeed becomes questionable for applications. As a result, the positioning accuracy is supplemented with a confidence level [86], e.g., the upper limit of the 90% confidence level is the

Algorithm 8 Annealed Particle Filter (Annealed-PF)

Output and input: $\left[\hat{\mathbf{x}}_t, \{\mathbf{x}_t^i\}_{i=1:N_\mathrm{p}}, \{w_t^i\}_{i=1:N_\mathrm{p}}\right] = \text{Annealed} - \text{PF}\left[\mathbf{z}_t, \mathbf{A}_t, \{\mathbf{x}_{t-1}^i\}_{i=1:N_\mathrm{p}}, \{w_{t-1}^i\}_{i=1:N_\mathrm{p}}\right]$
Setting: N_p, $p(\mathbf{x}_t|\mathbf{x}_{t-1})$, $p(r|\,\|\mathbf{x}-\mathbf{a}\|)$, K_Ann, $\{\beta_k\}_{k=1:K_\mathrm{Ann}}$
Initialization:

- μ_0, Σ_0
- Importance sampling $\left\{\mathbf{x}_0^i \sim \mathcal{N}(\mathbf{x}_0^i; \mu_0, \Sigma_0)\right\}_{i=1:N_\mathrm{p}}$
- Initial weights $\left\{w_0^i = \frac{1}{N_\mathrm{p}}\right\}_{i=1:N_\mathrm{p}}$
- $t = 1$

1: Importance sampling $\left\{\mathbf{x}_t^i \sim q(\mathbf{x}_t|\mathbf{x}_{t-1}^i, \mathbf{z}_t)\right\}_{i=1:N_\mathrm{p}}$

2: Assign weights similar to Generic-PF $\left\{w_t^i = w_{t-1}^i \frac{p(\mathbf{z}_t|\mathbf{x}_t^i)p(\mathbf{x}_t^i|\mathbf{x}_{t-1}^i)}{q(\mathbf{x}_t^i|\mathbf{x}_{t-1}^i, \mathbf{z}_t)}\right\}_{i=1:N_\mathrm{p}}$, and normalization $\left\{w_t^i = \frac{w_t^i}{\sum_{j=1}^{N_\mathrm{p}} w_t^j}\right\}_{i=1:N_\mathrm{p}}$

3: Resampling using **Algorithm** 1

$$\left[\{\mathbf{x}_t^i\}_{i=1:N_\mathrm{p}}, \{w_t^i\}_{i=1:N_\mathrm{p}}\right] = \text{Resampling}\left[\{\mathbf{x}_t^i\}_{i=1:N_\mathrm{p}}, \{w_t^i\}_{i=1:N_\mathrm{p}}\right]$$

4: Annealing

Initialization: $\left\{\mathfrak{x}_{K_\mathrm{Ann}}^i = \mathbf{x}_t^i\right\}_{i=1:N_\mathrm{p}}$

FOR $k = K_\mathrm{Ann} - 1$ down to 0

Annealed importance sampling $\left\{\mathfrak{x}_k^i \sim q(\mathfrak{x}_k|\mathfrak{x}_{k+1}^i, \mathbf{z}_t)\right\}_{i=1:N_\mathrm{p}}$

Assign annealed weights $\left\{\pi_k^i = (w_t^i)^{\beta_k} \frac{p(\mathfrak{x}_k^i\|\mathfrak{x}_{k+1}^i|)}{q(\mathfrak{x}_k^i|\mathfrak{x}_{k+1}^i, \mathbf{z}_t)}\right\}_{i=1:N_\mathrm{p}}$

Normalization $\left\{\pi_k^i = \frac{\pi_k^i}{\sum_{j=1}^{N_\mathrm{p}} \pi_k^j}\right\}_{i=1:N_\mathrm{p}}$

Resampling using **Algorithm** 1

$$\left[\{\mathfrak{x}_k^i\}_{i=1:N_\mathrm{p}}, \{\pi_k^i\}_{i=1:N_\mathrm{p}}\right] = \text{Resampling}\left[\{\mathfrak{x}_k^i\}_{i=1:N_\mathrm{p}}, \{\pi_k^i\}_{i=1:N_\mathrm{p}}\right]$$

END FOR

5: Update weights $\left\{w_t^i = \pi_0^i\right\}_{i=1:N_\mathrm{p}}$ and particles $\{\mathbf{x}_t^i = \mathfrak{x}_0^i\}_{i=1:N_\mathrm{p}}$

6: Estimate position $\hat{\mathbf{x}}_t$ (4.19)

7: Set $t = t + 1$ and iterate to item 1.

95th percentile of the positioning error (PCT_{95p}).

Another perspective of robustness is that the positioning algorithm should work well in some tough conditions, i.e., the sparse density of anchors, the small number of samples, the impropriate models and imprecise initialization, etc.

Cost

The cost is a critical issue of whether the positioning algorithms are actually applicable or not, in terms of complexity, implementation, memory and etc.

1) Computation complexity

The computation trend of the algorithms can be easily compared using their execution times or the Big-O notation.

2) Space complexity

In sample-based estimation, space complexity is also important, which is defined as essentially the number of memory cells needed.

3) Implementation

The implementation difficulty is quantified by measuring the number of multiplication, division or generating random numbers for sampling and resampling.

4.2 Constrained Sampling Methods

The state probabilistic density is represented by a set of weighted discrete samples

$$p(\mathbf{x}|\mathbf{z},\theta) \approx \sum_{i=1}^{N_s} w^i \delta(\mathbf{x}-\mathbf{x}^i) \ . \tag{4.26}$$

The accuracy of the sample-based representation is dominated by two factors: the density of the state samples and how closely the samples approach the true state [143]. However, dense samples pose high demands are prohibitive for the low-end devices. Even worse, a severe mismatch between the sampling density and the true state can produce many irrelevant samples, leading to sample divergence (all the samples diverge from the true position [134]).

There is much work on the state sampling methods. For efficient sampling, a tight sampling density is preferred [98], e.g., the kernel mean-shift sampling [31] is efficient but may lock to local optima; the adaptive sampling [96, 149, 153] averagely reduces the sample size, but the sampling quality cannot be improved. To keep sample diversity, the samples should be representative for

all the possibilities of the complete posterior, e.g., a flat sampling density allows the samples to be spread widely, however, it has been criticized for a low effective sample size [11, 17]; although sampling from mixture models prevents a single mode of the sample density [14, 158], it causes difficulty in maintaining the mixture components. The resampling procedure duplicates the samples with high weights and remove the ones with low probability, however, it brings additional variance on the state estimation [52]. However, the resampling methods

This section concers the main problem of the sample-based positioning is the lack of constraint on the sample-space, which results in numerically intractable solutions and severely deteriorates the posterior. It is hold that the constraints can be extracted from physical laws (such as the construction of indoor environments), the simply upper and lower limits of ranging models or the motion estimation, etc. This section proposes four constrained sampling methods, including

- a sensible bound on the sample-space to reduce the size of samples;
- a geometric sampling to produce geometrically meaningful samples;
- a polar sampling to retain the sampling diversity;
- a gradual Gaussian sampling to incrementally relocate the samples to the true posterior.

4.2.1 Bounded grid-based approximation

Since the prior may be erroneous, it is interesting to uniformly generate the samples, such as the grid-based sampling.

Problem statement

Generally, the choice of the sampling density is rather subjective. Since the state density is unpredictable, nonlinear and non-Gaussian, the subjective prior cannot be accurate, e.g., our previous work reveals that sampling with informative priors does not work out well [180]

Grid-based position estimations have been successfully used for the multi-modal state densities [25, 47]. The conventional grid-based positioning explores the grid covering a large region, i.e., the whole indoor area [53] or the maximum range of RF communication [135], which poses three problems: 1) the estimate can be easily misguided by the NLOS ranging; 2) a high memory and computation exponentially growing with the grid-space; 3) the estimate is dominated by the likelihood which strongly relies on a precise measurement model.

Since what constitutes the grid region is far from clear, this subsection proposes an instantaneous upper bound and a recursive upper bound that the state must satisfy.

Bounded Grid-based Estimation (BGE)

Inspired by the definition of a positioning error bound in literature [84], a bounded Grid-based estimation (BGE) is proposed, assuming an upper bound from the current ranging measurements.

1) Instantaneous grid region (R_t)

The bound is derive with the algebraic inequality relationships by the Bounding-box algorithm [103, 162]. The Bounding-box algorithm, also known as Min-Max algorithm, is a simple and straightforward method. The Bounding-box algorithm builds a square (a bounding box) around each anchor using its location ($a_l = (a_{xl}, a_{yl})$) and the ranging measurement (r_l), instead of the circles with the radius of r_l (see Eq. (4.30) and Fig. 4.3).

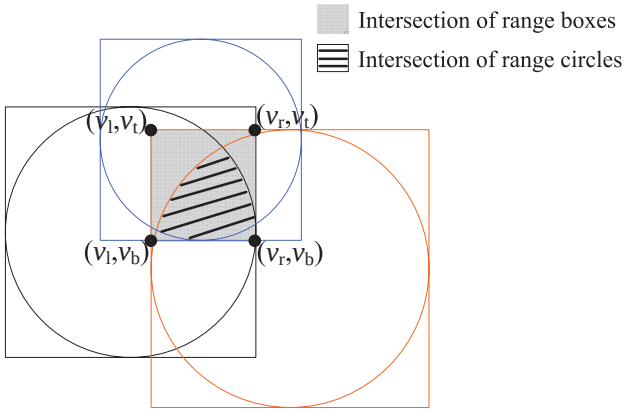

Figure 4.3: Circles/boxes intersection for the instantaneous grid region (R_t) with three ranging measurements

The target's position satisfies every ranging box, thus the position is inside the box intersection region with four vertices

$$\mathbf{V} = \{(v_\mathrm{l}, v_\mathrm{b}), (v_\mathrm{r}, v_\mathrm{b}), (v_\mathrm{l}, v_\mathrm{t}), (v_\mathrm{r}, v_\mathrm{t})\} , \tag{4.27}$$

and the center of the box intersection is $(\frac{v_\mathrm{l}+v_\mathrm{r}}{2}, \frac{v_\mathrm{t}+v_\mathrm{b}}{2})$.

The Bounding-box intersection at each instance of time is calculated as

$$R_t = \bigcap_{l=1}^{N^t_{\mathrm{anc}}} \{a^t_{xl} - r^l_t, a^t_{xl} + r^l_t, a^t_{yl} - r^l_t, a^t_{yl} + r^l_t\} , \tag{4.28}$$

where N^t_{anc} denotes the number of anchors at time t and with

$$\begin{cases} v^t_{\text{l}} = \max\{a^t_{xl} - r^l_t\}_{l=1:N^t_{\text{anc}}} \\ v^t_{\text{r}} = \min\{a^t_{xl} + r^l_t\}_{l=1:N^t_{\text{anc}}} \\ v^t_{\text{t}} = \min\{a^t_{yl} + r^l_t\}_{l=1:N^t_{\text{anc}}} \\ v^t_{\text{b}} = \max\{a^t_{yl} - r^l_t\}_{l=1:N^t_{\text{anc}}}. \end{cases} \tag{4.29}$$

The circle intersection region is particularly difficult to calculate; moreover, all the range circles often fail to overlap due to ranging errors [36]. In comparison with the circles overlap, the Bounding-box intersection is computationally efficient. The Bounding-box intersection has been found as a highly probable region for the true position to lie inside [69, 182].

Suppose the ranging measurements only observe positive errors, then the target is guaranteed to be within the intersection. Due to the multi-path effect, most of the measured ranges are larger than the actual distance[2]. Moreover, the box has a larger area than the corresponding range circle. Even though the ranging measurements are imprecise, the target is very likely to resist in R_t or be close to R_t. Consequently, the Bounding-box intersection is a highly probable region, which can be used as an instantaneous upper bound for the grid region.

In the case of large negative ranging errors, the Bounding-box intersection may not cover the target. Thus, it is extended by a constant (nega_r)

$$\begin{cases} v^t_{\text{l}} = \max\{a^t_{xl} - r^l_t - \text{nega}_r\}_{l=1:N^t_{\text{anc}}} \\ v^t_{\text{r}} = \min\{a^t_{xl} + r^l_t + \text{nega}_r\}_{l=1:N^t_{\text{anc}}} \\ v^t_{\text{t}} = \min\{a^t_{yl} + r^l_t + \text{nega}_r\}_{l=1:N^t_{\text{anc}}} \\ v^t_{\text{b}} = \max\{a^t_{yl} - r^l_t - \text{nega}_r\}_{l=1:N^t_{\text{anc}}}. \end{cases} \tag{4.30}$$

The value of nega_r should be carefully chosen: if nega_r is too small, it is not robust in the case of large negative ranging error; in contrary, it is computationally inefficient since more grid cells are needed to accommodate the large bound. We set the constant nega_r as the absolute value of the 5th

[2]Indoor ranging statistically observes positive errors, as the percentage of the positive ranging errors is 80%-90% in our indoor experiments; there are only a few negative ranging errors with the absolute value at the most about three meters; especially, NLOS ranging errors can be tens of meters [178].

percentile[3] of the experimental ranging errors. It is easy to understand that the target has a high probability to be inside R_t, as the large negative ranging errors are removed.

2) Grid-based approximation without a prior

The continuous state-space bounded in R_t is uniformly decomposed into N_g grid cells ($\mathbf{G}_t = \{\mathbf{x}_t^i\}_{i=1:N_\mathrm{g}}$), as illustrated Fig. 4.4 [19].

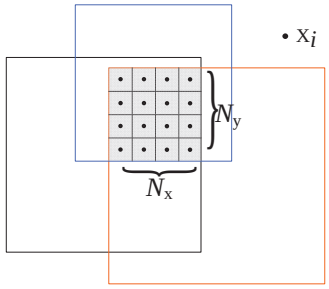

Figure 4.4: Bounded grid-based sampling: the bounded grid region (R) is decomposed into uniform grid cells ($N_\mathrm{g} = N_\mathrm{x} \times N_\mathrm{y}$)

The state density at each time instance is approximated by the weighted grid cells as (4.26). The weight of each grid cell is estimated by the likelihood ($p(\mathbf{z}_t|\mathbf{x}_t^i)$) with in the bound

$$w_t^i = \frac{p(\mathbf{z}_t|\mathbf{x}_t^i)}{\gamma},\ i \in \{i\}_{i=1}^{N_\mathrm{g}}, \tag{4.31}$$

where γ is the normalization factor. The joint likelihood of ranging from N_anc^t reachable anchors at t ($\mathbf{A} = \{\mathbf{a}^l\}_{l=1}^{N_\mathrm{anc}}$) is

$$p(\mathbf{z}_t|\mathbf{x}_t^i) = \prod_{l=1}^{N_\mathrm{anc}^t} p(r_t^l|\left\|\mathbf{x}_t^i - \mathbf{a}_t^l\right\|),\ i \in \{i\}_{i=1}^{N_\mathrm{g}}\ , \tag{4.32}$$

with the measurement model obtained from measurement statistics.

The position is commonly estimated by the expectation of $p(\mathbf{x}_t|\mathbf{z}_t)$ w.r.t. the grid and the normalized weights

$$\hat{\mathbf{x}}_t = \mathrm{E}[p(\mathbf{x}_t|\mathbf{z}_t)] = \mathbf{w}_t \cdot \mathbf{G}_t. \tag{4.33}$$

The pseudo-code of BGE is given by **Algorithm** 9.

[3]Ignoring the 5th percentile of the ranging errors is a reasonable compromise for setting the lower limit of the negative errors, whereas, other values are also applicable.

Algorithm 9 Bounded Grid-based estimation (BGE)

Output and input: $[\hat{\mathbf{x}}_t] = \mathrm{BGE}\,[\mathbf{z}_t, \mathbf{A}_t]$
Setting: N_g, $p(r|\,\|\mathbf{x}-\mathbf{a}\|)$ and nega_r

1: Derive instantaneous bound R_t by (4.29) or (4.30)
2: Grid-based sampling $\mathbf{G}_t$ from R_t
3: Assign weights $\{w_t^i\}_{i=1:N_\mathrm{g}}$ (4.31)
4: Estimate position $\hat{\mathbf{x}}_t$ (4.33)

Incorporation of the instantaneous upper bound on the grid region greatly reduces the sample size required for accurate positioning. The idea is that, rather than predefining the grid region or involving the history measurements, the bound R is derived from the ranging measurements of each positioning trial.

Recursively Bounded Grid-based Filter (RBGF)

In sequential estimation, the time-series measurements, position estimation and motion information are potential to refine the bound. Thus, the posterior of the target's position is recursively evaluated by the weighted samples in the bounded region, namely, a recursively bounded Grid-based filter (RBGF).

1) A recursive upper bound (B_t)

Grid-based filter sequentially performs numerical integration by uniformly discretizing the continuous state-space into a finite number (N_g) of an evenly spaced grid of points. The sample-space at t is confined by an intersection operation of B_{t-1} and R_t (see Fig. 4.5(a)), based on the assumption the target motion is slow

$$B_t = B_{t-1} \cap R_t \ . \tag{4.34}$$

The true state probably lies inside B_t, as the target has a high confidence to be inside in both R_t and B_{t-1}.

Obviously, the size of the bound (B_t) by (4.34) can only decrease with time. To avoid the bound to be too small after a few recursions, we take a union operation of (4.34) and $R_\mathrm{robust}(\hat{\mathbf{x}}_{t-1})$ (a square with the side length of l_robust and the center at the previous estimated position $\hat{\mathbf{x}}_{t-1}$)

$$B_t = (B_{t-1} \cap R_t) \cup R_\mathrm{robust}(\hat{\mathbf{x}}_{t-1}) \ . \tag{4.35}$$

As illustrated in Fig. 4.5(b), the bound (B_t) of (4.35) is the minimum box which covers both $B_{t-1} \cap R_t$ (4.34) and $R_\mathrm{robust}(\hat{\mathbf{x}}_{t-1})$. The $R_\mathrm{robust}(\hat{\mathbf{x}}_{t-1})$ should take a reasonable size. If l_robust is too large, then B_t might involve much posterior tail and cause higher computation. On the contrary, B_t can be

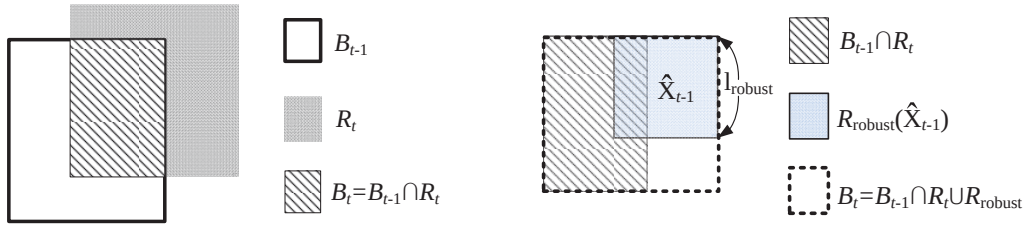

(a) The B_t of Eq. (4.34)

(b) The B_t of Eq. (4.35)

Figure 4.5: Recursive bound (B_t) on the grid-space derived from both the current ranging measurements and the previous position estimation

unrepresentable for the important posterior. Additionally, l_{robust} should be larger than the average motion of the target, as the target's movement has not been considered in $B_{t-1} \cap R_t$.

Then, the state-space is recursively bounded by B_t and decomposed into uniform grid-based samples ($\mathbf{G}_t = \{\mathbf{x}_t^i\}_{i=1:N_g}$). Since the bound maintains a reasonable size and focuses on the important posterior, the sample impoverishment problem does not exist. Moreover, the cells at each recursion are around the actual position as considering both the old estimation and the new observation. More importantly, the worst positioning error of NLOS ranges can be bounded inside B_t.

2) Grid-based Bayesian recursion

With the samples drawn from B_t, the weight of each grid cell is

$$w_{t|t}^i = \frac{p(\mathbf{z}_t|\mathbf{x}_t^i, \mathbf{z}_{1:t-1}) w_{t|t-1}^i}{\gamma},\ i \in \{i\}_{i=1}^{N_g}\ , \tag{4.36}$$

where the denominator (γ) is for normalization. Assuming current measurements are independent of the previous, we have

$$p(\mathbf{z}_t|\mathbf{x}_t^i, \mathbf{z}_{1:t-1}) = p(\mathbf{z}_t|\mathbf{x}_t^i)\ . \tag{4.37}$$

Similar to (2.83), the prior of the grid-based filter is numerically approximated into

$$w_{t|t-1}^i \approx \sum_{j=1}^{N_g} p(\mathbf{x}_t^i|\mathbf{x}_{t-1}^j) w_{t-1|t-1}^j,\ i \in \{i\}_{i=1}^{N_g}\ . \tag{4.38}$$

Then, the weight vector is expressed as

$$\mathbf{w}_t = \{w^i_{t|t}\}_{i=1:N_\mathrm{g}},\ w^i_{t|t} = p(\mathbf{z}_t|\mathbf{x}^i_t)\sum_{j=1}^{N_\mathrm{g}} p(\mathbf{x}^i_t|\mathbf{x}^j_{t-1})w^j_{t-1|t-1}\ , \tag{4.39}$$

and a normalization $\left\{ w^i_{t|t} = \frac{w^i_{t|t}}{\sum_{i=1}^{N_\mathrm{p}} w^i_{t|t}} \right\}_{i=1:N_\mathrm{p}}$.

The tracking estimate is the MMSE estimation of $p(\mathbf{x}_t|\mathbf{z}_{1:t})$

$$\hat{\mathbf{x}}_t = \mathrm{E}[p(\mathbf{x}_t|\mathbf{z}_{1:t})] = \mathbf{w}_t \cdot \mathbf{G}_t = \sum_{i=1}^{N_\mathrm{g}} \left(\mathbf{x}^i_t w^i_{t|t}\right)\ . \tag{4.40}$$

The pseudo-code of RBGF is given by **Algorithm** 10.

Algorithm 10 Recursively Bounded Grid-based Filter (RBGF)

Output and input: $[\hat{\mathbf{x}}_t, B_t, \{w^i_t\}_{i=1:N_\mathrm{g}}] = \mathrm{RBGF}\,[\mathbf{z}_t, \mathbf{A}_t, \hat{\mathbf{x}}_{t-1}, B_{t-1}, \mathbf{w}_{t-1}]$
Setting: N_g, l_robust, $p(\mathbf{x}_t|\mathbf{x}_{t-1})$, $p(r|\,\|\mathbf{x}-\mathbf{a}\|)$ and nega_r
Initialization: $B^0 = R_1$, $\hat{\mathbf{x}}^0$, $\left\{w^i_{0|0} = \frac{1}{N_\mathrm{g}}\right\}_{i=1:N_\mathrm{g}}$ and $t = 1$

1: Recurse B_t (4.35)
2: Grid-based sampling $\mathbf{G}_t$ from B_t, and $\mathbf{G}_{t-1}$ from B_{t-1}
3: Assign weights $\{w^i_{t|t}\}_{i=1:N_\mathrm{g}}$ (4.39)
4: Estimate position $\hat{\mathbf{x}}_t$ (4.40)
5: Set $t = t + 1$ and iterate to item 1.

Note that the prior at each grid sample according to (4.38) is calculated by the integral over the whole previous grid; consequently, the very small old weights cannot severely influence the prior, which combats the sample degeneracy. Moreover, only a small number of grid cells are needed to represent the posterior as the grid region is the recursive bounded.

3) Bounded Grid-based Filter with Approximated-prior (BGF-A and RBGF-A)

According to Eq. (4.38), calculating the prior of each grid cell needs to be integrated over the previous state samples. Obviously, if the prior of each grid sample can be approximated instead of the integral in (4.38), the computation can be substantially reduced. Therefore, the approximation is taken

$$\sum_{j=1}^{N_\mathrm{g}} p(\mathbf{x}^i_t|\mathbf{x}^j_{t-1})w^j_{t-1|t-1} \approx p(\mathbf{x}^i_t|\mathrm{E}[p(\mathbf{x}_{t-1}|\mathbf{z}_{t-1})]) \approx p(\mathbf{x}^i_t|\hat{\mathbf{x}}_{t-1})\ . \tag{4.41}$$

Then, the prior of (4.38) is approximated as

$$w^i_{t|t-1} \approx p(\mathbf{x}^i_t|\hat{\mathbf{x}}_{t-1}) \,, \tag{4.42}$$

with a time-invariant model $p(\mathbf{x}^i_t|\hat{\mathbf{x}}_{t-1}) \sim \mathcal{N}(\mu_{\text{prior}}, \sigma^2_{\text{prior}})$: μ_{prior} describes the average target motion between two time-steps, and σ_{prior} for the movement uncertainty.

The weight vector using an approximated prior is

$$\mathbf{w}_t = \{w^i_{t|t}\}_{i=1:N_\text{g}}, \; w^i_{t|t} = \frac{p(\mathbf{z}_t|\mathbf{x}^i_t)p(\mathbf{x}^i_t|\hat{\mathbf{x}}_{t-1})}{\gamma} \,. \tag{4.43}$$

The BGF-A or RBGF-A is more efficient in the weight update. Meanwhile, it can be expected that the approximation (4.41) will approximate the Chapman-Kolmogorov equation when the prior distribution has one significant mode. The pseudo-code is given by **Algorithm** 11.

Algorithm 11 Bounded Grid-based Filter with Approximated-prior (BGF-A/ RBGF-A)

Output and input: $[\hat{\mathbf{x}}_t, B_t] = \text{BGF} - \text{A/RBGF} - \text{A}\,[\mathbf{z}_t, \mathbf{A}_t, \hat{\mathbf{x}}_{t-1}, B_{t-1}]$
Setting: N_g, l_{robust}, $p(\mathbf{x}_t|\hat{\mathbf{x}}_{t-1})$, $p(r|\,\|\mathbf{x}-\mathbf{a}\|)$ and nega_r
Initialization: $B^0 = R_1$, $\hat{\mathbf{x}}^0$, $\left\{w^i_{0|0} = \frac{1}{N_\text{g}}\right\}_{i=1:N_\text{g}}$ and $t = 1$

1: Obtain R_t (4.30) or B_t (4.35)
2: Grid-based sampling $\mathbf{G}_t$ from the grid bound
3: Assign weights $\{w^i_t|t\}_{i=1:N_\text{g}}$ (4.43)
4: Estimate position $\hat{\mathbf{x}}_t$ (4.40)
5: Set $t = t + 1$ and iterate to item 1.

4.2.2 Geometric sampling

This subsection develops a sampling method based on the geometric relation of the current ranging measurements, namely geometric sampling. The key idea is to obtain the crossing points of every pair-wise ranging circles.

Motivation

Figure 4.6 illustrates the likelihood of the position estimation with three simulated ranging. The ranging measurements in Fig. 4.6 (a) is the true range; while the ranging in Fig. 4.6 (b) observes a an additive Gaussian error ($\mathcal{N}(3, 3^2)$). The likelihood is calculated using a Gaussian model $\mathcal{N}(3, 3^2)$.

Figure 4.6 indicates that, no matter whether the ranging is ideal (Fig. 4.6 (a)) or noisy (Fig. 4.6 (b)), the state density is extremely non-Gaussian and non-convex. As a consequence, direct Monte Carlo sampling encounters difficulty of the non-Gaussian and nonlinear state space. Furthermore,

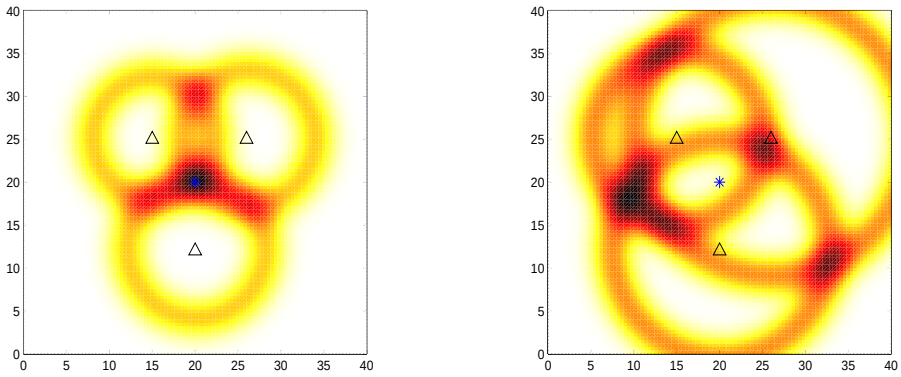

(a) Probability with three ideal ranges

(b) Probability with three noisy ranges

Figure 4.6: Probability distribution of 2D positioning with three ranges in the playing field of 40×40 unit^2 represented by 100×100 discrete points: two ranging cases are considered as the ideal (Fig. 4.6 (a)) and noisy (Fig. 4.6 (b)); '*' at the center ([20,20] unit) denotes the true position of the target; '△' for the anchors. The color of each point describes the probability of the target being located at the point: the darker the color is, the higher the probability is.

sampling from a prediction density can be questionable because of overlooking the newly arrived observations [17]. The bounded grid-based sampling introduced in the previous subsection remarkably improves the efficiency, but it still contains some irrelevant samples.

The geometric relation of one trial experimental ranging is depicted in Figure 4.7: among the six measurements, some observe LOS errors, whereas, the others get NLOS errors; as one can see, the true target position is close to some crossing points of the LOS circles, and far away from the other crossing points of the NLOS circles. It implies that the crossing points of LOS range circles can be good samples of the state estimation of the target's position. Therefore, the samples can be naturally drawn from the constraints of the current ranging geometry, instead of using the prediction density or grid-search.

Geometric Position Estimation (GeoE)

1) Geometric sampling

We hold that in the presence of a few line-of-sight (LOS) ranging, the state space can be effectively confined by the geometries of ranging measurements. These geometric points are obtained based on the relationship between a pairwise range circles, which is categorized into five types as shown in Fig. 4.8. There are five types of the two circle geometry, including the external circles,

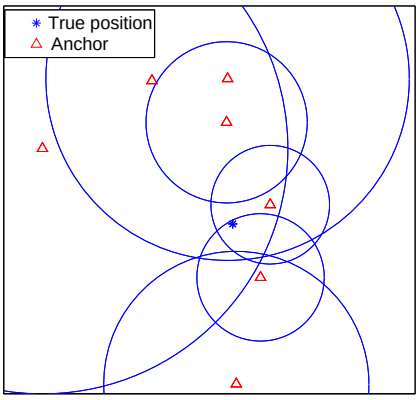

Figure 4.7: Geometry of one trial of real-world ranging: the circles represent the disk model of the ranging; △ denotes the anchors and '*' for the true position

internal circles, externally tangent, internally tangent and secant circles (the concentric circles are not considered, because the anchors are generally not deployed at the same place).

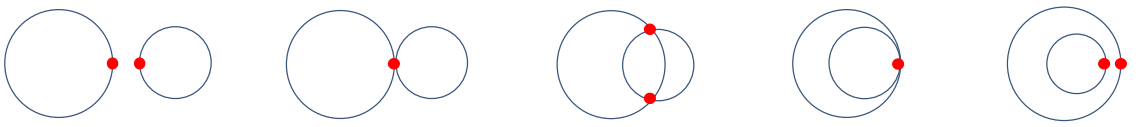

a) External circles b) Externally Tangent c) Secant circles d) Internally Tangent e) Internal circles

Figure 4.8: Geometry of two ranging circles

Let $\mathbf{A} = \{\mathbf{a}^l\}_{l=1}^{N_{\text{anc}}}$ be the 2D rectangular coordinates of N_{anc} reachable anchors, thus, the distances between two anchors is

$$d_{mn} = \left\|\mathbf{a}^m - \mathbf{a}^n\right\|, \; m \in \{\cdot\}_1^{N_{\text{anc}}^t}, \; n \in \{\cdot\}_1^{N_{\text{anc}}^t}, \; m \neq n \, . \tag{4.44}$$

Then, the geometric relationship can be derived with d_{mn} and the anchor deployments

$$\begin{cases} \textbf{if } d_{mn} > r_m + r_n, \textbf{then Fig.4.8(a)} \\ \textbf{elseif } d_{mn} == r_m + r_n, \textbf{then Fig.4.8(b)} \\ \textbf{elseif } d_{mn} < r_n + r_m \\ \quad \textbf{if } d_{mn} > |r_n - r_m|, \textbf{ then Fig.4.8(c)} \\ \quad \textbf{elseif } d_{mn} == |r_n - r_m|, \textbf{ then Fig.4.8(d)} \\ \quad \textbf{else Fig.4.8(e)} \\ \quad \textbf{endif} \\ \textbf{endif} \end{cases} \tag{4.45}$$

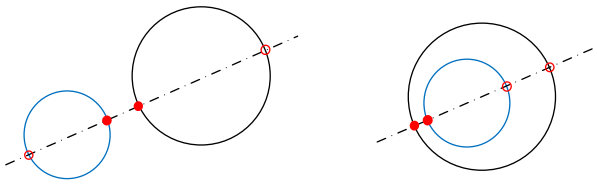

a) External circles b) Internal circles

Figure 4.9: Two nearest points (the solid dots) of the external/internal circles

The geometric points of Fig. 4.8 (b), (c) and (d) are the solutions of the two circle equations. Additionally, the tangent point is duplicated as two geometric samples. For the external and the internal cases in Fig. 4.8 (a) and (e), the line through the two circle centers makes four crossing points with the two circles (see Fig. 4.9). The two nearest points between the two circles are more rational to be close to the target. Hence, the pair of the crossing points nearest to each other are selected as the geometric samples. With N_{anc} ranging circles, one can obtain $N_{\text{anc}} \times (N_{\text{anc}} - 1)$ tangent points, crossing points or nearest points, which are defined as the state samples.

2) Geometric position estimation (GeoE)

Based on the geometric samples $(\{\mathbf{x}_t^i\}_{i=1:N_{\text{anc}}^t(N_{\text{anc}}^t-1)})$, the position estimation in (4.26) is evaluated

with the associated weights ($\mathbf{w}_t = \{w_t^i\}_{i=1:N_{\text{anc}}^t(N_{\text{anc}}^t-1)}$):

$$p(\mathbf{x}_t|\mathbf{z}_t) \approx \sum_{i=1}^{N_{\text{anc}}^t\times(N_{\text{anc}}^t-1)} w_t^i \delta(\mathbf{x}_t - \mathbf{x}_t^i)\,, \tag{4.46}$$

where $\mathbf{x}_t^i$ is the ith samples based on the range geometry and the sample size ($N_{\text{anc}}^t \times (N_{\text{anc}}^t - 1)$) varies at different time. The weights are the normalized likelihood

$$w_t^i = \frac{p(\mathbf{z}_t|\mathbf{x}_t^i)}{\sum_{j=1}^{N_{\text{anc}}^t\times(N_{\text{anc}}^t-1)} p(\mathbf{z}_t|\mathbf{x}_t^j)},\ i \in \{\cdot\}_1^{N_{\text{anc}}^t\times(N_{\text{anc}}^t-1)}\,. \tag{4.47}$$

The likelihood ($p(\mathbf{z}_t|\mathbf{x}_t^i)$) is the joint probability of N_{anc}^t measurements as (4.32).

The position is estimated by the weighted geometric samples

$$\hat{\mathbf{x}}_t = \text{E}(p(\mathbf{x}_t|\mathbf{z}_t)) = \sum_{i=1}^{N_{\text{anc}}^t\times(N_{\text{anc}}^t-1)} \mathbf{x}_t^i w_t^i\,. \tag{4.48}$$

The pseudo-code of GeoE is described in **Algorithm** 12.

Algorithm 12 Geometric Position Estimation (GeoE)

Output and input: $[\hat{\mathbf{x}}_t] = \text{GeoE}\,[\mathbf{z}_t, \mathbf{A}_t]$
Setting: $p(r|\,\|\mathbf{x}-\mathbf{a}\|)$

1: Geometric sampling $\{\mathbf{x}_t^i\}_{i=1}^{N_{\text{anc}}^t\times(N_{\text{anc}}^t-1)}$ (4.45)
2: Weights assignment $\{w_t^i\}_{i=1:N_{\text{p}}}$ (4.32) and (4.47)
3: Estimate position $\hat{\mathbf{x}}_t$ (4.48)

Geometric Bayesian Filter (GeoF)

In sequential state estimation, the state propagation trusting the previous state density can be problematic. The geometric interpretation of the latest ranging measurements is an intuitive solution to predict the state. Applying the geometric sampling on the filter frame, it is similar to other Bayesian filters in the numerical integration but differs in the way of drawing the samples.

1) Geometric Bayesian filter (GeoF)

Given the ranging measurements ($\mathbf{z}_t$) up to t, the posterior density of the target's position at t is numerically approximated by $N_{\text{anc}}^t(N_{\text{anc}}^t - 1)$ geometric samples associated with weights (w_t^i) as (4.46). The weights are jointly determined by the measurement model ($p(r_t^l|\mathbf{x}_t^i)$), the state propaga-

tion model ($p(\mathbf{x}_t^i|\hat{\mathbf{x}}_{t-1})$) and the old posterior ($p(\mathbf{x}_{t-1}^i|\hat{\mathbf{x}}_{t-1})$)

$$w_t^i \approx \frac{p(\mathbf{z}_t|\mathbf{x}_t^i)p(\mathbf{x}_t^i|\mathbf{z}_{1:t-1})}{\gamma},\ i \in \{\cdot\}_1^{N_{\text{anc}}^t \times (N_{\text{anc}}^t - 1)}, \tag{4.49}$$

with γ denoting the normalization constant over all the weights. The likelihood is the joint probability of N_{anc}^t measurements as (4.32). By assuming the state propagation as a Markov process of order one, we obtain

$$p(\mathbf{x}_t^i|\mathbf{z}_{1:t-1}) = \sum_{j=1}^{N_{\text{anc}}^{t-1} \times (N_{\text{anc}}^{t-1} - 1)} p(\mathbf{x}_t^i|\mathbf{x}_{t-1}^j) w_{t-1}^j,\ i \in \{\cdot\}_1^{N_{\text{anc}}^t \times (N_{\text{anc}}^t - 1)}. \tag{4.50}$$

Then the position of GeoF is the posterior expectation as (4.48), with the pseudo-code in **Algorithm** 13.

Algorithm 13 Geometric Bayesian Filter (GeoF)

Output and input: $\left[\hat{\mathbf{x}}_t, \left\{\mathbf{x}_t^i, w_t^i\right\}_{i=1}^{N_{\text{anc}}^t \times (N_{\text{anc}}^t - 1)}\right] = \text{GeoF}\left[\mathbf{z}_t, \mathbf{A}_t, \left\{\mathbf{x}_{t-1}^i, w_{t-1}^i\right\}_{i=1}^{N_{\text{anc}}^{t-1} \times (N_{\text{anc}}^{t-1} - 1)}\right]$

Setting: $p(\mathbf{x}_t|\mathbf{x}_{t-1})$, $p(r|\,\|\mathbf{x} - \mathbf{a}\|)$

Initialization: $\{\mathbf{x}_0^i, w_0^i\}_{i=1}^{N_{\text{anc}}^0 \times (N_{\text{anc}}^0 - 1)}$ and $t = 1$

1: Geometric sampling $\{\mathbf{x}_t^i\}_{i=1}^{N_{\text{anc}}^t \times (N_{\text{anc}}^t - 1)}$ (4.45)
2: Weights assignment $\{w_t^i\}_{i=1:N_{\text{anc}}^t \times (N_{\text{anc}}^t - 1)}$ (4.50), (4.32) and (4.49)
3: Estimate position $\hat{\mathbf{x}}_t$ (4.48)
4: Set $t = t + 1$ and iterate to item 1.

The probabilistic estimation turns to interpret and evaluate these geometric points, which efficiently reduces the sampling complexity the and skips resampling. One can expect that a majority of the geometric samples will be present nearby the true target's position.

2) Geometric Filter with Approximated-prior (GeoF-A)

Similar to the prior approximation in (4.41), the integral over the previous samples can be avoided by

$$p(\mathbf{x}_t^i|\mathbf{z}_{1:t-1}) = \sum_{j=1}^{N_{\text{anc}}^t \times (N_{\text{anc}}^t - 1)} p(\mathbf{x}_t^i|\mathbf{x}_{t-1}^j) w_{t-1|t-1}^j \approx p(\mathbf{x}_t^i|\hat{\mathbf{x}}_{t-1}). \tag{4.51}$$

Compared with GeoF, GeoF-A neither keeps all the samples in memory nor updates for integral of (4.50), which is more efficient. The pseudo-code of GeoF-A is described in **Algorithm** 14.

The downside of the geometric sampling is that it causes high computation, and the sampling

Algorithm 14 Geometric Bayesian Filter with Approximated-prior (GeoF-A)

Output and input: $[\hat{\mathbf{x}}_t] = \text{GeoF} - \text{A}\,[\mathbf{z}_t, \mathbf{A}_t, \hat{\mathbf{x}}_{t-1}]$
Setting: $p(\mathbf{x}_t|\mathbf{x}_{t-1})$, $p(r|\,\|\mathbf{x}-\mathbf{a}\|)$
Initialization: $\hat{\mathbf{x}}_0$ and $t = 1$

1: Geometric sampling $\{\mathbf{x}_t^i\}_{i=1}^{N_{\text{anc}}^t \times (N_{\text{anc}}^t - 1)}$ (4.45)
2: Weights assignment $\{w_t^i\}_{i=1:N_{\text{p}}}$ (4.51), (4.32) and (4.49)
3: Estimate position $\hat{\mathbf{x}}_t$ (4.48)
4: Set $t = t + 1$ and iterate to item 1.

solely depends on the current observation rather than all the history observations. Thus, the valuable history information is thereby ignored. It is hoped that the prior in (4.50) or (4.51) can be an informative density (such as a peaked distribution), so as to make a good evaluation of the geometric samples.

4.2.3 Polar sampling

The state density of 2D position estimation is a highly complex distribution requiring a greater number of samples to correctly represent [19]. Even if the measurement error is assumed to be Gaussian, the constellation of the state density can be significantly multi-modal, as depicted in Fig. 4.10.

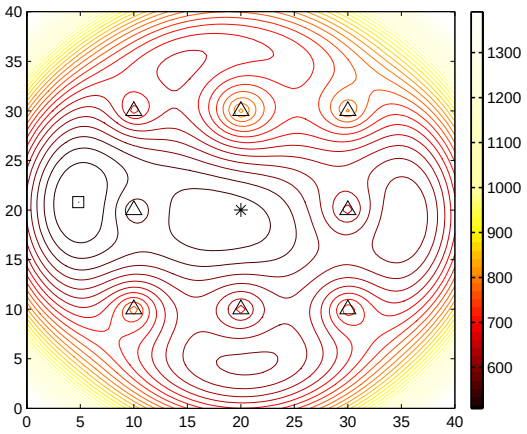

Figure 4.10: Multi-modal state-space of 2D positioning

The commonly used sampling density is a unimodal density, failing to represent the highly irregular state density. Additionally, the resampling step always tends to cluster to one mode and

becomes cumbersome in NLOS conditions. Instead of rendering the state in rectangular coordinate, this subsection proposes to sample in polar coordinate, namely, polar sampling. The very aim of the polar sampling is to maintain a multi-modal sampling density.

Polar coordinates of 2D positioning

The model structure of polar sampling is represented by the polar coordinates (ρ, φ)

$$\rho = \sqrt{(x - a_{xl})^2 + (y - a_{yl})^2} \tag{4.52}$$

$$\varphi = \arctan\left(\frac{y - a_{yl}}{x - a_{xl}}\right), \tag{4.53}$$

where ρ is the ranging measurement, and φ is the angle of the state with each anchor's position being the pole.

The uncertainty in polar coordinate is

$$\hat{\rho} = \rho + u \tag{4.54}$$

$$\hat{\varphi} = \varphi + v\,, \tag{4.55}$$

where u and v are assumed as the measurement error model and the motion model, respectively.

The model transformation from polar coordinate to rectangular coordinate is

$$\mathbf{x} = \begin{cases} x = \rho\cos(\varphi) + a_{xl} \\ y = \rho\sin(\varphi) + a_{yl} \end{cases}. \tag{4.56}$$

with (a_{xl}, a_{yl}) be the rectangular coordinates of the anchors.

Sequential estimation with polar sampling

For sequential estimation, the optimal sampling density $p(\mathbf{x}_t|\mathbf{x}_{t-1}, \mathbf{z}_t)$ is transformed into polar coordinate with two independent components $(p(\mathbf{z}_t), p(\varphi_t|\varphi_{t-1}, \mathbf{z}_t))$. The first component is the ranging measurement, which can be easily sampled in radial coordinate; the second one is the motion model $(p(\varphi_t|\varphi_{t-1}))$ in angular coordinate. Thus, the polar coordinates of the sequential state given the lth range measurement at t is expressed as

$$\rho_t^l = r_t^l + u, \quad l \in \{\cdot\}_1^{N_{\text{anc}}^t}, \tag{4.57}$$

$$\varphi_t^l = f(\varphi_{t-1}^l) + v, \quad l \in \{\cdot\}_1^{N_{\text{anc}}^t}. \tag{4.58}$$

Known the models of u and v, the state samples in polar coordinate are generated as

$$\rho_t^{l,i} \sim r_t^l + u, \quad l \in \{\cdot\}_1^{N_{\text{anc}}^t}, \quad i \in \{\cdot\}_1^{N_{r,\varphi}} \tag{4.59}$$

$$\varphi_t^{l,i} \sim p(\varphi_t^l | \varphi_{t-1}^l), \quad l \in \{\cdot\}_1^{N_{\text{anc}}^t}, \quad i \in \{\cdot\}_1^{N_{r,\varphi}} . \tag{4.60}$$

where $N_{r,\varphi}$ is the number of samples per ranging measurement. Then, the state samples are transformed into rectangular coordinate

$$\mathbf{x}_t^{l,i} = \begin{cases} x_t^{l,i} = \rho_t^{l,i} \cos(\varphi_t^{l,i}) + a_{xl}, & l \in \{\cdot\}_1^{N_{\text{anc}}^t}, \quad i \in \{\cdot\}_1^{N_{r,\varphi}} \\ y_t^{l,i} = \rho_t^{l,i} \sin(\varphi_t^{l,i}) + a_{yl}, & l \in \{\cdot\}_1^{N_{\text{anc}}^t}, \quad i \in \{\cdot\}_1^{N_{r,\varphi}} \end{cases} . \tag{4.61}$$

The polar sampling is illustrated in Fig. 4.11(a). To reduce the total sample size, deterministic sampling is employed in radial coordinate, which takes only two values: the current ranging measurements and the predicted ranges

$$\rho_t^{l,i} = \{r_t^l, \hat{r}_t^l\}, \quad l \in \{\cdot\}_1^{N_{\text{anc}}^t}, \quad i \in \{\cdot\}_1^{N_{r,\varphi}} , \tag{4.62}$$

where $\hat{r}_t^l = \|\hat{\mathbf{x}}_{t-1} - \mathbf{a}_t^l\|$ is the predicted range. The polar sampling with deterministic sampling in radial coordinate is depicted in Fig. 4.11(b).

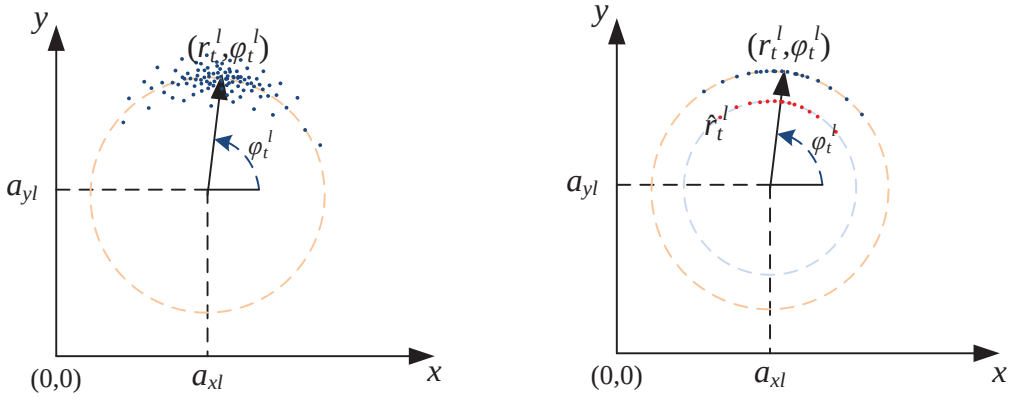

(a) Random sampling in both angular coordinate and radial coordinate assuming Gaussian models

(b) Random sampling in angular coordinate with a Gaussian model, and deterministic sampling in radial coordinate taking the two values: the current measured range (r_t) and the predicted range ($\hat{r}_t$)

Figure 4.11: Polar sampling of one ranging measurement in 2D rectangular coordinate

Since the velocity of the target is small, the state propagation in angular coordinate is defined to a Gaussian model $p(\varphi_t^l|\varphi_{t-1}^l) \sim \mathcal{N}(\varphi_{t-1}^l, \sigma_\varphi^2)$

$$\sigma_\varphi = \arctan(\sigma_{\mathbf{x}_t|\mathbf{x}_{t-1}}/r) \,, \tag{4.63}$$

where $\sigma_{\mathbf{x}_t|\mathbf{x}_{t-1}}$ is the standard deviation of $p(\mathbf{x}_t|\mathbf{x}_{t-1})$ in rectangular coordinate.

Then, the sample set in polar coordinate is $\{\{r_t^l, \hat{r}_t^l\},\ \varphi_t^{l,i}\}_{\{i=1:N_{r,\varphi},\ l=1:N_{\text{anc}}^t\}}$. This sample set are converted into rectangular coordinate (4.61)

$$\{\mathbf{x}_t^{l,i}\}_{\{i=1:2\times N_{r,\varphi},\ l=1:N_{\text{anc}}^t\}} \,. \tag{4.64}$$

On the Bayesian frame, the samples in rectangular coordinate is weighted as

$$w_t^{l,i} = \frac{p(\mathbf{z}_t|\mathbf{x}_t^{l,i})p(\mathbf{x}_t^{l,i}|\mathbf{z}_{1:t-1})}{\gamma},\ \ l \in \{\cdot\}_1^{N_{\text{anc}}^t},\ \ i \in \{\cdot\}_1^{2\times N_{r,\varphi}} \,, \tag{4.65}$$

with γ denoting the normalization constant. The likelihood of the (l,i)th sample is

$$p(\mathbf{z}_t|\mathbf{x}_t^{l,i}) = \prod_{k=1}^{N_{\text{anc}}^t} p(r_t^k|\left\|\mathbf{x}_t^{l,i} - \mathbf{a}_t^l\right\|),\ \ l \in \{\cdot\}_1^{N_{\text{anc}}^t},\ \ i \in \{\cdot\}_1^{2\times N_{r,\varphi}} \,, \tag{4.66}$$

where $\mathbf{a}_t^l$ is the rectangular coordinates of lth anchor. The prior with a first-order Markov chain over the state propagation is

$$p(\mathbf{x}_t^{l,i}|\mathbf{z}_{1:t-1}) = \sum_{k=1}^{N_{\text{anc}}^{t-1}} \sum_{j=1}^{2\times N_{r,\varphi}} p(\mathbf{x}_t^{l,i}|\mathbf{x}_{t-1}^{k,j}) w_{t-1}^{k,j},\ \ l \in \{\cdot\}_1^{N_{\text{anc}}^t},\ \ i \in \{\cdot\}_1^{2\times N_{r,\varphi}} \,. \tag{4.67}$$

The pseudo-code of the Bayesian Filter with Polar Sampling (PolarF) is in **Algorithm** 15.

2) Bayesian Filter with Polar Sampling and Approximated-prior (PolarF-A)

According to (4.41), the prior is approximated

$$p(\mathbf{x}_t^{l,i}|\mathbf{z}_{1:t-1}) \approx p(\mathbf{x}_t^{l,i}|\hat{\mathbf{x}}_{t-1}) \,. \tag{4.68}$$

The pseudo-code of PolarF-A is described in **Algorithm** 16.

Algorithm 15 Bayesian Filter with Polar Sampling (PolarF)

Output and input: $\left[\hat{\mathbf{x}}_t,\ \left\{\mathbf{x}_t^{l,i},\ w_t^{l,i}\right\}_{\{i=1:2\times N_{r,\varphi},\ l=1:N_{\text{anc}}^t\}}\right] = \text{PolarF}\left[\mathbf{z}_t,\ \mathbf{A}_t,\ \left\{\mathbf{x}_{t-1}^{l,i},\ w_{t-1}^{l,i}\right\}_{\{i=1:2\times N_{r,\varphi},\ l=1:N_{\text{anc}}^{t-1}\}}\right]$
Setting: $p(\mathbf{x}_t|\mathbf{x}_{t-1})$, $p(r|\,\|\mathbf{x}-\mathbf{a}\|)$
Initialization: $\left\{\mathbf{x}_0^{l,i},\ w_0^{l,i}\right\}_{\{i=1:2\times N_{r,\varphi},\ l=1:N_{\text{anc}}^0\}}$ and $t=1$

1: Polar sampling $\left\{\mathbf{x}_t^{l,i},\ w_t^{l,i}\right\}_{\{i=1:2\times N_{r,\varphi},\ l=1:N_{\text{anc}}^t\}}$ (4.61)
2: Assign weights $\{w_t^i\}_{i=1:N_{\text{anc}}^t\times 2\times N_{r,\varphi}}$ (4.67), (4.66) and (4.65)
3: Estimate position $\hat{\mathbf{x}}_t$ (4.48)
4: Set $t=t+1$ and iterate to item 1.

Algorithm 16 Bayesian Filter Polar Sampling with Approximated-prior (PolarF-A)

Output and input: $\left[\hat{\mathbf{x}}_t,\ \left\{\mathbf{x}_t^{l,i},\ w_t^{l,i}\right\}_{\{i=1:2\times N_{r,\varphi},\ l=1:N_{\text{anc}}^t\}}\right] = \text{PolarF}-\text{A}\,[\mathbf{z}_t,\ \mathbf{A}_t,\ ,\hat{\mathbf{x}}_{t-1}]$
Setting: $p(\mathbf{x}_t|\mathbf{x}_{t-1})$, $p(r|\,\|\mathbf{x}-\mathbf{a}\|)$
Initialization: $\hat{\mathbf{x}}_0$ and $t=1$

1: Polar sampling $\left\{\mathbf{x}_t^{l,i},\ w_t^{l,i}\right\}_{\{i=1:2\times N_{r,\varphi},\ l=1:N_{\text{anc}}^t\}}$ (4.61)
2: Assign weights $\{w_t^i\}_{i=1:N_{\text{anc}}^t\times 2\times N_{r,\varphi}}$ (4.68), (4.66) and (4.65)
3: Estimate position $\hat{\mathbf{x}}_t$ (4.48)
4: Set $t=t+1$ and iterate to item 1.

4.2.4 Gradual Gaussian approximation

In the case of vague prior or likelihood, sample-based probabilistic solutions are subject to the problem of sample divergence. Thus, the Gradual Gaussian sampling (GGS) is developed, using an iteration method with a small step size.

Gradual Gaussian Sampling (GGS)

After obtaining the $p(\mathbf{x}_t|\mathbf{z}_t)$, the posterior can be refined by the gradual sampling as

$$p(\mathbf{x}^*{}_{t,k}|\mathbf{z}_t) = \frac{p(\mathbf{z}_t|\mathbf{x}^*{}_{t,k}) \int p(\mathbf{x}^*{}_{t,k}|\mathbf{x}_t)p(\mathbf{x}_t)\, d\mathbf{x}_t}{\gamma} , \tag{4.69}$$

where $k \in \{\cdot\}_{k=1}^{N_{\text{Gradu}}}$ is the index of the gradual iteration; $\mathbf{x}^*{}_{t,k}$ is the state samples of the kth gradual iteration.

The key idea of the gradual sampling is to gradually converge the samples from the prediction density to the true posterior by a series of sampling. To keep a simple implementation, the gradual sampling should employ an easy-to-sample-from density. Thus, this subsection uses the Gradual Gaussian Sampling (GGS).

At each time-step of positioning, the GGS-based position estimation consists of two components:

1. **A general probabilistic frame:** the state samples are generated and evaluated by a sample-based probabilistic frame, such as the Generic-PF (without resampling) in **Algorithm** 4;
2. **GGS:** the state $(\{\mathbf{x}^*{}^i_{t,k},\ w^{*i}_{t,k}\}_{i=1:N_s})$ are iteratively approximated by a Gaussian density. Firstly, the Gaussian density is obtained $(\mathcal{N}(\mu^*_{t,k}, \sigma^{*2}_{t,k}))$

$$\mu^*_{t,k} = \sum_{i=1}^{N_s} \mathbf{x}^*{}^i_{t,k} w^{*i}_{t,k} , \tag{4.70}$$

$$\sigma^{*2}_{t,k} = \sum_{i=1}^{N_s} w^{*i}_{t,k} \left\| \mathbf{x}^*{}^i_{t,k} - \mu^*_{t,k} \right\|^2 . \tag{4.71}$$

Then, the state samples are drawn from $\mathcal{N}(\mu^*_{t,k}, \sigma^{*2}_{t,k})$. On the Generic-PF frame, the weights is assigned

$$\left\{ w^{*i}_{t,k} = w^i_{t-1} \frac{p(\mathbf{z}_t|\mathbf{x}^{*i}_{t,k}) p(\mathbf{x}^{*i}_{t,k}|\mathbf{x}^i_{t-1})}{\mathcal{N}(\mathbf{x}^{*i}_{t,k}; \mu^*_{t,k}, \sigma^{*2}_{t,k})} \right\}_{i=1:N_s} . \tag{4.72}$$

The illustration of GGS is depicted in Fig. 4.12, as the sample cloud gradually moves to the true state by a Gaussian approximation. The pseudo-code of Gradual Gaussian Estimation (GGE) is in **Algorithm** 17.

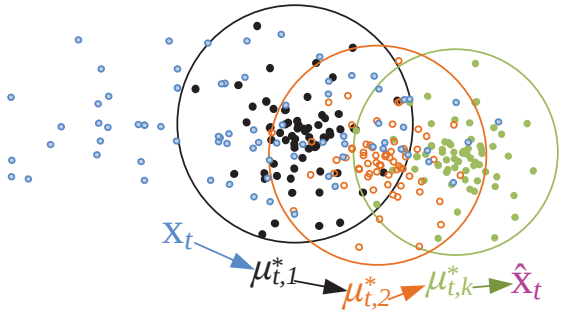

Figure 4.12: Gradual Gaussian sampling: the samples gradually converge to the true state ($\mathbf{x}_t$)

Algorithm 17 Gradual Gaussian Estimation (GGE)

Output and input: $[\hat{\mathbf{x}}_t,\ \left\{\mathbf{x}_t^i,\ w_t^i\right\}_{i=1}^{N_s}] = \text{GGE}[\mathbf{z}_t,\ \mathbf{A}_t,\ \left\{\mathbf{x}_{t-1}^i,\ w_{t-1}^i\right\}_{i=1}^{N_s}]$
Setting: N_s, N_{Gradu}, $p(r|\|\mathbf{x}-\mathbf{a}\|)$, $p(\mathbf{x}_t|\mathbf{x}_{t-1})$

1: Obtain $\left\{\mathbf{x}_t^{*i},\ w_t^i\right\}_{i=1}^{N_s}$ from the sample-based estimation, i.e., **Algorithm** 6
2: Initialization for the gradual sampling step $\left\{\mathbf{x}_{t,0}^{*i},\ w_{t,0}^{*i}\right\}_{i=1}^{N_s} = \left\{\mathbf{x}_t^i,\ w_t^i\right\}_{i=1}^{N_s}$,
3: Gradual Gaussian approximation, initializing $k = 1$
    FOR $k = 1$ to N_{Gradu}
        Gaussian sampling $\left\{\mathbf{x}_{t,k}^{*i} \sim \mathcal{N}(\mu_{t,k}^*, \sigma_{t,k}^{*2})\right\}_{i=1:N_s}$ (4.70) (4.71)
        Assign weights $\{w_{t,k}^{*i}\}_{i=1}^{N_s}$ (4.72)
        Weights normalization $\left\{w_{t,k}^{*i} = \frac{w_{t,k}^{*i}}{\sum_{j=1}^{N_s} w_{t,k}^{*j}}\right\}_{i=1:N_s}$
    END FOR
4: Modify the state samples and weights $\left\{\mathbf{x}_t^i,\ w_t^i\right\}_{i=1}^{N_s} = \left\{\mathbf{x}_{t,N_{\text{Gradu}}}^{*i},\ w_{t,N_{\text{Gradu}}}^{*i}\right\}_{i=1}^{N_s}$
5: Estimate position $\hat{\mathbf{x}}_t$ (4.19)
6: Set $t = t + 1$ and iterate to item 1.

In fact, the GGS aims to incrementally converge the mean of the gradual samples to the true position, rather than representing the complete state density. Note that, the step 3 in **Algorithm** 17 recursively runs until reaching up to N_{Gradu} or the sample-based posterior is evaluated to converge to the true posterior. The number of the iteration should be set to a small number.

4.2.5 Results and analysis

The aforementioned sampling methods are evaluated in the experiment M1.

Positioning performance

The quantitative results of the sample-based positioning through different sampling algorithms are listed in Table 4.1. The MEAN_p and RMSE_p represent the positioning accuracy, σ_p describes the positioning precision; MAX_p and PCT_{95} stand for the estimation robustness. For the compared algorithms the sample size is set to be $N_\text{s} = 100$, and the proposed methods averagely have $N_\text{s} = 49$[4].

It presents that RBGF achieves the best results considering the accuracy, precision and robustness; whereas, LLS is the worst as its linearization step can be severely affected by the noise ranging. The ML estimation remarkably outperforms NLS as considering the positive bias of the real ranging error into the measurement model. Except the conventional GLE and GF, all the sample-based algorithms result in an acceptable accuracy, e.g., GLE and GF can be improved by taking finer resolution or the bound grid-space as BGE, BGF and RBGF.

Comparing ML, BGE and GeoE with BGF and GeoF, one can know that mobility causes no damage to the positioning performance. In fact, the sequential positioning benefits from mobility and exploits it to enhance the efficiency and accuracy.

Note that the Gaussian-PF greatly outperforms the other PFs, although the PFs are often considered to be better [145]; it is because that the Gaussian sampling has a very low variance which limits the effect of the NLOS error. This Gaussian-PF seems sensible at first, however, it is questionable if the posterior is highly non-Gaussian.

The improved versions of PF (Auxiliary-PF and Annealed-PF) are theoretically sound, but they achieve almost no improvements compared with SIR and Generic-PF. It is explained that the auxiliary sampling only emphasize the good parent samples, but it does not allocate the samples to the true state. The Annealed-PF relocates the samples by annealing, nevertheless, it inevitably leads to lose the prior power at the first few annealing steps.

Compare with the conventional grid-based representations (GLE and GF), the bounded grid-based sampling markedly improves the efficiency by adding only a few arithmetic operations. The benefits

[4]The average anchor connectivity throughout our experiments is 7.5, thus, the size of the geometric samples is $N_\text{anc}^{t-1} \times (N_\text{anc}^{t-1} - 1) \approx 48.75$; the ; for the performance comparison, all the other proposed sampling methods set $Ns = 49$.

Table 4.1: Comparison of the sampling methods in positioning error (/meter) of M1, employing a Gaussian measurement model ($\varepsilon_r \sim \mathcal{N}(2.5, 3^2)$)

Category	Algorithms	MEAN_p	RMSE_p	σ_p	MAX_p	$\text{PCT}_{95\text{p}}$
Non-sampling	NLS	4.49	5.35	2.69	30.39	9.40
	LLS	6.88	10.79	8.31	120.94	19.21
	ML	2.10	2.67	1.65	20.65	5.23
	EKF	3.37	3.83	1.83	11.65	6.74
Compared sampling	GLE ($N_\text{g} = 10 \times 10$)	2.37	2.78	1.45	11.74	5.12
	GF ($N_\text{g} = 10 \times 10$)	2.34	2.60	1.13	6.20	4.72
	SIR ($N_\text{s} = 100$)	1.57	1.82	0.94	6.66	3.22
	Generic-PF ($N_\text{s} = 100$)	1.57	1.81	0.90	6.56	3.27
	Auxiliary-PF ($N_\text{s} = 100$)	1.51	1.77	0.91	7.03	3.11
	Gaussian-PF ($N_\text{s} = 100$)	1.30	1.46	0.68	5.06	2.63
	Annealed-PF ($N_\text{s} = 100$, $N_\text{Ann} = 3$)	1.53	1.77	0.90	6.84	3.19
Proposed sampling	BGE ($N_\text{g} = 7 \times 7$)	1.74	2.08	1.14	10.04	3.83
	BGF ($N_\text{g} = 7 \times 7$)	1.36	1.57	0.80	6.37	2.71
	RBGF ($N_\text{g} = 7 \times 7$)	1.19	1.36	0.70	4.92	2.34
	GeoE (averagely $N_\text{s} = 49$)	1.87	2.34	1.41	11.78	4.60
	GeoF (averagely $N_\text{s} = 49$)	1.53	1.95	1.21	8.21	4.02
	PolarF (averagely $N_\text{s} = 45$)	1.10	1.30	0.68	6.20	2.38
	GGE ($N_\text{s} = 49$, $N_\text{Gradu} = 3$)	1.25	1.41	0.62	3.44	2.46

of the bounded grid-based sampling are 1) a deterministic sampling; 2) relatively easier to implement; 3) robust to the error of the prior, as it does not assume any other knowledge of the state than in the grid region. It is believed that, in the case of an erroneous prior, a predictive sampling density is problematic; thus, it is better to use the uniform sampling within a bounded region.

The geometric sampling obtains a satisfied accuracy, but it is not robust as the values of $\mathrm{MAX_p}$ and $\mathrm{PCT_{95}}$ are large. It is because that the NLOS measurements generate irrelevant samples far away from the true state, which severely affect the posterior approximation.

The PolarF obtains better accuracy but higher $\mathrm{MAX_p}$ than RBGF and GGE, by reason that the polar sampling can neither bound the state-space nor reduce the sample divergence.

Both the Annealed-PF and GGE employ three steps of iteration, but the GGE is superior because it samples from the gradually refined posterior. GGE obtains the best robustness, indicating that the gradual sampling can address the sample divergence in NLOS conditions. If $N_{\mathrm{Gradu}} = 0$, the GGF is the same as Gaussian-PF. Additionally, the GGS is similar to the idea of Annealed-PF, which splits the sampling into a sequence of progressive sampling. The GGS uses a Gaussian approximation on the posterior, whereas, Annealed-PF is based on the annealing function and the prediction density. Therefore, the GGS is suitable for point estimation.

Overall, the proposed constrained sampling requires a small sample size, and yields satisfied results by taking into account the latest observation.

Sampling quality

The performance of the sample-based estimation is dominated by the quality of the state samples. A good sampling method should work well in the aspects: the sample efficiency, divergence and diversity, as illustrated in Fig. 4.13. Figure 4.13 (a) depicts that good sample density should concentrate most samples around the true state, meanwhile, is should maintain sufficient sample diversity. Figure 4.13 (b), (c) and (d) represent the sampling degeneracy, divergence and low diversity problems, respectively.

1) Sampling degeneracy

The sampling degeneracy happens when the sampling density is non-informative rather than a peaky density. Figure 4.13 (b) depicts a sample density with low efficiency, as the samples spread widely rather than concentrating to the true state. As a consequence, a large computational effort is wasted on updating the samples with very small probability. The sample efficiency is usually indicated by the effective sample size (N_{eff}) via (2.98). The N_{eff} of Generic-PF and RBGF (bounded grid sampling) with the time sequence is plotted in Fig. 4.14.

From Fig. 4.14, the N_{eff} of the sampling methods varies with time: 1) the N_{eff} of Generic-PF

a) Good sample density b) Sample degeneracy c) Sample divergence d) Low sample diversity

Figure 4.13: Illustration of the sample quality: the true state is denoted by the filled circle, and the state samples as the small dots

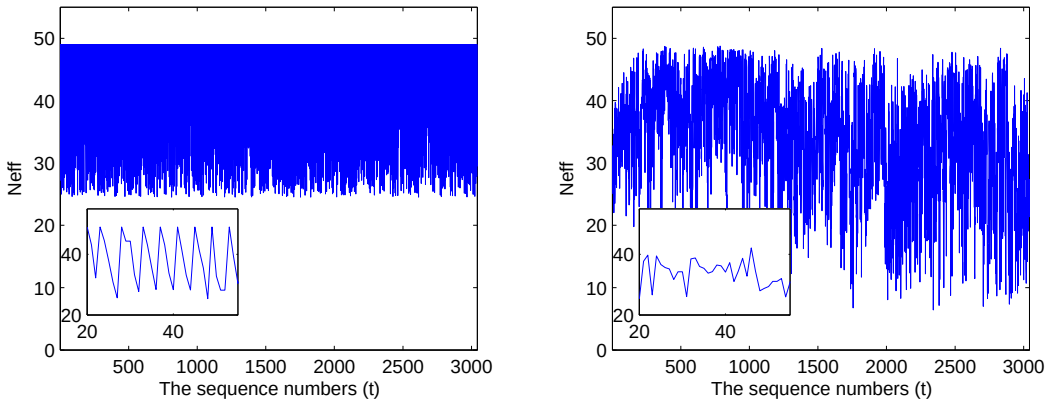

(a) The N_{eff} of Generic-PF (selective resampling) (b) The N_{eff} of RBGF (bounded grid sampling)

Figure 4.14: Effective sample size (N_{eff}) of the sampling algorithms varying over time, with the sample size $N_{\text{s}} = 49$

shows cyclical fluctuations with time, by reason that the resampling is carried out when N_{eff} decreases to ${N_{\text{eff}}}^{threshold}$; 2) N_{eff} of RBGF is not periodically changes, and the average N_{eff} is comparable to Generic-PF. Thus, RBGF can mitigate the sampling degeneracy without resampling.

In order to measure the sample degeneracy of sampling with different sample sizes, the effective sample rate ($k_{N_{\text{eff}}}$) is defined

$$k_{N_{\text{eff}}} = \frac{N_{\text{eff}}}{N_{\text{s}}} , \tag{4.73}$$

with the results listed in Table 4.2.

2) Sampling divergence

Even if the sampling is effective, the samples cannot be guaranteed to converge to the true state, as shown in Fig. 4.13 (c). Thus, another crucial criterion is the sample divergence (*div*) defined as the average distance between the samples and the true state

$$div = \left\| \mathbf{x} - \frac{1}{N_{\text{s}}} \sum_{i=1}^{N_{\text{s}}} \mathbf{x}^i \right\| . \tag{4.74}$$

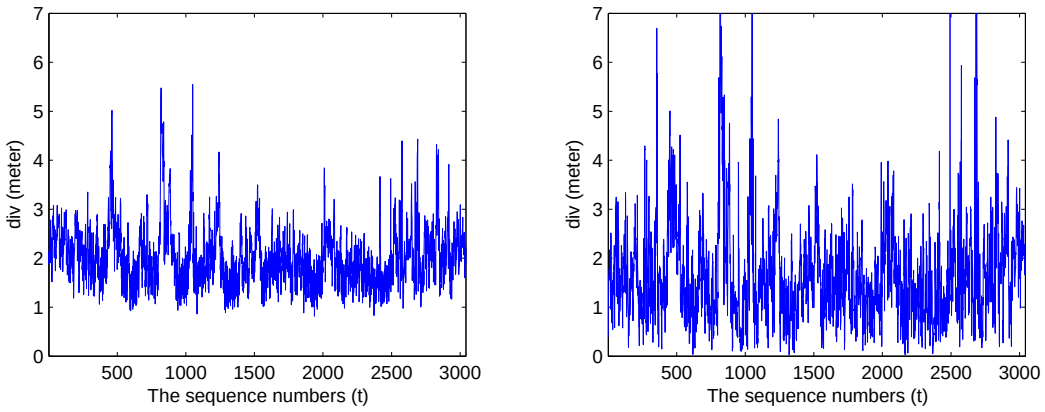

(a) The *div* of PF (selective resampling)

(b) The *div* of RBGF (bounded grid sampling)

Figure 4.15: Sample divergence (*div*) of the sampling algorithms varying over time, with the sample size $N_{\text{s}} = 49$

The sample divergence of the selective sampling and bounded grid sampling is described in Fig. 4.15, which presents an averagely improvement of BRGF in comparison with Generic-PF in the sampling divergence.

3) Sampling diversity

With good sampling efficiency and convergence, the sample-based estimation can become quite representative regarding the true state density, and require a small sample size. On the other hand, it may be problematic in robustness, due to the loss of sample diversity. The sample diversity is defined as the standard divination of the state samples

$$\text{diversity} = \sqrt{\frac{1}{N_s}\sum_{i=1}^{N_s}\left\|\mathbf{x}^i - \sum_{j=1}^{N_s}\mathbf{x}^j w^j\right\|^2}. \tag{4.75}$$

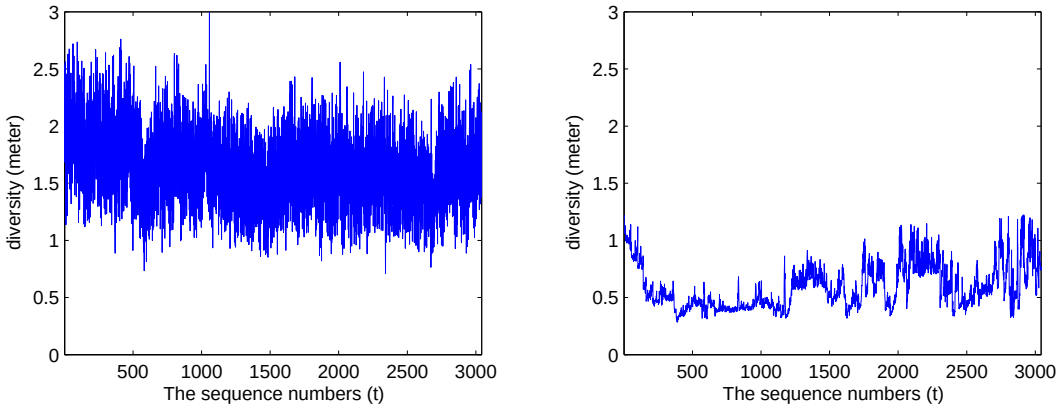

(a) The diversity of PF (selective resampling)

(b) The diversity of RBGF (bounded grid sampling)

Figure 4.16: Sample diversity (*diversity*) of the sampling algorithms varying over time, with the sample size $N_s = 49$

As can be seen in Fig. 4.16, the bounded sampling of RBGF maintain a very low sample diversity. Thus, it interprets that RBGF should extend the bound in the case of extremely uncertain prior or the target with a high velocity.

The sampling quality of the experiment M1 is shown in Table 4.2, indicating that:

- The effective sample size ($k_{N_{\text{eff}}}$) is inversely proportional to sampling diversity (*div*); in other words, $k_{N_{\text{eff}}}$ can be improved at the expense of losing the sample diversity, e.g., the Gaussian-PF conquers sample degeneracy, but may stick to a single mode due to its low diversity; the GLE and GF can represent an arbitrary posterior, but they are severely ineffective.
- According to the $corr(\varepsilon_p, div)$, if $k_{N_{\text{eff}}}$ is high, the positioning accuracy is more dependent on *div*; otherwise, the sample divergence does not necessarily leading to estimating divergence.
- With the same $k_{N_{\text{eff}}}$, the sampling with the smaller *div* obtains a better accuracy;
- The PolarF achieves good accuracy, high $k_{N_{\text{eff}}}$ and sufficient *diversity*, which is more desirable

Table 4.2: Sampling quality of the sampling algorithms in the experiment M1: the effective sample rate ($k_{N_{\text{eff}}}$), divergence (div) and diversity

Algorithms	$k_{N_{\text{eff}}}$ (%)	div (m)	$diversity$ (m)	$corr(\varepsilon_{\text{p}}, div)$
GLE ($N_{\text{g}} = 10 \times 10$)	1	20.97	32.92	-0.02
GF ($N_{\text{g}} = 10 \times 10$)	2	20.97	33.07	-0.08
SIR ($N_{\text{s}} = 100$)	75	1.56	1.28	0.99
Generic-PF ($N_{\text{s}} = 100$)	75	1.56	1.29	0.99
Auxiliary-PF ($N_{\text{s}} = 100$)	83	1.50	1.55	0.98
Gaussian-PF ($N_{\text{s}} = 100$)	86	1.28	1.02	0.96
Annealed-PF ($N_{\text{s}} = 100$, $K_{\text{Ann}} = 3$)	75	1.52	1.28	0.99
BGE ($N_{\text{g}} = 7 \times 7$)	49	2.08	3.72	0.53
BGF ($N_{\text{g}} = 7 \times 7$)	21	2.08	3.85	0.24
RBGF ($N_{\text{g}} = 7 \times 7$)	53	1.12	1.62	0.83
GeoE (averagely $N_{\text{s}} = 49$)	25	2.57	12.51	0.24
GeoF (averagely $N_{\text{s}} = 49$)	11	2.57	12.62	-0.01
PolarF (averagely $N_{\text{s}} = 45$)	65	1.41	2.56	0.87
GGE ($N_{\text{s}} = 49$, $N_{\text{Gradu}} = 3$)	76	1.27	0.52	0.99

for a practical positioning.

To conclude, the performance of the sample-based estimation is conjointly determined by how closely the samples mimics the true state and the sample diversity and the sampling degeneracy.

4.2.6 Discussion

The effect of the sample size

The selection of the sample size is the key factor of the efficiency of sample-based estimations. The sample size is typically fixed, whereas, some work adaptively determines the sample size [135]. We believe that the real number of samples needed can be much smaller than it is commonly set. The experiments confirm this as the positioning accuracy is slightly dependent on the sample size (see Fig. 4.17).

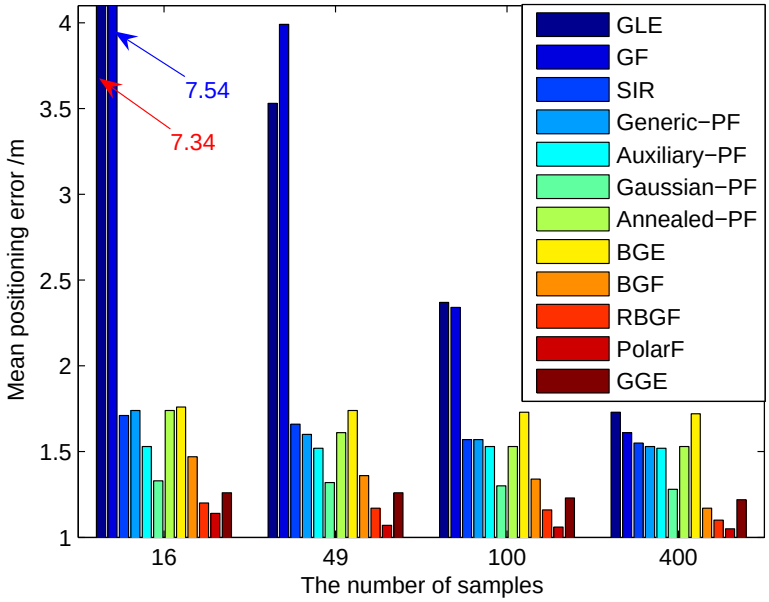

Figure 4.17: Positioning error versus the sample size

Figure 4.17 plots the mean accuracy of the sample-based positioning over different sample sizes: except the GLE and GF, the accuracy of the other algorithms reports small improvements as increasing the sample size from 16 to 400. It is explained that the $k_{N_{\text{eff}}}$ of GLE and GF is too low and their grid resolutions are too coarse to represent the continuous posterior; the other algorithms retain a sufficient $k_{N_{\text{eff}}}$, thus, their estimation accuracy highly relies on the sample divergence rather than

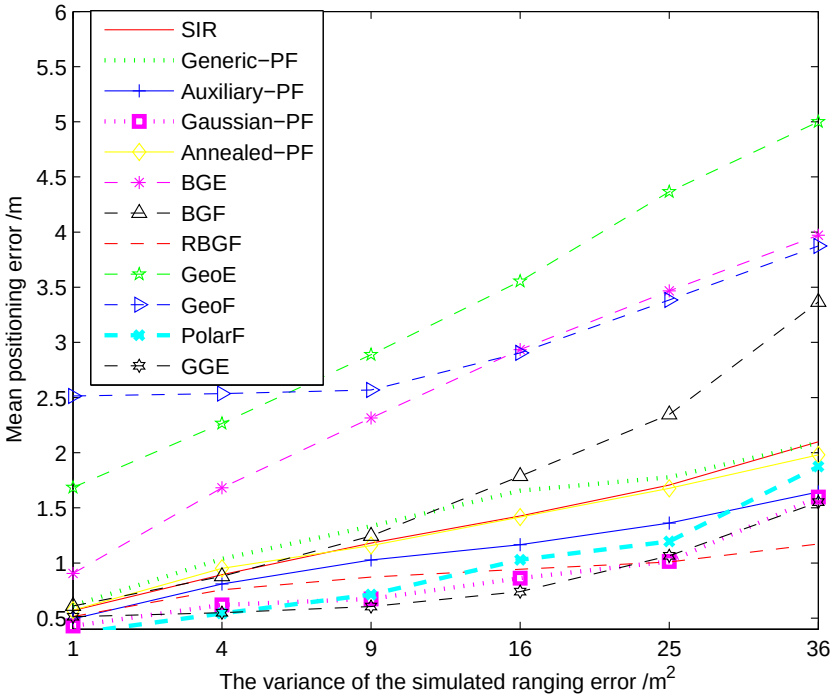

Figure 4.18: Positioning error versus the ranging uncertainty, assuming the simulated ranging error $\varepsilon_r \sim \mathcal{N}(2.5, \sigma^2_{\varepsilon_r})$

how dense the samples are. Therefore, to enhance the sample-based positioning, a more efficient way is to reduce the sample divergence rather than setting a large number of samples.

The effect of ranging uncertainty

To characterize the effect of ranging uncertainty on the positioning, we conduct the simulation with the same anchor deployment and connectivity as the real-world experiment. The simulation sets the ranging error $\varepsilon_r \sim \mathcal{N}(2.5, \sigma^2_{\varepsilon_r})$, consequently, all the compared algorithms assumes the same measurement model ($\mathcal{N}(2.5, \sigma^2_{\varepsilon_r})$). All the algorithms are set with the same sample size ($N_s = 49$) and initialization, with the results depicted in Fig. 4.18.

The simulation results (Fig. 4.18) confirm the error propagation analysis in Subsection 4.1.1, as the positioning error increases with the ranging error. In addition, the simulated results are almost consistent with the real-world experiments, as the algorithms GGE, Gaussian-PF, RBGF and PolarF achieve good performance. The Auxiliary-PF achieves higher improvement in the simulation than

in the experiment, due to that the auxiliary sampling is more effective with Gaussian ranging errors. Unexpectedly, the geometric sampling methods result in much worse accuracy. It is because that, in the experiment, there are always good ranging measurements to produce good geometric samples, which is not the case of the simulations using the model $\mathcal{N}(2.5, \sigma^2_{\varepsilon_r})$. Consequently, it is suggested to choose the sampling method according to the real-world measurement characteristics.

The effect of the state bound

Compared with the conventional grid-based methods in Table 4.1, the bounded ones significantly improve the accuracy as the samples are concentrated in the probable grid-region. The derived bound can also be applied to other sampling methods, with the idea that the weights of the samples outside the bound is set to zero. Figure 4.19 and **Algorithm** 18 take the bound on the GeoF as an example, namely bounded GeoF (GeoF-B).

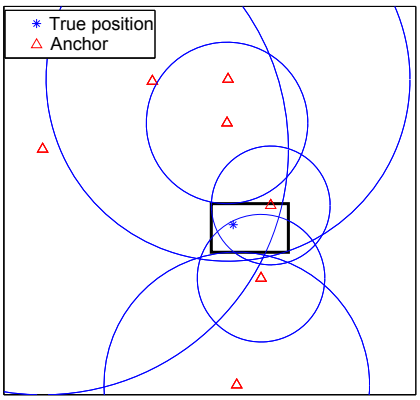

Figure 4.19: Geometry of one trial of real-world ranging: the circles are the disk model of ranging; △ represents the anchors and '*' for the true position; □ is the bound derived from (4.35)

The sample-space with the box constraint derived from both the current ranging measurements and the previous position estimation. Consequently, the GeoF-B not only takes into account the current ranging geometry, but is also projected to the bound.

Unfortunately, if the bound is too tight, then the bounded sampling is dangerous, as the sample diversity discussed in Table 4.2. The size of the instantaneous bound (R) of (4.30) and the recursive bound (R_t) of (4.35) from the experimental positioning is illustrated in Fig. 4.20. It indicates that, although the recursive bound retains a more stable and rational size, it can be too small. Therefore, using B_t to constrain sampling, there might be no sample falling inside the bound, with the risk of

Algorithm 18 Bounded Geometric Filter (GeoF-B)

Output and input: $[\hat{\mathbf{x}}_t] = \text{GeoF} - \text{B}\,[\mathbf{z}_t, \mathbf{A}_t, \hat{\mathbf{x}}_{t-1}]$
Setting: $p(\mathbf{x}_t|\mathbf{x}_{t-1})$, $p(r|\,\|\mathbf{x}-\mathbf{a}\|)$
Initialization: $\hat{\mathbf{x}}_0$ and $t = 1$

1: Geometric sampling $\{\mathbf{x}_t^i\}_{i=1}^{N_{\text{anc}}^t \times (N_{\text{anc}}^t - 1)}$ from (4.45)
2: Select the geometric samples within R_t (4.30)
3: Weights assignment $\{w_t^i\}_{i=1:N_{\text{p}}}$ (4.51), (4.32) and (4.49)
4: Estimate position $\hat{\mathbf{x}}_t$ (4.48)
5: Set $t = t + 1$ and iterate to item 1.

losing track of the target. Thus, the bound should be carefully constructed, which is suggested to retain a wide size.

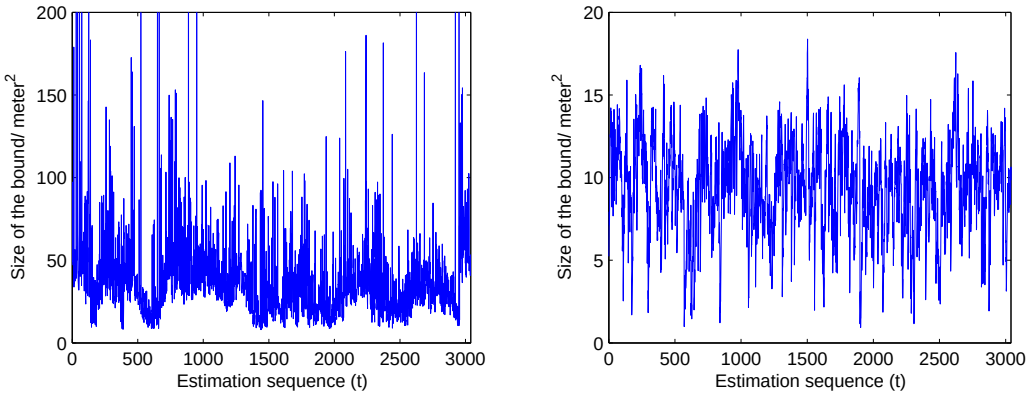

(a) The size of the instantaneous bound (R_t) of (4.30) (b) The size of the recursive bound (B_t) of (4.35)

Figure 4.20: Size of the bound of (4.30) and (4.35) over time

The bounded sampling scheme is applied to the aforementioned algorithms. The improvements in the mean positioning error of bounding these sampling algorithms are plotted in Fig. 4.21. The results demonstrate that, the bounded sampling improve the mean positioning, which verifies that the bound effectively cancels the effect of the irrelevant samples. It seems that the higher the accuracy of the algorithm is, the less the improvement of the bounded sampling obtains, due to that the better sampling method has much less irrelevant samples.

Complexity

The time and space complexity of all the sample-based algorithms are compared in Table 4.3. Since generating the random number and resampling are source-consuming, they are also used to in-

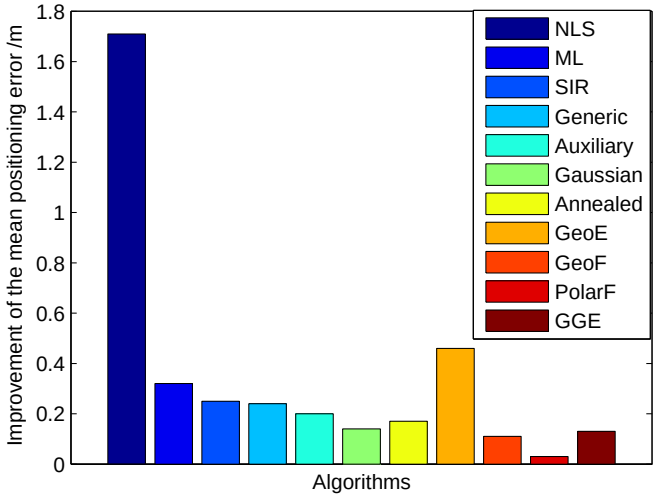

Figure 4.21: Improvement of the bounded sampling compared with the corresponding unbounded ones in the mean positioning error (/meter)

dicate the implementation difficulty. In comparison, the majority of the proposed sampling methods avoid producing random numbers and resampling, which lead to an easy implementation. However, they impose a larger time complexity arising from the integral over the complete state in (2.55). Additionally, most aforementioned sampling methods cause a large memory burden proportional to the sample size.

The complexity can be reduced by approximating the prior by a parametric density. Thus, the Gaussian-PF, BGF-A, RBGF-A, GeoF-A and PolarF-A approximate the prior by a Gaussian density as (4.41). The mean positioning accuracy of the algorithms using the Gaussian prior and their original algorithms is illustrated in Fig. 4.22. The results demonstrate that the positioning accuracy of exploring the Chapman-Kolmogorov equation (2.55) and the Gaussian prior (4.41) is almost the same. The time complexity of the Gaussian-PF is linear of the sample size. Furthermore, the space complexity is significantly reduced, as the Gaussian prior does not require to keep the sample and the weight vector in memory.

Summary

The characteristics of the used sampling methods are concluded in Table 4.4. In conclusion, we find that the proposed constrained sampling outperform the importance sampling and other methods in the sampling efficiency and convergence, but at the expense of losing some sampling diversity.

Table 4.3: Time, space and implementation complexity of the sampling algorithms

Algorithms	Time	Space	Size of random number	Resampling
GLE	$O(N_s \times N_{anc}^t)$	$O(1)$	0	no
GF	$O(N_s \times \max(N_s, N_{anc}^t))$	$O(N_s)$	0	no
SIR	$O(N_s \times N_{anc}^t)$	$O(N_s)$	$3 * N_s$	yes
Generic-PF	$O(N_s \times N_{anc}^t)$	$O(N_s)$	$> 2 * N_s$	yes
Auxiliary-PF	$O(N_s \times N_{anc}^t)$	$O(N_s)$	$5 * N_s$	yes
Gaussian-PF	$O(N_s \times N_{anc}^t)$	$O(1)$	$2 * N_s$	no
Annealed-PF	$O(N_s \times N_{anc}^t \times (1 + K_{Ann}))$	$O(N_s)$	$3 * (1 + K_{Ann}) * N_s$	yes
BGE	$O(N_s \times N_{anc}^t)$	$O(1)$	0	no
BGF	$O(N_s \times \max(N_s, N_{anc}^t))$	$O(N_s)$	0	no
RBGF	$O(N_s \times \max(N_s, N_{anc}^t))$	$O(N_s)$	0	no
GeoE ($N_s^t = N_{anc}^t \times (N_{anc}^t - 1)$)	$O(N_s^t * N_{anc}^t)$	$O(1)$	0	no
GeoF ($N_s^t = N_{anc}^t \times (N_{anc}^t - 1)$)	$O(N_s^t * \max(N_s^{t-1}, N_{anc}^t))$	$O(N_s)$	0	no
PolarF ($N_s^t = N_{anc}^t \times 2 \times N_{r,\varphi}$)	$O(N_s^t * \max(N_s^{t-1}, N_{anc}^t))$	$O(N_s)$	$2 * N_s^t$	no
GGE	$O(N_s \times N_{anc}^t \times N_{Gradu})$	$O(1)$	$2 * N_s \times N_{Gradu}$	no
BGF-A	$O(N_s \times N_{anc}^t)$	$O(1)$	0	no
RBGF-A	$O(N_s \times N_{anc}^t)$	$O(1)$	0	no
GeoF-A ($N_s^t = N_{anc}^t \times (N_{anc}^t - 1)$)	$O(N_s^t * N_{anc}^t)$	$O(1)$	0	no
PolarF-A ($N_s^t = N_{anc}^t \times 2 \times N_{r,\varphi}$)	$O(N_s^t * N_{anc}^t)$	$O(1)$	$2 * N_s^t$	no

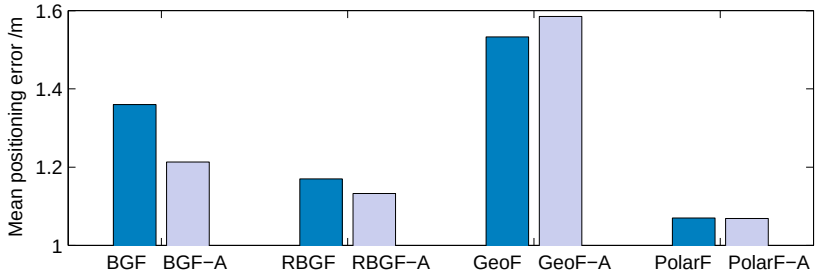

Figure 4.22: Comparison of the positioning error of using the prior form the Chapman-Kolmogorov equation (2.55) and the Gaussian approximation (4.41)

Table 4.4: Characteristics of the sampling methods (+, 0 and - represent good, intermediate and weak, respectively)

Sampling method	Computation efficiency	Sampling simplicity	Memory efficiency	Sample degeneracy	Sample diversity	Representation of probability density
Single Gaussian	+	+	+	+	0	Gaussian
Gaussian sum	–	0	+	0	+	Gaussian mixture
Grid-based method	–	+	0	0	+	arbitrary
Importance sampling	+	0	0	–	0	arbitrary
SIR	0	–	0	+	–	arbitrary
Bounded Grid-based method	+	+	+	+	0	arbitrary
Geometric sampling	0	+	0	+	+	arbitrary
Polar sampling	+	+	0	0	+	arbitrary
Gradual Gaussian sampling	$\propto \frac{1}{N_{\text{Gradu}}}$	+	+	+	0	Gaussian

4.3 NLOS Mitigation

Chapter 3.3 has discussed that the NLOS error cannot be described as a Gaussian distribution, or indeed any specific distribution. To suppress the NLOS effect, this section proposes three nonparametric measurement models.

4.3.1 Existing NOLS mitigation

The simplest way is to identify and discard the NLOS measurements [22, 105]. However, there is always the possibility of false identifications of the NLOS measurements. Even if the LOS and NLOS ranges can be correctly distinguished, positioning with a hard decision of discarding the NLOS ranges may lose much information (see Subsection 4.1.1). Moreover, if the number of LOS measurements is insufficient, the NLOS ranges cannot be discarded. Thus, NLOS mitigation approaches are more promising, with a comprehensive overview in Table 4.5 [92, 117, 147].

From Table 4.5, these NLOS mitigation methods have one of the following requirements: 1) the knowledge of the LOS or NLOS status; 2) the ranging error is well modeled; 3) redundant ranging measurements; 4) large measurement database for online training and learning; 5) the radio environment is time invariant; 6) the channel condition is completely known. For practical positioning, the NLOS mitigation methods are developed as follows.

4.3.2 Biased nonparametric measurement models

Considerable work [108, 163, 164] has accumulated that a biased ranging model tends to be more robust than the frequently referred Gaussian model. Some literature employs a biased parametric model, such as the Negative Exponential distribution [8, 69, 77] or Lognormal distribution [8]. These parametric models often get overfitting due to arbitrary NLOS errors. To capture the feature of NLOS errors, two biased models are formed from off-line statistics.

A triangular Membership Function (MF)

Chapter 3.3 has shown a statistical model can be a good interpretation of the ranging. Since it is impossible to cache all the information about the frequency histogram, we construct a heuristic model of the ranging error using a triangular Membership Function (MF).

1) Experimental frequency histogram

The first step to understand the ranging error is to build an experimental frequency histogram (see Fig. 4.23 (a-b)) of the ranging error, and the typical properties are presented in Chapter 3.3.

2) MF Configuration

Table 4.5: Existing NLOS mitigation approaches for range-based indoor range-based positioning

Facts	Methods	Drawbacks
the ranging errors appear a positively biased distribution	the mixture or nonparametric models from measurement statistics [6, 8]	difficulty in determining the joint probability distributions of the models; the algorithm in [141] requires to know the number of NLOS ranging
the variance of time-series ranging increases in NLOS conditions	the measurements with a higher variance can be excluded or given less weights [22, 169, 170]	a running variance of time-series ranging measurements cannot be estimated in a short observation window
the ranging error depends on channel conditions or link quality	the channel impulse response indicates the probability of the NLOS error [15, 70, 77, 105]	it is difficult to obtain the complete knowledge of the channel profile; it is not suitable for the scenario with unknown wireless interference
the NLOS ranging causes considerably larger residuals at the true target's position	the residual weighting algorithms (RWGH) in [33, 107, 107] is a weighted combination of the partial position estimates	the algorithms require redundant ranging measurements, which is not available with a sparse anchor density; a higher computation is imposed
the NLOS ranging is not consistent with the LOS measurements at the true position	the methods [117, 173] use machine learning to find the most consistent candidate for position estimation	the training and learning procedures cause high calculation and latency, which is prohibitive in low-end networks
the NLOS error is related to the physical environment	the calibration methods comes from a signal database of a given indoor environment [15, 83]	the environment information is costly to incorporate, i.e., the exact floor plan, wall material, ray tracing results and signal database, etc.; additionally, these methods are inefficient in variable environments

The triangular[5] MF is a piecewise function as shown Fig. 4.23 (c-d), constructed from the experimental frequency histogram. The procedure and one example of the MF configuration are summarized in **Algorithm** 19. The strength of the MF configuration requires no mathematical derivation of the ranging model.

Algorithm 19 Triangular MF configuration

Output $[MF_{\text{low}}, MF_{\text{median}}, MF_{\text{up}}]$

1: Get the sample pool of the ranging measurements, and then draw the frequency histogram of the ranging error (ε_r) as Fig. 4.23 (a-b);
2: Compute the percentiles of 1%, 50% and 99%[6] of ε_r as the lower limit (MF_{low}), the median (MF_{median}) and the upper limit (MF_{up}) of MF, respectively; remove the left and the right-side outliers as Fig. 4.23 (c-d);
3: Configure the MF with the three parameters $[MF_{\text{low}}, MF_{\text{median}}, MF_{\text{up}}]$ as Fig. 4.23 (c-d).

Example of the MF configuration from the ranging measurements of M2

Step 1: Gather the sample set of ε_r, as the histogram in Fig. 4.23 (b);
Step 2: Compute $MF_{\text{low}} = -1.97$ meters, $MF_{\text{median}} = 2.29$ meters and $MF_{\text{up}} = 13.19$ meters
Step 3: Join dots $(-1.97, 0)$, $(2.29, 1)$, $(13.19, 0)$ by straight lines, as the triangular profile in Fig. 4.23 (d)

3) MF-based likelihood (L_{MF})

Given the state samples ($\{\mathbf{x}^i\}_{i=1}^{Ns}$), the $[MF_{\text{low}}, MF_{\text{median}}, MF_{\text{up}}]$ converts the measurements to the likelihood

$$p(r^l | \left\|\mathbf{x}^i - \mathbf{a}^l\right\|) = \begin{cases} \frac{(r^l - \left\|\mathbf{x}^i - \mathbf{a}^l\right\|) - MF_{\text{up}}}{MF_{\text{median}} - MF_{\text{up}}} + \epsilon_{\text{small}} & \text{if } MF_{\text{median}} \leq (r^l - \left\|\mathbf{x}^i - \mathbf{a}^l\right\|) < MF_{\text{up}} \\ \frac{(r^l - \left\|\mathbf{x}^i - \mathbf{a}^l\right\|) - MF_{\text{low}}}{MF_{\text{median}} - MF_{\text{low}}} + \epsilon_{\text{small}} & \text{if } MF_{\text{low}} < (r^l - \left\|\mathbf{x}^i - \mathbf{a}^l\right\|) < MF_{\text{median}} \\ \epsilon_{\text{small}} & \text{otherwise} \end{cases} \tag{4.76}$$

with $l \in \{\cdot\}_1^{N_{\text{anc}}}$ and $i \in \{\cdot\}_1^{N_{\text{s}}}$. The constant ϵ_{small} is a very small number ($\epsilon_{\text{small}} = 0.0001$) to avoid the likelihood to be zero.

[5]The triangular MF is not the only shape for the heuristic model, as other shapes of the MF can be used, i.e., a trapezoidal or rectangular MF. The triangular MF is conceptually simple and computational efficiency.

[6]There is no particular rule for choosing the three parameters of MF: for a 98% confidence level, we set the three percentiles as 1%, 50% and 99%.

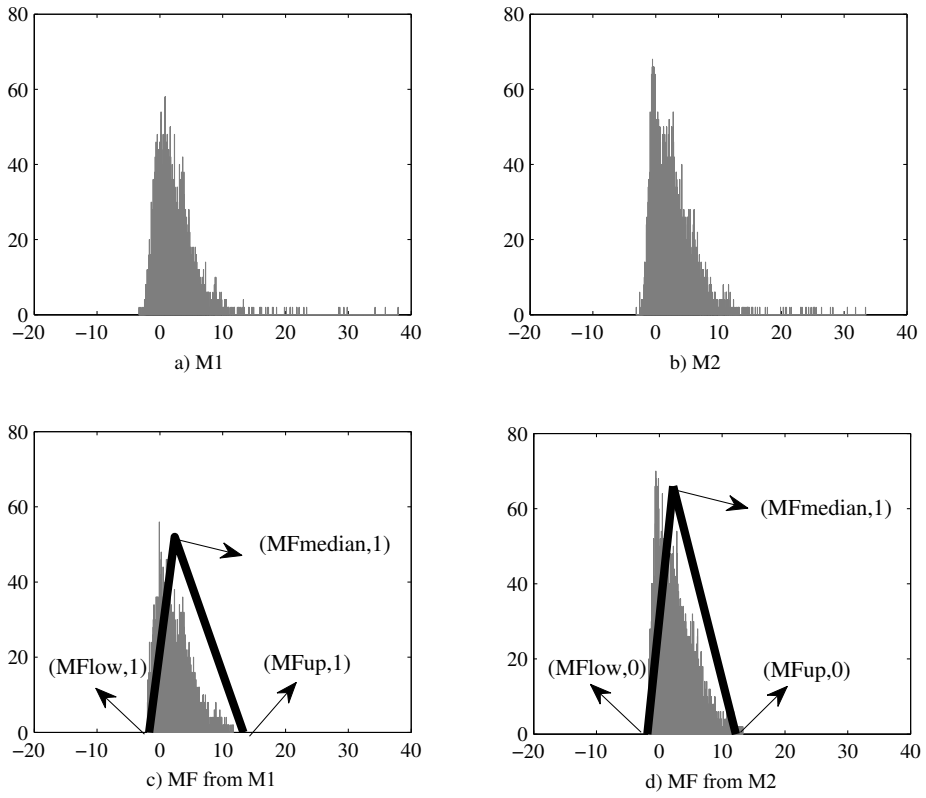

Figure 4.23: Triangular MF configured from the frequency histogram of ranging errors, in the experiments M1 and M2: Fig. 4.23 (a-b) depict the histograms, and Fig. 4.23 (c-d) illustrate the MF configuration.

Similar to the joint likelihood using a parametric model in (4.32), the MF-based likelihood can be incorporated into the probabilistic positioning frame.

A bias function (b) on the measurement model

To imitate the NLOS bias, a bias function (b) is imposed on the lth ranging residual at the ith state sample

$$Res_l^b(\mathbf{x}^i) = Res_l(\mathbf{x}^i) \cdot b \,, \tag{4.77}$$

where $Res_l(\mathbf{x}^i) = r^l - \left\|\mathbf{x}^i - \mathbf{a}^l\right\|$ is the residual of the lth ranging at the ith state sample. The bias function denoted by b is set as a negative exponential function adding a constant[7]

$$b = \exp\left\{-\mathrm{c}_1^b * Res_l(\mathbf{x}^i)\right\} + \mathrm{c}_2^b \,. \tag{4.78}$$

The joint likelihood of N_{anc} ranging measurements is

$$p(\mathbf{z}|\mathbf{x}^i) = \prod_{l=1}^{N_{\text{anc}}} p(Res_l^b(\mathbf{x}^i)),\ i \in \{i\}_{i=1}^{N_s} \,, \tag{4.79}$$

with $p(Res_l^b) \sim \mathcal{N}(\mu_{\varepsilon_r}, \sigma_{\varepsilon_r}^2) \cdot b$.

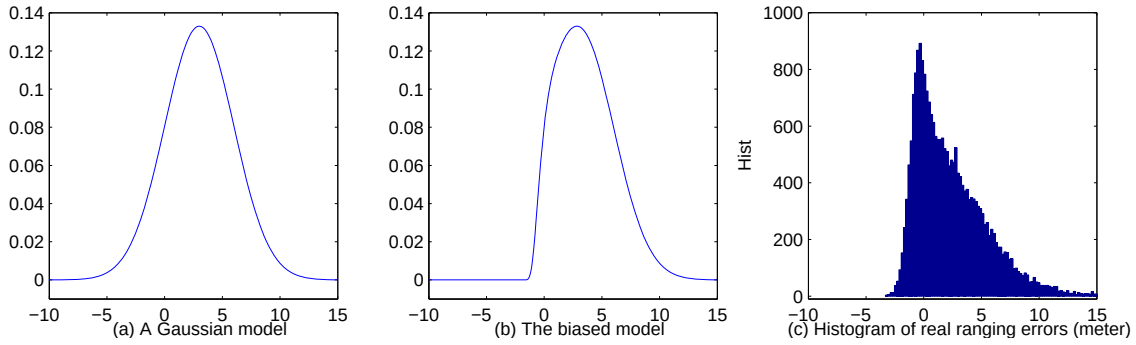

Figure 4.24: The fitted Gaussian model, the model tuned by the bias function, and the histogram of the ranging errors with real-world measurements

Figure 4.24 illustrates the measurement model modified by the bias function: Fig. 4.24(a) is a Gaussian model, and Fig. 4.24(b) is the model biased by b. It is explicit that the model with b imitates the bias and tailed histogram, which tunes the likelihood in the following two ways

[7]The bias function is a negative exponential function parameterized ($\mathrm{c}_1^b = 1, \mathrm{c}_2^b = 1$), additionally, other parameterize values or bias functions can be chosen according to the experiment statistics.

1. The state samples with negative Res are probably not the actual position, whose likelihood is deemphasized;
2. The large positive Res may be caused by the NLOS error; thus, the samples with large Res are still possible to be the true state, whose likelihood is slightly emphasized.

Note that in statistics literatures, there are biased distributions for the measurement model, which are impracticable due to either the multi-parameter configuration or high computation. While the proposed bias function allows to enjoy the simplicity of a Gaussian model, meanwhile, flexibly interpret the NLOS bias.

Algorithm 20 A bias function (b) on the ranging model

Output: $[p(Res_l^b)]$

1: Get the sample pool of the ranging measurements, and then do distribution fitting to a Gaussian model $\varepsilon_r \sim \mathcal{N}(\mu_{\varepsilon_r}, \sigma^2_{\varepsilon_r})$; as for our experiments, we take $\mathcal{N}(2.5, 3^2)$
2: Configure the bias function $(\mathrm{c}_1^b, \mathrm{c}_2^b)$ according to statistical analysis; for our experiments, we take $\mathrm{c}_1^b = 1, \mathrm{c}_2^b = 1$
3: Set the biased ranging error model as (4.77)

4.3.3 Adaptive measurement model

In most cases, the probabilistic positioning framework explores an adaptive prior but a fixed empirical measurement model [17]. Since the presence of NLOS errors can vary drastically over time and space, the fixed measurement model may seriously affect the performance. Hence, NLOS mitigation can be achieved by extending the measurement models to using adaptive parameters [136].

The idea is that if there is an initial position estimation ($\hat{\mathbf{x}}_{\text{initial}}$) having much lower uncertainty than the NLOS error, then $\hat{\mathbf{x}}_{\text{initial}}$ can be confident to help turning the NLOS ranging back into regular ranging. Thus, an adaptive Gaussian model is proposed as

$$p_{\text{adapt}}(r^l|\mathbf{x}) \sim \mathcal{N}(r^l - \mu^l_{\text{adapt}}, (\sigma^l_{\text{adapt}})^2), \;\; l \in \{\cdot\}_1^{N_{\text{anc}}} , \tag{4.80}$$

with the adaptive parameters $(\mu^l_{\text{adapt}}, \sigma^l_{\text{adapt}})$. In this adaption, the ranging measurement is modified by the residual $(r^l - \hat{r}^l)$ with a correction degree (c_{corr})

$$\mu^l_{\text{adapt}} = c_{\text{corr}} \times (r^l - \hat{r}^l) + (1 - c_{\text{corr}}) \times \mu_{\varepsilon_r} , \tag{4.81}$$

with the predicted range $\hat{r}^l = \left\| \hat{\mathbf{x}}_{\text{initial}} - \mathbf{a}^l \right\|$. The larger c_{corr} is, the higher the leverage the correction

has. The c_{corr} is a number between 0 and 1, which is defined as

$$c_{\text{corr}} = \frac{\sigma^2_{\varepsilon_r}}{\sigma^2_{\varepsilon_r} + \sigma^2_{\varepsilon_{\hat{r}}}} \ . \tag{4.82}$$

with $\sigma^2_{\varepsilon_r}$ denoting the uncertainty of the measured ranging and $\sigma^2_{\varepsilon_{\hat{r}}}$ for predicted one. Since the measured and predicted ranges determine the likelihood and initial estimation, respectively, Eq. (4.82) is approximated as

$$c_{\text{corr}} \approx \frac{\sigma^2_{\text{likelihood}}}{\sigma^2_{\text{likelihood}} + \sigma^2_{\text{initial}}} \ , \tag{4.83}$$

where $\sigma^2_{\text{initial}}$ and $\sigma^2_{\text{likelihood}}$ are the sample-based variance of the initial and likelihood density, respectively.

The prior uncertainty is

$$\hat{\sigma}^2_{\text{initial}} = \sum_{i=1}^{Ns} w^i_{\text{initial}} \ \|\mathbf{x}^i - \hat{\mathbf{x}}_{\text{initial}}\|^2 \ , \tag{4.84}$$

with w_{initial} being the initial weighted.

The likelihood uncertainty is

$$\hat{\sigma}^2_{\text{likelihood}} = \sum_{i=1}^{Ns} p(r^l|\mathbf{x}^i) \ \|\mathbf{x}^i - \hat{\mathbf{x}}_{\text{likelihood}}\|^2 \ , \tag{4.85}$$

where $\hat{\mathbf{x}}_{\text{likelihood}}$ is the expectation of the likelihood weighted samples; the statistical measurement model is $p(r|\mathbf{x}) \sim \mathcal{N}(r - \mu_{\varepsilon_r}, \sigma^2_{\varepsilon_r})$.

The variance of the adaptive measurement model is a weighted mean of the ranging residual and the statistical variance

$$(\sigma^l_{\text{adapt}})^2 = c_{\text{corr}} \times (r^l - \hat{r}^l)^2 + (1 - c_{\text{corr}}) \times \sigma^2_{\varepsilon_r}, \ \ l \in \{\cdot\}_1^{N_{\text{anc}}} \ , \tag{4.86}$$

which describes that the larger the ranging residual is, the higher uncertain the measurement is.

As the measurements of neighboring time-steps are temporary and spacial correlated, the adaptive measurement model uses the difference between the likelihood and the prediction density to parameterize the model of each ranging measurement. The pseudo-code of NLOS is described in **Algorithm** 21.

Algorithm 21 Adaptive measurement model for NLOS mitigation

Output and input: $[\left\{\mathcal{N}(\mu^l_{\text{adapt}}, (\sigma^l_{\text{adapt}})^2)\right\}_{l=1}^{N_{\text{anc}}}] = [p(r|\mathbf{x})]$

1: Obtain the initial state $(\{\mathbf{x}^i, w^i_{\text{initial}}\}_{i=1}^{N_s})$ from a previous estimation or initial estimation
2: Calculate the sample-based likelihood from the statistical measurement model $p(r|\mathbf{x})$
3: Adapt the Gaussian parameters $(\mu^l_{\text{adapt}}, (\sigma^l_{\text{adapt}})^2)$ from (4.81) and (4.86)

4.3.4 Results and analysis

The effectiveness of the proposed NLOS mitigation methods (the biased MF model, the bias function (b) and the adaptive Gaussian model) is compared by applying on the used sample-based algorithms, with the results shown in Fig. 4.25.

Through Fig. 4.25, one can find out the notable improvements of using the proposed biased models (the MF and bias function), indicating that the bias model can imitate the NLOS errors well enough. The other biased parametric models discussed in Chapter 3.3, i.e., the Log-normal, Gamma, Weibull distribution or mixture distributions, have not been compared, due to the multi-parameter and non-negative features. Thus, the two proposed biased models take the benefit of the flexibility without parametric modeling. The adaptive approach also reduces positioning error, except for applying on the GeoF algorithm. This deviation is because that using an erroneous prior to adapt the measurement model can introduce extra uncertainty.

Comparing the simplicity of the three NLOS mitigation, the biased models (the MF and bias function) are more effective in both the performance improvement and implementation efficiency. The adaptive method allows for modifying the measurement model over time, unlike the biased model being fixed over time.

The positioning behavior of the two basic filters (Generic-PF and RBGF) is plotted in Fig 4.26, comparing with and without the NLOS mitigation. Compared with the original Generic-PF and RBGF, the scatter plot of positioning using NLOS mitigation achieves a smaller variance. As marked by an ellipse in each sub-figure, the ranging at that site is more likely to observe an NLOS error due to the metal wall; from Fig 4.26 (c-h), the positioning behavior demonstrates that the NLOS mitigation methods remove the large positioning errors.

4.3.5 Discussion

1) MF model

As one may question the generality of the MF model, the MF configuration is changed with different confidence levels (from 90% to 99%). Additionally, a Gaussian model and two faulty MF

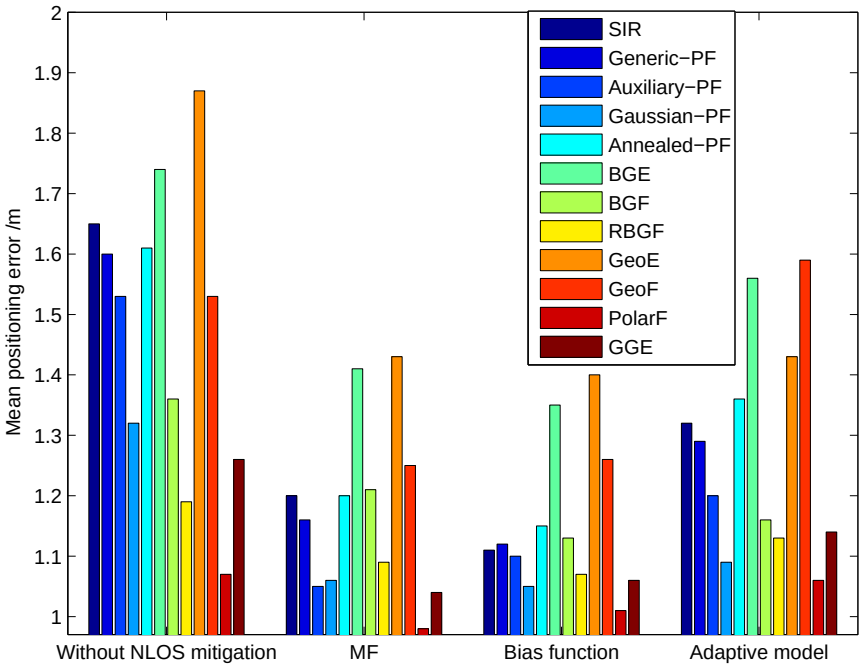

Figure 4.25: Mean positioning error (/meter) of the proposed NLOS mitigation methods

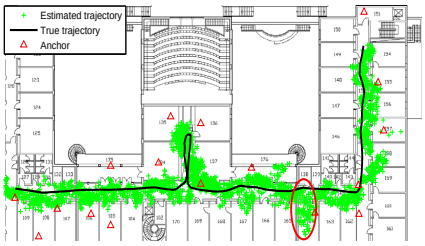

(a) Generic-PF without NLOS mitigation

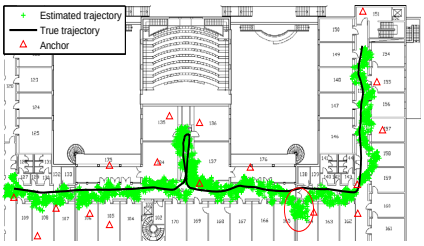

(b) RBGF without NLOS mitigation

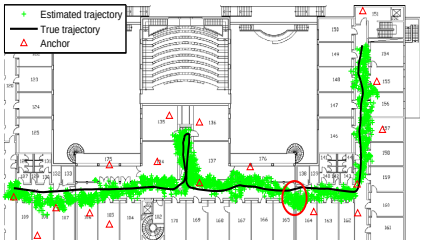

(c) Generic-PF with MF

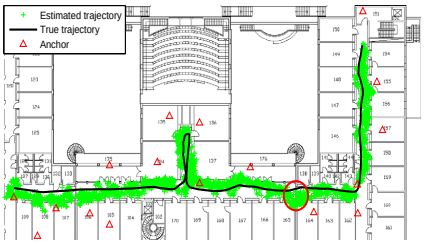

(d) RBGF with MF

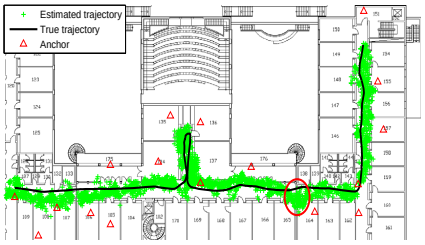

(e) Generic-PF with b

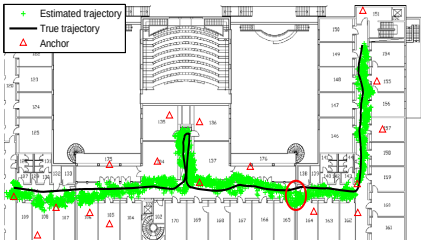

(f) RBGF with b

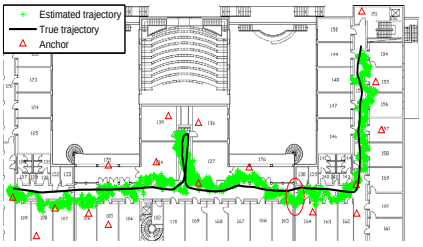

(g) Generic-PF with $\mathcal{N}(\mu^l_{\text{adapt}}, (\sigma^l_{\text{adapt}})^2)$

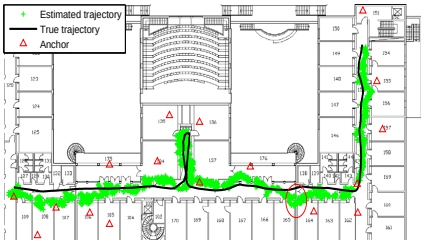

(h) RBGF with $\mathcal{N}(\mu^l_{\text{adapt}}, (\sigma^l_{\text{adapt}})^2)$

Figure 4.26: Positioning behavior of the proposed NLOS mitigation methods applied to Generic-PF and RBGF, in the experiment M1 on the floor plan: the scatterplot is estimated trajectory; the solid line is the true mobile trajectory; $\triangle$ denotes anchors; the location marked by the ellipse is nearby a metal fire-protect wall which causes NLOS ranging.

models (on purpose) are compared. The MF model is configured with the measurements from M2, while, the positioning is performed in M1, with the results presented in Table 4.6.

Table 4.6: Effect of the MF parameters on BGF, with the positioning error (/meter) of the experiment M1

MF Model (confidence level)	Parameters $[\eta_{\text{low}}, MF_{\text{median}}, \eta_{\text{up}}]$	MEAN_p	RMSE_p	MAX_p
MF 99%	[-2.51, 2.07, 19.17]	1.16	1.30	4.29
MF 98%	[-1.97, 2.29, 13.19]	1.19	1.32	3.90
MF 90%	[-1.45, 1.85, 7.69]	1.29	1.51	6.37
Faulty MF 1	[-1, 0, 5]	1.52	1.86	9.32
Faulty MF 2	[-15, 0, 15]	1.61	2.18	9.84
Gaussian model	$\mathcal{N}(2.5, 3^2)$	1.36	1.57	6.37

Table 4.6 presents that: 1) the MF configured by the experiment M2 works well for positioning of M1, which implies that the ranging model of the same building or similar scenarios can be stationary and configured by a few statistics; 2) different MF configurations or even the faulty MF still lead to acceptable results, telling that the performance of MF method is not sensitive to the three parameters; the BGF with the Gaussian model performs worse, demonstrating that the MF solution is suitable for non-Gaussian ranging errors. Nevertheless, a careful choice of the MF shape and MF parameters are necessary for promising improvements.

2) Adaptive measurement model

The variable c_{corr} used to correct the NLOS error is adaptive in (4.83). To exam the effect of the c_{corr}, the comparison of setting c_{corr} to fixed values is investigated, see Fig. 4.27. By varying the values of the c_{corr}, the mean positioning are almost the same. Compared with the NLOS mitigation with fixed c_{corr} and the Generic-PF without NLOS mitigation, the adaptive c_{corr} results in a notable improvement. It implies that, the adaptive c_{corr} can feasibly indicate the quality of the measurement and make a correction on the NLOS ranging.

Overall, the measurement model is the most important aspect for the NLOS mitigation purpose. In NLOS conditions, the measurement model can be oversimplified (the Gaussian model) or overly complicated (such as the mixture models, ray-tracing based models, empirical histogram models and online data training). The strengths of proposed nonparametric models are that they are easy to set up and require no analytical derivation.

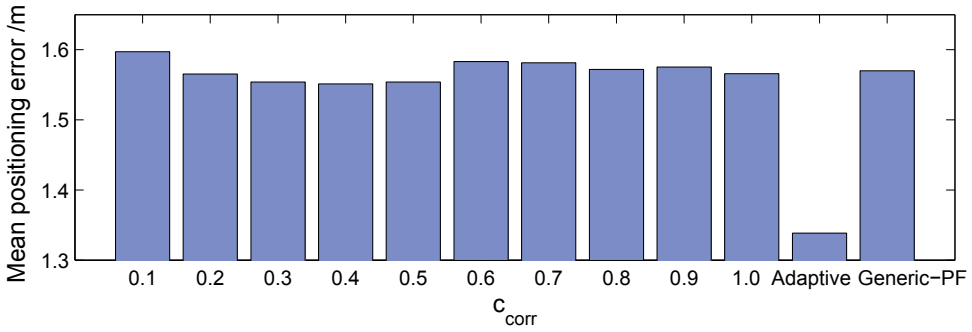

Figure 4.27: Positioning error of the Generic-PF using the adaptive measurement model, with the fixed or adaptive c_{corr} in the experiment M1

4.4 Summary

The error propagation analysis implies that, the positioning performance is related to the anchor deployment, the position estimator, the number of measurements and the measurement model. Therefore, this chapter investigates the practical anchor deployment, the sampling algorithms for probabilistic positioning and the NLOS mitigation to refine the measurement model.

According to theoretical CRLB-2D analysis and the practical considerations to real-world indoor scenarios, the anchor placement is suggested that: 1) it should first guarantee sufficient anchors be placed around the borderline of the positioning field; 2) it is also necessary to deploy some anchors in the interior field, corners or NLOS regions, in case that the borderline anchors are not reachable.

The key idea of the constrained sampling is to focus the samples on the probable region instead of exhaustively covering all possibilities of the state. Therefore, the sample size is notably reduced. Furthermore, the resampling step is avoided.

The weakness of the sample-based methods is that the samples' properties have to be stored. The algorithms BGF-A, RBGF-A, GeoF-A and PolarF-A achieve comparable accuracy, confirming that the Gaussian prior works well and considerablely reduces the complexity.

To mitigate the NLOS effect, the choice of the measurement model should take into account the features of indoor ranging. Thus, three measurement models are introduced: the two bias models are able to parameterize the bias of the NLOS errors; the adaptive model optimizes the hyperparameters based on the variance of the prediction density and likelihood. The proposed models achieve both substantial improvements and good flexibility.

Chapter 5

One Time-step Smoothing for Real-time Positioning

Since the ranging uncertainty is severe, the positioning estimation observes a high amplitude of variance. Specially, due to the high failure of RF communication, the sparse anchor deployment and the NLOS conditions, indoor positioning often encounters the problem of sparse ranging measurements. In non-sequential positioning, the estimation variance and sparsity problems can be solved by data fusion after waiting for more measurements. For sequential estimation, the smoothing frame is of particular interest as being able to make the state probability from not only the past and present observations ($\mathbf{z}_{1:t}$) but also the future observations ($\mathbf{z}_{t:T}$, $t < T$) [144].

Aiming of real-time positioning, it is impractical to apply the smoothing frame involving a high dimension of the future observation. Therefore, this chapter focuses on the smoothing implementation with the measurements one time-step ahead, which includes: 1) the popular smoothing solutions: Forward Filtering Backward Smoothing (FFBS) [93], Two-filter Smoothing (TFS) [57] and Rauch-Tung-Striebel (RTS) smoothing [78]; 2) a new method the smoothed filtering (SF).

5.1 Motivation and Problem Statement

5.1.1 Motivation

To generate a smooth representation of the positioning trajectory, Bayesian smoothing methods have been extensively studied. The smoothing frame ($p(\mathbf{x}_t|\mathbf{z}_{1:t})$) is beneficial by deriving the state probability from the past, present and future observations, which generally provides better approximations of marginal smoothing distributions compared with filtering methods [89, 94].

Beside that the sense of a smooth representation of tracking trajectory, the smoothing frame has more definite meaning for a relatively small number of observations of indoor ranging techniques. It is defined as a *sparsity problem* of LOS ranging measurements, which is categorized into two types:

- scarce measurements: the number of ranging measurements is insufficient due to the sparse anchor deployment or temporary packet loss;
- NLOS case: there are enough ranging measurements, but the LOS measurements are the minority.

Figure 5.1 depicts the sparsity problem, indicating that the measurement sparsity only occurs in a few ranging instances, e.g., the ranging neighboring the scarce instance can still obtain sufficient measurements; moreover, the NLOS error appears randomly rather than presenting continuously. Therefore, the sparsity problem is a temporary problem.

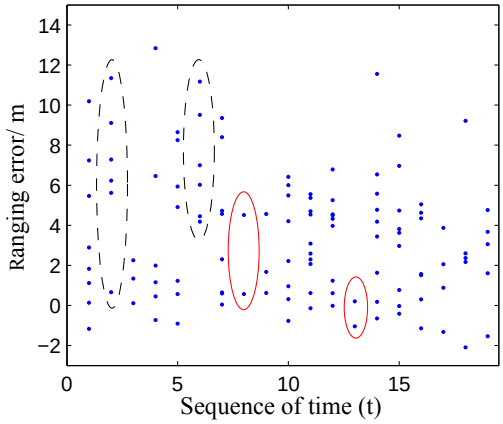

Figure 5.1: Scarce LOS ranging measurements due to either the sparse anchor deployment or the NLOS conditions: the samples surrounded by the dashed ellipse describe NLOS scenarios; the samples circled by the ellipse represent the condition of sparse reachable anchors

The smoothing frame is likely to work well in the sparse conditions, as it computes the state by conditioning not only on the observations up to current time but also on future ones.

5.1.2 Problem statement

The Bayesian smoothing approaches are promising in both smoothing the tracking trajectory and solving the sparsity problem. The smoothing density is to estimate the state given past, present and future observation

$$p(\mathbf{x}_t|\mathbf{z}_{1:T}) \,, \tag{5.1}$$

where $t \leq T$. In the case that the time-step size of the future observations is fixed, it is called as the *smoothing lag*

$$\triangle T = T - t \,. \tag{5.2}$$

To apply the smoothing frame in real-time range-based positioning, the challenge is twofold:

- *Problem 1*: Tractable solution
  For 2D range-based positioning, it cannot typically generate an exact solution to the nonlinear and non-Gaussian models. Particle methods (Monte Carlo methods) [50] offer an approximate solution, unfortunately, they are intractable if the sample size is large.
- *Problem 2*: Implementation issue
  If the smoothing recursion involves the observations many time-steps ahead ($t \ll T$), it can be computation, storage, and time consuming. In other words, it is impractical to obtain overall smoothed estimates using the observations from the end to the beginning.

The closed-form solution for 2D range-based positioning often does not exist, which is generally necessary to resort to Monte Carlo sampling methods. Sequential Monte Carlo with importance sampling [53] solves problems 1, which provide efficient solutions for nonlinear smoothing. However, the performance and applicability of the smoothing framework greatly depend on how much and how the future observations are incorporated. Aiming at real-time position tracking, it is preferable to formulate the smoothing density from the observations a few time-steps ahead. Overall, we are interested in the smoothing density of one time-step recursion ($p(\mathbf{x}_t|\mathbf{z}_{1:t+1})$) using SMC.

5.2 One Time-step Smoothing

The sequential position estimation or position tracking is defined as the time-series estimation of the posterior given all the available observations. The 2D position can be estimated by either filtering or smoothing frames.

- *Filtering* $p(\mathbf{x}_t|\mathbf{z}_{1:t})$: to estimate the distribution of the state $\mathbf{x}_t$ conditionally to the observations up to t.
- *Smoothing* $p(\mathbf{x}_t|\mathbf{z}_{1:T})$: to estimate the distribution of the state $\mathbf{x}_t$ conditionally to the observations up to T (with $t < T$).

To recur the Bayesian frame, it essentially applies a hidden Markov model (HMM) of order one [155] as follows.

State transition model

$$\mathbf{x}_t = f(\mathbf{x}_{t-1}, \mathbf{q}_t) \,, \tag{5.3}$$

where $\mathbf{x}_t = (x_t, y_t)$ is the 2D coordinates; $\mathbf{q}_t$ denotes the process noise. The state propagation from $t-1$ to t is $p(\mathbf{x}_t|\mathbf{x}_{t-1}, \mathbf{z}_{1:t-1}) \approx p(\mathbf{x}_t|\mathbf{x}_{t-1})$, assuming that the state at time t is stochastically dependent on the state at $t-1$.

Measurement model

$$\mathbf{z}_t = g(\mathbf{x}_t, \mathbf{n}_t) \,, \tag{5.4}$$

with $\mathbf{n}_t$ being the measurement noise. It assumes the observation at t is conditionally independent given the state at t, leading to $p(\mathbf{z}_t|\mathbf{x}_t, \mathbf{z}_{1:t-1}) \approx p(\mathbf{z}_t|\mathbf{x}_t)$. The vector of the current observations ($\mathbf{z}_t$) from N^t_{anc} reachable anchors ($\{\mathbf{a}^t_l = (a^t_{xl}, a^t_{yl})\}_{l=1:N^t_{\text{anc}}}$) is

$$\mathbf{z}_t = \{r^t_l\}_{l=1:N^t_{\text{anc}}}, \tag{5.5}$$

with r^t_l the ranging measurement from the lth anchor at t.

To smooth the estimated trajectory, improve accuracy, and deal with the sparsity problem, the sequential smoothing can be promising. However, the complexity of the smoothing method is proportional to the smoothing lag ($\triangle T$): the larger the $\triangle T$ is, the higher the computation and latency are. Consequently, two Bayesian smoothing methods are applied with one time-step future observation, Forward Filtering Backward Smoothing (FFBS) and Two Filter Smoothing (TFS) [144]

$$\triangle\, T = 1 \,. \tag{5.6}$$

Both these two smoothing methods compute the same sequence of conditional distribution $p(\mathbf{x}_t|\mathbf{z}_{1:t+1})$, which is defined as *one time-step smoothing*.

5.2.1 Forward Filtering Backward Smoothing (FFBS)

The smoothing density can be deduced from a forward-backward recursive expression, namely, Forward Filtering Backward Smoothing (FFBS) [23]. The smoothing density of FFBS on one time-

step frame is

$$
\begin{aligned}
p(\mathbf{x}_t|\mathbf{z}_{1:t+1}) &= \int p(\mathbf{x}_t, \mathbf{x}_{t+1}|\mathbf{z}_{1:t+1})\, d\mathbf{x}_{t+1} \\
&= \int p(\mathbf{x}_{t+1}|\mathbf{z}_{1:t+1}) p(\mathbf{x}_t|\mathbf{x}_{t+1}, \mathbf{z}_{1:t+1})\, d\mathbf{x}_{t+1} \\
&\overset{\text{Markov}}{=} \int p(\mathbf{x}_{t+1}|\mathbf{z}_{1:t+1}) p(\mathbf{x}_t|\mathbf{x}_{t+1}, \mathbf{z}_{1:t})\, d\mathbf{x}_{t+1} \qquad (5.7) \\
&= \int \frac{p(\mathbf{x}_{t+1}|\mathbf{z}_{1:t+1}) p(\mathbf{x}_t, \mathbf{x}_{t+1}|\mathbf{z}_{1:t})}{p(\mathbf{x}_{t+1}|\mathbf{z}_{1:t})}\, d\mathbf{x}_{t+1} \\
&= p(\mathbf{x}_t|\mathbf{z}_{1:t}) \int \frac{p(\mathbf{x}_{t+1}|\mathbf{z}_{1:t+1}) p(\mathbf{x}_{t+1}|\mathbf{x}_t, \mathbf{z}_{1:t})}{p(\mathbf{x}_{t+1}|\mathbf{z}_{1:t})}\, d\mathbf{x}_{t+1} \\
&\overset{\text{Markov}}{=} p(\mathbf{x}_t|\mathbf{z}_{1:t}) \int \frac{p(\mathbf{x}_{t+1}|\mathbf{z}_{1:t+1}) p(\mathbf{x}_{t+1}|\mathbf{x}_t)}{\int p(\mathbf{x}_{t+1}|\mathbf{x}_t) p(\mathbf{x}_t|\mathbf{z}_{1:t})\, d\mathbf{x}_t}\, d\mathbf{x}_{t+1} \ . \qquad (5.8)
\end{aligned}
$$

The filtering density ($p(\mathbf{x}_{t+1}|\mathbf{z}_{1:t+1})$) is computed by your favorite forward filter, such as the Generic Particle Filter (GPF) [11] as

$$
w^i_{t+1|t+1} \propto w^i_{t|t} p(\mathbf{z}_{t+1}|\mathbf{x}^i_{t+1}),\ i \in \{\cdot\}_1^{N_\mathrm{p}} \ , \qquad (5.9)
$$

where $w^i_{t+1|t+1}$ is the filtering weight of the ith particle at $t+1$.

The smoothing density (5.8) is numerically represented as

$$
p(\mathbf{x}_t|\mathbf{z}_{1:t+1}) \approx \sum_{i=1}^{N_\mathrm{p}} w^i_{t|t+1} \delta(\mathbf{x}_t - \mathbf{x}^i_t) \ , \qquad (5.10)
$$

with the ith smoothing weight

$$
\begin{aligned}
w^i_{t|t+1} &\approx w^i_{t|t} \sum_{j=1}^{N_\mathrm{p}} \left\{ w^j_{t+1|t+1} \frac{p(\mathbf{x}^j_{t+1}|\mathbf{x}^i_t)}{p(\mathbf{x}^j_{t+1}|\mathbf{z}_{1:t})} \right\} \\
&\approx w^i_{t|t} \sum_{j=1}^{N_\mathrm{p}} \left\{ w^j_{t+1|t+1} \frac{p(\mathbf{x}^j_{t+1}|\mathbf{x}^i_t)}{\sum_{k=1}^{N_\mathrm{p}} w^k_{t|t} p(\mathbf{x}^j_{t+1}|\mathbf{x}^k_t)} \right\},\ i \in \{\cdot\}_1^{N_\mathrm{p}} \ . \qquad (5.11)
\end{aligned}
$$

Then, the position estimation at t by the smoothing density is

$$\hat{\mathbf{x}}_t = \mathrm{E}(p(\mathbf{x}_t|\mathbf{z}_{1:t+1})) = \sum_{i=1}^{N_\mathrm{p}} \mathbf{x}_t^i w_{t|t+1}^i \ . \tag{5.12}$$

The FFBS (5.11) consists of the filtering distribution ($p(\mathbf{x}_t|\mathbf{z}_{1:t})$) and the backward re-weighting probability from the future ($\mathbf{z}_{t+1}$). The pseudo-code of FFBS is in **Algorithm** 22.

Algorithm 22 Forward Filtering Backward Smoothing (FFBS)

Output and input: $\left[\hat{\mathbf{x}}_t,\ \{\mathbf{x}_{t+1}^i,\ w_{t+1|t+1}^i\}_{i=1:N_\mathrm{p}}\right] = \mathrm{FFBS}\left[\mathbf{z}_{t+1},\ \mathbf{A}_{t+1},\ \{\mathbf{x}_t^i,\ w_{t|t}^i\}_{i=1:N_\mathrm{p}}\right]$
Setting: N_p, $p(\mathbf{x}_t|\mathbf{x}_{t-1})$, $p(\mathbf{z}_t|\mathbf{x}_t)$, ${N_\mathrm{eff}}^{threshold} = 0.5N_\mathrm{p}$
Initialization:

- $p(\mathbf{x}_1)$
- $\left\{\mathbf{x}_1^i \sim p(\mathbf{x}_1)\right\}_{i=1:N_\mathrm{p}}$
- $\left\{w_1^i = \frac{1}{N_\mathrm{p}}\right\}_{i=1:N_\mathrm{p}}$
- $t = 1$

1: Importance sampling $\left\{\mathbf{x}_{t+1}^i \sim p(\mathbf{x}_{t+1}|\mathbf{x}_t^i)\right\}_{i=1:N_\mathrm{p}}$
2: Update the filtering weights $\left\{w_{t+1|t+1}^i\right\}_{i=1:N_\mathrm{p}}$ (5.9) and normalization $\left\{w_{t+1|t+1}^i = \frac{w_{t+1|t+1}^i}{\sum_{j=1}^{N_\mathrm{p}} w_{t+1|t+1}^j}\right\}_{i=1:N_\mathrm{p}}$
3: Assign the smoothing weights $\left\{w_{t|t+1}^i\right\}_{i=1:N_\mathrm{p}}$ (5.11), and normalization $\left\{w_{t|t+1}^i = \frac{w_{t|t+1}^i}{\sum_{j=1}^{N_\mathrm{p}} w_{t|t+1}^j}\right\}_{i=1:N_\mathrm{p}}$
4: Estimate position $\hat{\mathbf{x}}_t^{\mathrm{FFBS}}$ (5.12)
5: If $\widehat{N_\mathrm{eff}} < {N_\mathrm{eff}}^{threshold}$, then resampling
6: Set $t = t + 1$ and iterate to item 1

5.2.2 Two Filter Smoothing (TFS)

The two-filter smoothing (TFS) [41] is a well-established alternative to FFBS, which obtains the smoothing density ($p(\mathbf{x}_t|\mathbf{z}_{1:t+1})$) from two independent filters (the forward and the backward filters).

Given observations up to $t+1$, the smoothing density of TFS is

$$\begin{aligned}
p(\mathbf{x}_t|\mathbf{z}_{1:t+1}) &= p(\mathbf{x}_t|\mathbf{z}_{1:t-1}, \mathbf{z}_{t:t+1}) \\
&= \frac{p(\mathbf{x}_t, \mathbf{z}_{t:t+1}|\mathbf{z}_{1:t-1})}{p(\mathbf{z}_{t:t+1}|\mathbf{z}_{1:t-1})} \\
&\propto p(\mathbf{x}_t|\mathbf{z}_{1:t-1})p(\mathbf{z}_{t:t+1}|\mathbf{x}_t) \\
&= p(\mathbf{x}_t|\mathbf{z}_{1:t-1})p(\mathbf{z}_t|\mathbf{x}_t)p(\mathbf{z}_{t+1}|\mathbf{x}_t) \\
&= p(\mathbf{x}_t|\mathbf{z}_{1:t-1})p(\mathbf{z}_t|\mathbf{x}_t, \mathbf{z}_{1:t-1})p(\mathbf{z}_{t+1}|\mathbf{x}_t) \\
&\propto p(\mathbf{x}_t|\mathbf{z}_{1:t})p(\mathbf{z}_{t+1}|\mathbf{x}_t) \\
&\propto \underbrace{p(\mathbf{x}_t|\mathbf{z}_{1:t})}_{\text{Forward filter}} \underbrace{\int p(\mathbf{z}_{t+1}|\mathbf{x}_{t+1})p(\mathbf{x}_{t+1}|\mathbf{x}_t)\, d\mathbf{x}_{t+1}}_{\text{Backward filter}} .
\end{aligned} \tag{5.13}$$

The first filter is the forward filter, which calculates the posterior distribution $p(\mathbf{x}_t|\mathbf{z}_{1:t})$; the second filter calculates a series of backward functions $p(\mathbf{z}_{t+1:T}|\mathbf{x}_t)$, that in the one time-step case is $p(\mathbf{z}_{t+1}|\mathbf{x}_t)$. Together, these two filters construct the smoothing density of TFS.

An important requirement of TFS is that $p(\mathbf{z}_{t+1:T}|\mathbf{x}_t)$ should be a probability density, in other words, the integral of this function is finite. Thus, the smoothing density of (5.13) is rewritten as

$$p(\mathbf{x}_t|\mathbf{z}_{1:t+1}) = \frac{p(\mathbf{x}_t|\mathbf{z}_{1:t})\frac{\int p(\mathbf{z}_{t+1}|\mathbf{x}_{t+1})p(\mathbf{x}_{t+1}|\mathbf{x}_t)\, d\mathbf{x}_{t+1}}{\lambda_2}}{\lambda_1} , \tag{5.14}$$

where λ_1 and λ_2 are the normalization factors of the smoothing and backward density, respectively. The smoothing density is represented as (5.9) with the weights

$$w^i_{t|t+1} = \frac{w^i_{t|t}\frac{\sum_{j=1}^{N_\mathrm{p}}\left\{p(\mathbf{z}_{t+1}|\mathbf{x}^j_{t+1})p(\mathbf{x}^j_{t+1}|\mathbf{x}^i_t)\right\}}{\lambda_2}}{\lambda_1}, \; i \in \{\cdot\}_1^{N_\mathrm{p}} . \tag{5.15}$$

The pseudo-code of the TFS is described in **Algorithm** 23.

5.2.3 Smoothed Filtering (SF)

The FFBS and TFS formulate the smoothing density ($p(\mathbf{x}_t|\mathbf{z}_{1:t+1})$) from the current ($p(\mathbf{x}_t|\mathbf{z}_{1:t})$) and future ($p(\mathbf{x}_{t+1}|\mathbf{z}_{1:t+1})$) density. They are theoretically sound, as taking into account the future measurements. The shortcoming is that the smoothing density only influence the point estimation in (5.12) rather than improving the density propagation.

Algorithm 23 Two Filter Smoothing (TFS)

Output and input: $\left[\hat{\mathbf{x}}_t,\ \{\mathbf{x}^i_{t+1},\ w^i_{t+1|t+1}\}_{i=1:N_\mathrm{p}}\right] = \mathrm{TFS}\left[\mathbf{z}_{t+1},\ \mathbf{A}_{t+1},\ \{\mathbf{x}^i_t,\ w^i_{t|t}\}_{i=1:N_\mathrm{p}}\right]$
Setting: N_p, $p(\mathbf{x}_t|\mathbf{x}_{t-1})$, $p(\mathbf{z}_t|\mathbf{x}_t)$, ${N_\mathrm{eff}}^{threshold} = 0.5N_\mathrm{p}$
Initialization:

- $p(\mathbf{x}_1)$
- $\left\{\mathbf{x}^i_1 \sim p(\mathbf{x}_1)\right\}_{i=1:N_\mathrm{p}}$
- $\left\{w^i_1 = \frac{1}{N_\mathrm{p}}\right\}_{i=1:N_\mathrm{p}}$
- $t = 1$

1: Importance sampling $\left\{\mathbf{x}^i_{t+1} \sim p(\mathbf{x}_{t+1}|\mathbf{x}^i_t)\right\}_{i=1:N_\mathrm{p}}$
2: Assign filtering weights $\left\{w^i_{t+1|t+1}\right\}_{i=1:N_\mathrm{p}}$ (5.9) and normalization $\left\{w^i_{t+1|t+1} = \frac{w^i_{t+1|t+1}}{\sum_{j=1}^{N_\mathrm{p}} w^j_{t+1|t+1}}\right\}_{i=1:N_\mathrm{p}}$
3: Assign smoothing weights $\left\{w^i_{t|t+1}\right\}_{i=1:N_\mathrm{p}}$ as (5.15)
4: Estimate position $\hat{\mathbf{x}}^{\mathrm{TFS}}_t$ (5.12)
5: If $\widehat{N_\mathrm{eff}} < {N_\mathrm{eff}}^{threshold}$, then resampling
6: Set $t = t + 1$ and iterate to item 1

Since FFBS and TFS have not incorporated the smoothing density into the state recursion, we propose to propagate the posterior from the smoothing density, formulated as

$$p(\mathbf{x}_{t+1}|\mathbf{z}_{1:t+1}) = \int p(\mathbf{x}_t|\mathbf{z}_{1:t+1})p(\mathbf{x}_{t+1}|\mathbf{x}_t, \mathbf{z}_{1:t+1})\, d\mathbf{x}_t\ , \tag{5.16}$$

namely, Smoothed Filtering (SF). Indeed, the only difference to FFBS and TFS is that instead of propagating the posterior from the prediction density, the SF is derived from one time-step smoothing density.

Form a Markov process of order one, it means that

$$\begin{aligned} p(\mathbf{x}_{t+1}|\mathbf{x}_t, \mathbf{z}_{1:t+1}) &\overset{\text{Markov}}{=} p(\mathbf{x}_{t+1}|\mathbf{x}_t, \mathbf{z}_{t+1}) \\ &= \frac{p(\mathbf{x}_{t+1}, \mathbf{z}_{t+1}|\mathbf{x}_t)}{p(\mathbf{z}_{t+1}|\mathbf{x}_t)} \\ &= \frac{p(\mathbf{z}_{t+1}|\mathbf{x}_{t+1}\mathbf{x}_t)p(\mathbf{x}_{t+1}|\mathbf{x}_t)}{p(\mathbf{z}_{t+1}|\mathbf{x}_t)} \\ &= \frac{p(\mathbf{z}_{t+1}|\mathbf{x}_{t+1})p(\mathbf{x}_{t+1}|\mathbf{x}_t)}{p(\mathbf{z}_{t+1}|\mathbf{x}_t)} \\ &= \frac{p(\mathbf{z}_{t+1}|\mathbf{x}_{t+1})p(\mathbf{x}_{t+1}|\mathbf{x}_t)}{\int p(\mathbf{z}_{t+1}|\mathbf{x}_{t+1})p(\mathbf{x}_{t+1}|\mathbf{x}_t)\, d\mathbf{x}_{t+1}} . \end{aligned} \tag{5.17}$$

The factor $p(\mathbf{x}_{t+1}|\mathbf{x}_t, \mathbf{z}_{1:t+1})$ can be derived by (5.17), alternatively, by the approximation $p(\mathbf{z}_{t+1}|\mathbf{x}_{t+1}) \approx p(\mathbf{z}_{t+1}|\mathbf{x}_t)$ leading to

$$p(\mathbf{x}_{t+1}|\mathbf{x}_t, \mathbf{z}_{1:t+1}) \approx p(\mathbf{x}_{t+1}|\mathbf{x}_t) . \tag{5.18}$$

It is based on two facts of indoor RF positioning: 1) the difference of the state at neighborhood time-steps is very small, in other words, the target has a low velocity; 2) the uncertainty of the ranging measurements is much larger than that of the position estimation.

Similar to the TFS, the smoothing density of SF is

$$p(\mathbf{x}_t|\mathbf{z}_{1:t+1}) \propto p(\mathbf{x}_t|\mathbf{z}_{1:t})p(\mathbf{z}_{t+1}|\mathbf{x}_t) . \tag{5.19}$$

Hence, Eq. (5.16) is reformulated as

$$p(\mathbf{x}_{t+1}|\mathbf{z}_{1:t+1}) \propto \int p(\mathbf{x}_t|\mathbf{z}_{1:t})p(\mathbf{z}_{t+1}|\mathbf{x}_t)p(\mathbf{x}_{t+1}|\mathbf{x}_t)\, d\mathbf{x}_t . \tag{5.20}$$

Note that the posterior $p(\mathbf{x}_{t+1}|\mathbf{z}_{1:t+1})$ in (5.16) is a filtering density derived from the smoothing density, which can be numerically represented as

$$w^i_{t+1|t+1} \approx \sum_{j=1}^{N_\mathrm{p}} \left\{ w^i_{t|t+1} p(\mathbf{x}^i_{t+1}|\mathbf{x}^j_t) \right\},\ i \in \{\cdot\}_1^{N_\mathrm{p}} , \tag{5.21}$$

with the smoothing density deduced from (5.19) as

$$w^i_{t|t+1} \propto w^i_{t|t} p(\mathbf{z}_{t+1}|\mathbf{x}^i_t) . \tag{5.22}$$

The $p(\mathbf{z}_{t+1}|\mathbf{x}_t)$ in (5.20) can either be performed from the component of (5.14), or simply be approximated $p(\mathbf{z}_{t+1}|\mathbf{x}_t) \sim \mathcal{N}(\mu_{\varepsilon_r}, \sum^2_{\varepsilon_r})$ as the target's motion is slow.

Differing from that the FFBS and TFS estimate the state based on the smoothing density $p(\mathbf{x}_t|\mathbf{z}_{1:t+1})$, the SF estimation is by the filtering density ($p(\mathbf{x}_t|\mathbf{z}_{1:t})$) as

$$\hat{\mathbf{x}}_t^{\mathrm{SF}} = \mathrm{E}(p(\mathbf{x}_t|\mathbf{z}_{1:t})) = \sum_{i=1}^{N_\mathrm{p}} \mathbf{x}_t^i w_{t|t}^i \,. \tag{5.23}$$

The pseudo-code of the SF is described in **Algorithm** 24.

Algorithm 24 Smoothed Filtering (SF)

Output and input: $\left[\hat{\mathbf{x}}_t,\ \{\mathbf{x}_{t+1}^i,\ w_{t+1|t+1}^i\}_{i=1:N_\mathrm{p}}\right] = \mathrm{SF}\left[\mathbf{z}_{t+1},\ \mathbf{A}_{t+1},\ \{\mathbf{x}_t^i,\ w_{t|t}^i\}_{i=1:N_\mathrm{p}}\right]$
Setting: N_p, $p(\mathbf{x}_t|\mathbf{x}_{t-1})$, ${N_\mathrm{eff}}^{threshold} = 0.5N_\mathrm{p}$, $p(\mathbf{z}_t|\mathbf{x}_t) \sim \mathcal{N}(\mu_{\varepsilon_r}, \sum^2_{\varepsilon_r})$
Initialization:

- $p(\mathbf{x}_1)$
- $\left\{\mathbf{x}_1^i \sim p(\mathbf{x}_1)\right\}_{i=1:N_\mathrm{p}}$
- $\left\{w_1^i = \frac{1}{N_\mathrm{p}}\right\}_{i=1:N_\mathrm{p}}$
- $t = 1$

1: Estimate position $\hat{\mathbf{x}}_t^{\mathrm{SF}}$ (5.23)
2: Assign smoothing weights $\left\{w_{t|t+1}^i\right\}_{i=1:N_\mathrm{p}}$ (5.22)
3: Importance sampling $\left\{\mathbf{x}_t^i \sim p(\mathbf{x}_{t+1}|\mathbf{x}_t^i)\right\}_{i=1:N_\mathrm{p}}$
4: Update filtering weights $\left\{w_{t+1|t+1}^i\right\}_{i=1:N_\mathrm{p}}$ (5.21) and normalization $\left\{w_{t+1|t+1}^i = \frac{w_{t+1|t+1}^i}{\sum_{j=1}^{N_\mathrm{p}} w_{t+1|t+1}^j}\right\}_{i=1:N_\mathrm{p}}$
5: If $\widehat{N_\mathrm{eff}} < {N_\mathrm{eff}}^{threshold}$, then resampling
6: Set $t = t + 1$ and iterate to item 1

The smoothed posterior involves the future observations in the density propagation, which are powerful information to mitigate the estimation instability and sparsity problem.

5.3 Combine Linear Smoother with Nonlinear Filtering Output

Nonlinear estimations are able to deal with nonlinear uncertainty, while linear smoother are good at revealing low-frequency features and removing severe variance. Hence, it is interesting to add a linear smoother to a nonlinear filter. The idea is that; take the output of GPF ($\hat{\mathbf{x}}^{\mathrm{GPF}}$) as an "observa-

tion", which is smoothed by a linear smoother (Moving Average (MA) or Kalman smoother).

5.3.1 Moving average

The moving average is the simplest case of kernel filtering as

$$\hat{\mathbf{x}}_t^{\mathrm{MA}} = \sum_{k=1}^{N_{\mathrm{win}}} w_k \hat{\mathbf{x}}_{t-k+\lceil \frac{N_{\mathrm{win}}}{2} \rceil}^{\mathrm{GPF}}, \tag{5.24}$$

by setting all the kernel weights equally ($\{w_k = \frac{1}{N_{\mathrm{win}}}\}_{k=1}^{N_{\mathrm{win}}}$, with N_{win} being the moving window size). The kernel filtering is able to reducing high-frequency errors, but unable to address the estimation divergence. Also, the performance of MA highly relies on the window size.

5.3.2 Kalman smoother

The Kalman smoother [3] is well known to address the linear Gaussian problem. The uncertainty of the GPF output can be deemed as linear dynamics, thus, we use the Rauch-Tung-Striebel (RTS) smoother [74] (also known as two-pass smoother) to recursively obtain the Gaussian distributions of the state

$$p(\mathbf{X}_t | \hat{\mathbf{x}}_{t:t+\triangle T}^{\mathrm{GPF}}) \tag{5.25}$$

where the vector $\mathbf{X}_t = [x_t, y_t, \dot{x}_t, \dot{y}_t]^{\mathrm{T}}$ denotes the Cartesian coordinates and velocities toward both axes at t. The RTS smoother is an efficient two-pass algorithm: forward pass (a regular Kalman filter) and backwards pass.

In our smoothing case, the Kalman models consist of the state transition model and the uncertainty of the GPF estimation. The state transition model is expressed as

$$\mathbf{X}_t = \mathbf{A}\mathbf{X}_{t-1} + \mathbf{Q}_{t-1}, \tag{5.26}$$

where $\mathbf{A}$ is the state transition matrix

$$\mathbf{A} = \begin{pmatrix} 1 & 0 & \triangle t & 0 \\ 0 & 1 & 0 & \triangle t \\ 0 & 0 & 1 & 0 \\ 0 & 0 & 0 & 1 \end{pmatrix}$$

with $\triangle t = 1$ as the time sequence is a dimensionless parameter; $\mathbf{Q}_{t-1} \sim \mathcal{N}(0, Q)$ for the process noise at $t-1$ and Q being the time-invariant covariance matrix. Assuming the acceleration as Gaussian

noise ($\mathcal{N}(0, \mathrm{c}_a)$), Q is the following matrix

$$Q = \mathrm{c}_a \begin{pmatrix} \frac{1}{4}\triangle t^4 & 0 & \frac{1}{2}\triangle t^3 & 0 \\ 0 & \frac{1}{4}\triangle t^4 & 0 & \frac{1}{2}\triangle t^3 \\ \frac{1}{2}\triangle t^3 & 0 & \triangle t^2 & 0 \\ 0 & \frac{1}{2}\triangle t^3 & 0 & \triangle t^2 \end{pmatrix}. \tag{5.27}$$

Then, the $\hat{\mathbf{x}}_t^{\mathrm{RTS}}$ is corrected by the Kalman update step with the measurement matrix

$$\hat{\mathbf{x}}_t^{\mathrm{RTS}} = \begin{pmatrix} 1 & 0 & 0 & 0 \\ 0 & 1 & 0 & 0 \end{pmatrix} \mathbf{X}_t + \mathbf{r}_t \,, \tag{5.28}$$

where $\mathbf{r}_t \sim \mathcal{N}(0, R)$ is the GPF estimation error with the statistical covariance R.

The backwards pass recursively update the smoothed means ($\mathbf{m}_t^{\mathrm{smooth}}$) and covariances ($\mathbf{P}_t^{\mathrm{smooth}}$) as following

$$\begin{aligned} \mathbf{m}_{t+1}^{-} &= \mathbf{A}\mathbf{m}_t, \\ \mathbf{P}_{t+1}^{-} &= \mathbf{A}\mathbf{P}_t\mathbf{A}^{\mathrm{T}} + \mathbf{Q}_t, \\ \mathbf{K}_t &= \mathbf{P}_t\mathbf{A}^{\mathrm{T}}[\mathbf{P}_{t+1}^{-}]^{-1}, \\ \mathbf{m}_t^{\mathrm{smooth}} &= \mathbf{m}_t + \mathbf{K}_t[\mathbf{m}_{t+1}^{\mathrm{smooth}} - \mathbf{m}_{t+1}^{-}], \\ \mathbf{P}_t^{\mathrm{smooth}} &= \mathbf{P}_t + \mathbf{K}_t[\mathbf{P}_{t+1}^{\mathrm{smooth}} - \mathbf{P}_{t+1}^{-}]\mathbf{K}_t^{\mathrm{T}} \,, \end{aligned} \tag{5.29}$$

with $\mathbf{K}_t$ being the smoothing gain at t.

Equation (5.29) represents that the recursion starts from the last time-step, as it needs to know ($\mathbf{m}_{t+1}^{\mathrm{smooth}}, \mathbf{P}_{t+1}^{\mathrm{smooth}}$) at t. To investigate the real-time behavior of RTS smoother, we also implement it in the one time-step recursion (denoted by RTS-1). The RTS-1 calculates $p(\mathbf{X}_t|\hat{\mathbf{x}}_{t:t+1}^{\mathrm{RTS}})$ at every time-step except the last time-step.

5.4 Results and analysis

Beside the aforementioned nonlinear smoothers, we also investigate two linear smoothers combined with GPF. All the smoothing algorithms are implemented in an indoor tracking test-bed as introduced in our previous work [146], which consists of a robot and wireless sensor networks. The ranging technique is Time-of-Flight (TOF) measuring. The experiment is carried out in a typical indoor scenario, the corridor of our Computer Science building.

5.4.1 Quantitative results

All the competing algorithms take the same initialization, particle size, Gaussian measurement model, Gaussian random motion model and resampling strategy. The quantitative positioning results of the smoothing methods in the experiment are listed in Table 5.1, on the terms of both the positioning performance and complexity.

Performance

Table 5.1 demonstrates as follows.

- The FFBS and TFS make almost no improvement compared with GPF. It is explained that the smoothing density only influences the point estimation rather than the probability recursion; thus, FFBS and TFS cannot be expected to modify the posterior.
- The proposed SF observes the lowest values of the $\mathrm{MEAN_p}$, $\mathrm{RMSE_p}$, $\mathrm{MAX_p}$ and σ_p (the variance of the positioning errors indicates the estimation stability); this is a consequence that the posterior propagation is derived from the smoothing density instead of the prediction density.
- Combining the RTS smoother with GPF output achieves better accuracy than GPF, because the GPF estimation error can be deemed as linear Gaussian models and be removed by the linear smoother. The MA also ameliorate the GPF estimation, by reason that the target's positions at neighborhood time-steps are quite nearby.
- The drawbacks of GPF+MA and GPF+RTS are that they can only achieve a good accuracy when the smooth lag or window size is sufficiently large. As setting $\triangle T = 1$ and $N_{\mathrm{win}} = 2$, the performance of GPF+MA and GPF+RTS1 significantly degrades. Furthermore, it is well known that the improvement of MA does not go infinitely by increasing the window size.

Complexity

The complexity column of Table 5.1 represents the computation and latency of the smoothing algorithms, which are also important factors in practical applications. According to the algorithm configuration (the particle size, the number of anchors, the smoothing lag and the MA window size), FFBS causes the highest complexity while GPF and GPF+RTS1 are the lowest. However, the GPF+RTS smoother requires a large smoothing lag to achieve effective smoothing. Moreover, SF results in better performance with lower complexity than the nonlinear smoothers. Overall, the SF makes a good tradeoff between the smoothing performance and complexity.

Table 5.1: Comparison of the smoothing methods on SMC ($N_p = 49$), with the positioning results (/meter) of the experiment

Algorithms	$MEAN_p$	$RMSE_p$	σ_p	MAX_p	Time complexity
GPF	1.57	1.84	0.94	7.19	$O(N_p \times N_{anc})$
FFBS	1.54	1.79	0.92	6.58	$O(N_p^3)$
TFS	1.57	1.83	0.94	6.77	$O(N_p^2 \times N_{anc})$
SF	1.29	1.46	0.69	3.95	$O(N_p \times \max(N_p, N_{anc}))$
GPF+RST	1.37	1.58	0.78	5.86	$O(N_p \times N_{anc} \times \triangle T)$
GPF+RST-1	1.55	1.72	0.94	6.72	$O(N_p \times N_{anc})$
GPF+MA ($N_{win} = 10$)	1.42	1.65	0.84	6.29	$O(N_p \times N_{anc} \times N_{win})$
GPF+MA ($N_{win} = 2$)	1.54	1.79	0.92	7.00	$O(N_p \times N_{anc} \times N_{win})$

5.4.2 Positioning behavior and smoothness

Positioning behavior

Figure 5.2 depicts the estimated trajectory with or without the smoothing methods on the floor plan. It demonstrates that FFBS and TFS perform almost similarly to the GPF estimated trajectory (see Fig. 5.2(b) and Fig. 5.2(c)), which makes no improvements on approaching the true trajectory. The GPF+RTS and GPF+MA obtain much clearer estimated trajectories, as the spreading of the position estimation is much narrower; however, their estimated trajectories sometimes deviate from the true trajectory. Despite the spreading of the SF estimation is slightly broader than that of GPF+RTS and GPF+MA, it has much smaller divergence to the ground truth position (see Fig. 5.2(d)). Therefore, SF performs the best tracking to the true trajectory.

Smoothness

The smoothness of the estimated trajectory is depicted in Fig. 5.3. Figure 5.3(a) displays that the estimation error of GPF fluctuates sharply over time. The FFBS (Fig. 5.3(b)) and TFS (Fig. 5.3(c)) obtain almost the same instability as GPF. The SF removes the extremely large positioning errors, whereas, it keeps the fluctuation of the small errors. The GPF+MA (Fig. 5.3(e)) and GPF+RTS (Fig. 5.3(f)) obviously remove the high-frequency errors, however, the very large positioning errors (the low-frequency errors) are not smoothed. Thus, the linear smoothers with a nonlinear filter are more a sense to smooth the representation of the position estimation. Over the whole moving trajectory, SF observes the satisfied smoothness and the best tracking behavior.

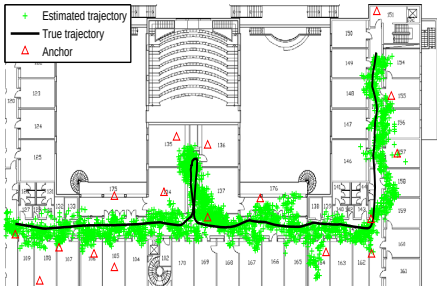

(a) GPF

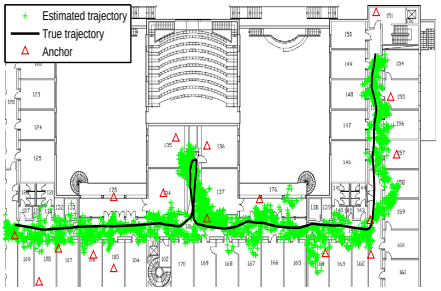

(b) FFBS

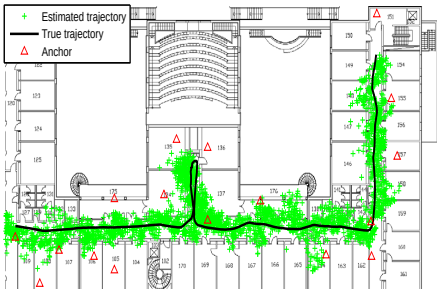

(c) TFS

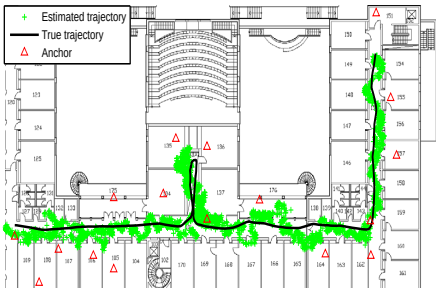

(d) SF

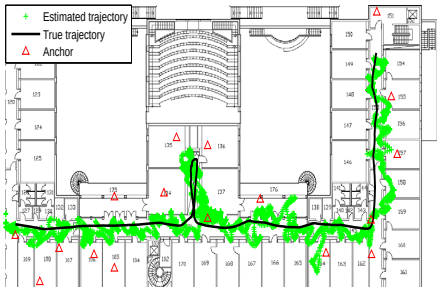

(e) GPF+MA ($N_{\text{win}} = 10$)

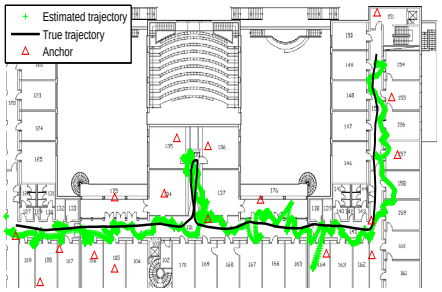

(f) GPF+RST

Figure 5.2: Positioning behavior of the smoothing methods on the floor plan: The solid line denotes the ground truth of the mobile trajectory; the scatter plot '+' is the estimated position; '△' for the anchors; the sample size of GPF is $N_{\text{p}} = 49$.

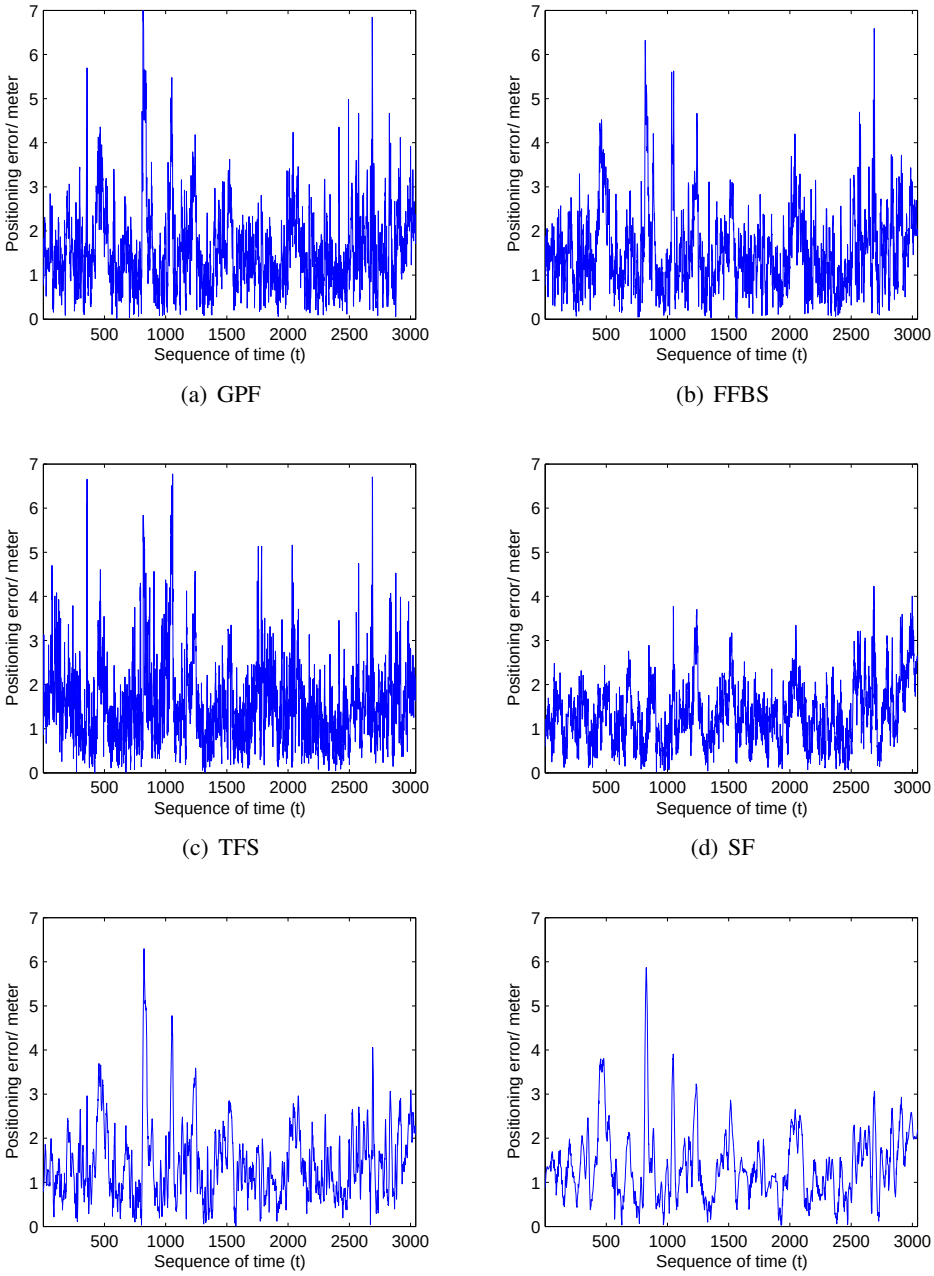

(a) GPF (b) FFBS

(c) TFS (d) SF

(e) GPF+MA ($N_{\text{win}} = 10$) (f) GPF+RTS

Figure 5.3: Positioning smoothness over time of the smoothing methods: the sample size of GPF is $N_{\text{p}} = 49$.

5.5 Summary

Due to the severe uncertainty of the indoor wireless environment and sensor system, range-based position tracking often encounters the accuracy and sparse problem. To combat the uncertainty, the smoothing frame is applied to the nonlinear non-Gaussian SMC models, including the FFBS, TFS, SF, GPF+MA and GPF+RST. Furthermore, to be aware of the real-time constraint, we focus on the smoothing frame using one time-step recursion. By validation in a real-world indoor tracking experiment, we summarize that

- One time-step smoothing is particularly relevant for both reducing the uncertainty and smooth the representation in real-time positioning.
- The nonlinear smoothers (FFBS and TFS) are not effective in one time-step recursion, by reason that the smoothing density is not propagated into the state recursion.
- The SF achieves much better accuracy and stability, as the smoothing density influences not only the position estimation but also the posterior recursion. In addition, its complexity is lower than the other nonlinear smoothers.
- The linear smoothing methods (GPF+MA and GPF+RST) notably reduce the high-frequency fluctuation of the positioning error, as removing the linear and Gaussian errors of the GPF estimation. However, they only work well when the smoothing lag or window size is sufficient. Moreover, they are more a sense to improve the estimation representation rather than filtering out the extremely large positioning errors. .

Our theoretical derivations and experimental verifications provide a better understanding of the one time-step smoothing frame on 2D position tracking. The GPF+RTS and GPF+MA is more a sense to improve the representation of the estimated trajectory, whereas, the SF filters out the estimation bias. The SF algorithm fits the scenarios of typical motion (the mobile target with a general acceleration) and high uncertainty. Since SF requires no other assumptions, offline training or high complexity, it is practical for its efficiency and effectiveness.

Chapter 6

Concluding Remarks

6.1 Conclusions

Real-world indoor experiments show that radio ranging observes a high uncertainty, which has to resort to a probabilistic framework. For the nonlinear and non-Gaussian positioning problem, a closed form estimation is impossible to be derived. Therefore, the probabilistic estimation often explores a sample-based approximation. The fundamental ingredients of applying sample-based probabilistic methods to practical indoor positioning are

1. to distribute the state samples properly, making a small sample size;
2. to specify a suitable measurement model, which should characterize the ranging reality.

The state sampling is a serious matter of the sample-based approximations, which should concern three aspects: 1) for robustness, the state samples should spread widely enough to represent the complete posterior; 2) for effectiveness, the samples should concentrate around the true state rather than spreading across the whole positioning area; 3) for efficiency, it should be easy to be implemented and the number of required samples should be reasonably small. The key idea of the proposed methods is to constrain the sample-space rather than exhaustively exploring all possibilities, thereby, the number of needed samples is small. More importantly, the constrained sampling alleviates the sample degeneracy.

The indoor ranging statistics have emphasized the insufficiency of the measurement modeling to reality, as the model can never be perfectly accurate. Concerning the NLOS effect, the modeling problem is more severe: the NLOS error practically violates the model and leads to a large estimation error or even loses the track. Chapter 3.3 finds that the indoor TOF ranging shows a positive bias and right-tailed distribution, thus, two biased measurement models are proposed. As the NLOS error is

time and space varying, an adaptive model is extracted from the previous position estimation or the prior. The proposed NLOS mitigation allows more accurate positioning to be performed in mixed LOS/NLOS conditions, with the advantage of requiring no analytical derivation.

In the case of the estimation instability and measurement sparsity, it is interested to apply the backward smoothing. Keeping in mind that the original aim is real-time positioning, one time-step smoothing is suitable. The two common smoothing frames (the FFBS and TFS) are ineffective in one time-step smoothing. Thus, it is proposed to incorporate the smoothing density into the filtering density, which notably improves the sequential positioning. Beside the smoothing frame, it is more efficient to apply a KF on the sample-based filters, which can remove the Gaussian estimation errors.

This thesis compares the proposed sampling, NLOS mitigation and smoothing methods, with both the simulations and a running test-bed validating the robustness, effectiveness and noise-tolerance. These positioning algorithms achieve meter level accuracy with 95% confidence level for both sequential and non-sequential positioning. The novelty of the proposed NLOS mitigation methods is their easy setup, thus, which significantly enhances the usability to other indoor scenarios. The one time-step smooth is computationally inexpensive and implementationally affordable. Furthermore, the proposed methods provide a general framework for either stationary or mobile positioning, and can be combined to yield superior performance. Overall, this study emphasizes the practical issues of probabilistic indoor positioning: the measurement models of reality, the tradeoff between accuracy and cost, and the representation of the indoor environment, etc.

6.2 Suggestions

One can find that the sample-based positioning algorithms differ in the requirements of the measurement models, parametric or nonparametric frames, computation and implementation complexity or whether they can handle non-Gaussian noise. Therefore, this study holds that there is no best localization algorithm for all positioning situations, e.g., an algorithm can perform many levels of performance in the conditions of different cost, scenarios, priori information. Some suggestions for setting indoor positioning are given:

1. Measurement analysis is an important part of indoor positioning, which should be done before choosing a positioning algorithm.
2. Anchor deployment is more an engineering problem than a theoretical analysis, which should be practical and robust.
3. Reduce the terms of the probabilistic state: some algorithms involve penalty variables of the state (i.e., the velocity, acceleration, orientation, and etc.), which is impractical for range-

based positioning under severe uncertainty.

4. Achieve the tradeoff between the positioning performance and cost, e.g., for emergency purposes, one can afford a high cost but require a high accuracy; in the case of goods tracking /positioning in warehouses, the sub-optimal accuracy with a low cost is preferred.
5. Form approximate solutions to the optimal Bayesian frame: rigorous mathematical derivations do not necessarily lead to the best performance. on the other hand, approximate derivations can greatly reduce the cost.
6. Assume practical measurement models, motion models and the state density, including their values, ranges and connections to physical world.
7. Make in a small number of the state samples: more attention should be paid to constrain the state space.
8. Pre-computation can significantly reduce the computational burden of the sample-based evaluation.

Bibliography

[1] Lpc2738 datasheet, eidhoven, neterlands. [online], available: http://www.nxp.com.

[2] Nanopan 5375 rf module datasheet, berlin, germany, 2009. [online], available: http://www.nanotron.com.

[3] Vincent J Aidala. Kalman filter behavior in bearings-only tracking applications. *Aerospace and Electronic Systems, IEEE Transactions on*, (1):29–39, 1979.

[4] S. Al-Jazzar, J. Caffery, and H.R. You. Scattering-model-based methods for toa location in nlos environments. *Vehicular Technology, IEEE Transactions on*, 56(2):583–593, 2007.

[5] S. Al-Jazzar and J. Caffery Jr. Ml and bayesian toa location estimators for nlos environments. In *Proc. IEEE VTC '02-Fall*, volume 2, pages 1178–1181, 2002.

[6] B. Alavi. *Distance measurement error modeling for time-of-arrival-based indoor geolocation*. PhD thesis, WORCESTER POLYTECHNIC INSTITUTE, 2006.

[7] B. Alavi and K. Pahlavan. Modeling of the toa-based distance measurement error using uwb indoor radio measurements. *IEEE Communications Letters*, 10(4):275–277, 2006.

[8] N.A. Alsindi, B. Alavi, and K. Pahlavan. Measurement and modeling of ultrawideband toa-based ranging in indoor multipath environments. *Vehicular Technology, IEEE Transactions on*, 58(3):1046–1058, 2009.

[9] Daniel L Alspach and Harold W Sorenson. Nonlinear bayesian estimation using gaussian sum approximations. *Automatic Control, IEEE Transactions on*, 17(4):439–448, 1972.

[10] Jeffrey L Anderson. Exploring the need for localization in ensemble data assimilation using a hierarchical ensemble filter. *Physica D: Nonlinear Phenomena*, 230(1):99–111, 2007.

[11] M Sanjeev Arulampalam, Simon Maskell, Neil Gordon, and Tim Clapp. A tutorial on particle filters for online nonlinear/non-gaussian bayesian tracking. *IEEE Transactions on Signal Processing*, 50(2):174–188, 2002.

[12] Sanjeev Arulampalam and Branko Ristic. Comparison of the particle filter with range-parameterized and modified polar ekfs for angle-only tracking. In *AeroSense 2000*, pages

288–299. International Society for Optics and Photonics, 2000.

[13] P. Barsocchi, S. Lenzi, S. Chessa, and F. Furfari. Automatic virtual calibration of range-based indoor localization systems. *Wireless Communications and Mobile Computing*, 2011.

[14] Matthew James Beal. *Variational algorithms for approximate Bayesian inference*. PhD thesis, University of London, 2003.

[15] Francesco Benedetto, Gaetano Giunta, Alessandro Toscano, and Lucio Vegni. Dynamic los/nlos statistical discrimination of wireless mobile channels. In *Vehicular Technology Conference, 2007. VTC2007-Spring. IEEE 65th*, pages 3071–3075. IEEE, 2007.

[16] James O Berger. *Statistical decision theory and Bayesian analysis*. Springer, 1985.

[17] James O Berger, Elías Moreno, Luis Raul Pericchi, M Jesús Bayarri, José M Bernardo, Juan A Cano, Julián De la Horra, Jacinto Martín, David Ríos-Insúa, Bruno Betrò, et al. An overview of robust bayesian analysis. *Test*, 3(1):5–124, 1994.

[18] Niclas Bergman. *Bayesian Inference in Terrain Navigation*. Linköping Studies in Science and Technology. Thesis No 649, 1997.

[19] Niclas Bergman. Recursive bayesian estimation. *Department of Electrical Engineering, Linköping University, Linköping Studies in Science and Technology. Doctoral dissertation*, (579), 1999.

[20] Niclas Bergman, Lennart Ljung, and Fredrik Gustafsson. Terrain navigation using bayesian statistics. *Control Systems, IEEE*, 19(3):33–40, 1999.

[21] Adrian N Bishop, Barış Fidan, Brian Anderson, Kutluyıl Doğançay, and Pubudu N Pathirana. Optimality analysis of sensor-target localization geometries. *Automatica*, 46(3):479–492, 2010.

[22] Joan Borras, Paul Hatrack, and Narayan B Mandayam. Decision theoretic framework for nlos identification. In *Vehicular Technology Conference, 1998. VTC 98. 48th IEEE*, volume 2, pages 1583–1587. IEEE, 1998.

[23] Mark Briers, Arnaud Doucet, and Simon Maskell. Smoothing algorithms for state–space models. *Annals of the Institute of Statistical Mathematics*, 62(1):61–89, 2010.

[24] Richard S Bucy and Kenneth D Senne. Digital synthesis of non-linear filters. *Automatica*, 7(3):287–298, 1971.

[25] Wolfram Burgard, Dieter Fox, Daniel Hennig, and Timo Schmidt. Estimating the absolute position of a mobile robot using position probability grids. In *Proceedings of the national conference on artificial intelligence*, pages 896–901, 1996.

[26] J. Caffery Jr and G.L. Stuber. Subscriber location in cdma cellular networks. *Vehicular Technology, IEEE Transactions on*, 47(2):406–416, 1998.

[27] James Carpenter, Peter Clifford, and Paul Fearnhead. Improved particle filter for nonlinear problems. *IEE Proceedings-Radar, Sonar and Navigation*, 146(1):2–7, 1999.

[28] D. Cassioli, M.Z. Win, and A.F. Molisch. The ultra-wide bandwidth indoor channel: from statistical model to simulations. *Selected Areas in Communications, IEEE Journal on*, 20(6):1247–1257, 2002.

[29] James Chaffee and Jonathan Abel. Gdop and the cramer-rao bound. In *Position Location and Navigation Symposium, 1994., IEEE*, pages 663–668. IEEE, 1994.

[30] Frankie KW Chan and Hing-Cheung So. Accurate distributed range-based positioning algorithm for wireless sensor networks. *IEEE Transactions on Signal Processing*, 57(10):4100–4105, 2009.

[31] Cheng Chang and Rashid Ansari. Kernel particle filter for visual tracking. *Signal processing letters, IEEE*, 12(3):242–245, 2005.

[32] Guanling Chen, David Kotz, et al. A survey of context-aware mobile computing research. Technical report, Technical Report TR2000-381, Dept. of Computer Science, Dartmouth College, 2000.

[33] P.C. Chen. A non-line-of-sight error mitigation algorithm in location estimation. In *Proc. IEEE WCNC'99*, pages 316–320, 1999.

[34] Zhe Chen. Bayesian filtering: From kalman filters to particle filters, and beyond. *Statistics*, 182(1):1–69, 2003.

[35] Xiuzhen Cheng, Andrew Thaeler, Guoliang Xue, and Dechang Chen. Tps: A time-based positioning scheme for outdoor wireless sensor networks. In *INFOCOM 2004. Twenty-third AnnualJoint Conference of the IEEE Computer and Communications Societies*, volume 4, pages 2685–2696. IEEE, 2004.

[36] KW Cheung, HC So, W.K. Ma, and YT Chan. A constrained least squares approach to mobile positioning: algorithms and optimality. *EURASIP journal on applied signal processing*, 2006:150–150, 2006.

[37] Rizwan A Choudrey. *Variational methods for Bayesian independent component analysis*. PhD thesis, University of Oxford, 2002.

[38] Andrea Conti, Davide Dardari, Matteo Guerra, Lorenzo Mucchi, and Moe Z Win. Experimental characterization of diversity navigation. 2014.

[39] Andrea Conti, Matteo Guerra, Davide Dardari, Nicolo Decarli, and Moe Z Win. Network experimentation for cooperative localization. *Selected Areas in Communications, IEEE Journal on*, 30(2):467–475, 2012.

[40] Gregory F Cooper. The computational complexity of probabilistic inference using bayesian

belief networks. *Artificial intelligence*, 42(2):393–405, 1990.

[41] Drew Creal. A survey of sequential monte carlo methods for economics and finance. *Econometric Reviews*, 31(3):245–296, 2012.

[42] N. Cressie and D.M. Hawkins. Robust estimation of the variogram: I. *Mathematical geology*, 12(2):115–125, 1980.

[43] D. Dardari, A. Conti, U. Ferner, A. Giorgetti, and M.Z. Win. Ranging with ultrawide bandwidth signals in multipath environments. *Proceedings of the IEEE*, 97(2):404–426, 2009.

[44] Davide Dardari, Chia-Chin Chong, and Moe Z Win. Threshold-based time-of-arrival estimators in uwb dense multipath channels. *Communications, IEEE Transactions on*, 56(8):1366–1378, 2008.

[45] M. Debbah and R.R. Muller. Mimo channel modeling and the principle of maximum entropy. *Information Theory, IEEE Transactions on*, 51(5):1667–1690, 2005.

[46] Frank Dellaert, Wolfram Burgard, Dieter Fox, and Sebastian Thrun. Using the condensation algorithm for robust, vision-based mobile robot localization. In *Computer Vision and Pattern Recognition, 1999. IEEE Computer Society Conference on.*, volume 2. IEEE, 1999.

[47] Frank Dellaert, Dieter Fox, Wolfram Burgard, and Sebastian Thrun. Monte carlo localization for mobile robots. In *Robotics and Automation, 1999. Proceedings. 1999 IEEE International Conference on*, volume 2, pages 1322–1328. IEEE, 1999.

[48] Benoit Denis, J-B Pierrot, and Chadi Abou-Rjeily. Joint distributed synchronization and positioning in uwb ad hoc networks using toa. *Microwave Theory and Techniques, IEEE Transactions on*, 54(4):1896–1911, 2006.

[49] V. Dizdarevic and K. Witrisal. On impact of topology and cost function on lse position determination in wireless networks. In *Proceedings of Workshop on Positioning, Navigation, and Communication (WPNC'06)*, pages 129–138. Citeseer, 2006.

[50] Arnaud Doucet, Mark Briers, and Stéphane Sénécal. Efficient block sampling strategies for sequential monte carlo methods. *Journal of Computational and Graphical Statistics*, 15(3), 2006.

[51] Arnaud Doucet, Nando De Freitas, Neil Gordon, et al. *Sequential Monte Carlo methods in practice*, volume 1. Springer New York, 2001.

[52] Arnaud Doucet, Simon Godsill, and Christophe Andrieu. On sequential monte carlo sampling methods for bayesian filtering. *Statistics and computing*, 10(3):197–208, 2000.

[53] Paul Fearnhead. *Sequential Monte Carlo methods in filter theory*. PhD thesis, University of Oxford, 1998.

[54] Andrew Fort, Claude Desset, Julien Ryckaert, Philippe De Doncker, Leo Van Biesen, and Piet

Wambacq. Characterization of the ultra wideband body area propagation channel. In *Ultra-Wideband, 2005. ICU 2005. 2005 IEEE International Conference on*, pages 6–pp. IEEE, 2005.

[55] Dieter Fox, Wolfram Burgard, Sebastian Thrun, and Armin B Cremers. Position estimation for mobile robots in dynamic environments. In *AAAI/IAAI*, pages 983–988, 1998.

[56] Eric Foxlin. Pedestrian tracking with shoe-mounted inertial sensors. *Computer Graphics and Applications, IEEE*, 25(6):38–46, 2005.

[57] D Fraser and J Potter. The optimum linear smoother as a combination of two optimum linear filters. *Automatic Control, IEEE Transactions on*, 14(4):387–390, 1969.

[58] Karl J Friston, W Penny, Christophe Phillips, S Kiebel, G Hinton, and John Ashburner. Classical and bayesian inference in neuroimaging: theory. *NeuroImage*, 16(2):465–483, 2002.

[59] Deepak Ganesan, Bhaskar Krishnamachari, Alec Woo, David Culler, Deborah Estrin, and Stephen Wicker. Complex behavior at scale: An experimental study of low-power wireless sensor networks. Technical report, Technical Report UCLA/CSD-TR 02, 2002.

[60] Alan E Gelfand and Adrian FM Smith. Sampling-based approaches to calculating marginal densities. *Journal of the American statistical association*, 85(410):398–409, 1990.

[61] John Geweke. Bayesian inference in econometric models using monte carlo integration. *Econometrica: Journal of the Econometric Society*, pages 1317–1339, 1989.

[62] S. Gezici and Z. Sahinoglu. Uwb geolocation techniques for ieee 802.15.4a personal area networks. *Mitsubishi Electric Research Laboratory Technical Report TR-2004-110*, 2004.

[63] Lewis David Girod. *A self-calibrating system of distributed acoustic arrays*. PhD thesis, Citeseer, 2005.

[64] Neil J Gordon, David J Salmond, and Adrian FM Smith. Novel approach to nonlinear/non-gaussian bayesian state estimation. In *IEE Proceedings F (Radar and Signal Processing)*, volume 140, pages 107–113. IET, 1993.

[65] G Grisettiyz, Cyrill Stachniss, and Wolfram Burgard. Improving grid-based slam with rao-blackwellized particle filters by adaptive proposals and selective resampling. In *Robotics and Automation, 2005. ICRA 2005. Proceedings of the 2005 IEEE International Conference on*, pages 2432–2437. IEEE, 2005.

[66] Yanying Gu, Anthony Lo, and Ignas Niemegeers. A survey of indoor positioning systems for wireless personal networks. *Communications Surveys & Tutorials, IEEE*, 11(1):13–32, 2009.

[67] F. Gustafsson and F. Gunnarsson. Mobile positioning using wireless networks: possibilities and fundamental limitations based on available wireless network measurements. *Signal Processing Magazine, IEEE*, 22(4):41–53, 2005.

[68] Fredrik Gustafsson, Fredrik Gunnarsson, Niclas Bergman, Urban Forssell, Jonas Jansson, Rickard Karlsson, and P-J Nordlund. Particle filters for positioning, navigation, and tracking. *Signal Processing, IEEE Transactions on*, 50(2):425–437, 2002.

[69] I. Guvenc and C.C. Chong. A survey on toa based wireless localization and nlos mitigation techniques. *Communications Surveys & Tutorials, IEEE*, 11(3):107–124, 2009.

[70] I. Guvenc, C.C. Chong, and F. Watanabe. Nlos identification and mitigation for uwb localization systems. In *Proc. IEEE WCNC '07*, pages 1571–1576, 2007.

[71] I. Güvenç, C.C. Chong, F. Watanabe, and H. Inamura. Nlos identification and weighted least-squares localization for uwb systems using multipath channel statistics. *EURASIP Journal on Advances in Signal Processing*, 2008:36, 2008.

[72] John Michael Hammersley and David Christopher Handscomb. *Monte carlo methods*, volume 1. Springer, 1964.

[73] Mudhafar Hassan-Ali and Kaveh Pahlavan. A new statistical model for site-specific indoor radio propagation prediction based on geometric optics and geometric probability. *Wireless Communications, IEEE Transactions on*, 1(1):112–124, 2002.

[74] Simon S Haykin, Simon S Haykin, and Simon S Haykin. *Kalman filtering and neural networks*. Wiley Online Library, 2001.

[75] Yu-Chi Ho and R Lee. A bayesian approach to problems in stochastic estimation and control. *Automatic Control, IEEE Transactions on*, 9(4):333–339, 1964.

[76] Jeroen D Hol. Resampling in particle filters. 2004.

[77] G. İsmail, C. Chia-Chin, W. Fujio, et al. Nlos identification and weighted least-squares localization for uwb systems using multipath channel statistics. *EURASIP on Advances in Signal Processing*, 2007.

[78] Kazufumi Ito and Kaiqi Xiong. Gaussian filters for nonlinear filtering problems. *Automatic Control, IEEE Transactions on*, 45(5):910–927, 2000.

[79] E.T. Jaynes. Information theory and statistical mechanics. ii. *Physical review*, 108(2):171, 1957.

[80] E.T. Jaynes. Information theory and statistical mechanics. *Statistical Physics. Brandeis Lectures*, 3:160–185, 1963.

[81] P. Jensfelt. *Approaches to mobile robot localization in indoor environments*. Tekniska högsk., 2001.

[82] Patric Jensfelt and Henrik Christensen. Laser based position acquisition and tracking in an indoor environment. In *International Symposium on Robotics and Automation-ISRA*, volume 98. Citeseer, 1998.

[83] Yung-Hoon Jo, Joon-Yong Lee, Dong-Heon Ha, and Shin-Hoo Kang. Accuracy enhancement for uwb indoor positioning using ray tracing. In *Proceedings of IEEE/ION PLANS 2006*, pages 565–568, 2001.

[84] Damien Jourdan, Davide Dardari, and Moe Z Win. Position error bound for uwb localization in dense cluttered environments. *Aerospace and Electronic Systems, IEEE Transactions on*, 44(2):613–628, 2008.

[85] Simon J Julier and Jeffrey K Uhlmann. A new extension of the kalman filter to nonlinear systems. In *Int. symp. aerospace/defense sensing, simul. and controls*, volume 3, pages 3–2. Orlando, FL, 1997.

[86] Kamol Kaemarungsi. *Design of Indoor Positioning Systems Based on Location Fingerprinting Technique*. PhD thesis, University of Pittsburgh, 2005.

[87] Kamol Kaemarungsi and Prashant Krishnamurthy. Modeling of indoor positioning systems based on location fingerprinting. In *INFOCOM 2004. Twenty-third AnnualJoint Conference of the IEEE Computer and Communications Societies*, volume 2, pages 1012–1022. IEEE, 2004.

[88] Rudolph Emil Kalman. A new approach to linear filtering and prediction problems. *Journal of basic Engineering*, 82(1):35–45, 1960.

[89] Bhargav Kanagal and Amol Deshpande. Online filtering, smoothing and probabilistic modeling of streaming data. In *Data Engineering, 2008. ICDE 2008. IEEE 24th International Conference on*, pages 1160–1169. IEEE, 2008.

[90] Nicholas Kantas, Arnaud Doucet, Sumeetpal Sindhu Singh, and Jan Marian Maciejowski. An overview of sequential monte carlo methods for parameter estimation in general state-space models. In *15th IFAC Symposium on System Identification (SYSID), Saint-Malo, France.(invited paper)*, volume 102, page 117, 2009.

[91] Rickard Karlsson. Particle filtering for positioning and tracking applications. 2005.

[92] Jasurbek Khodjaev, Yongwan Park, and Aamir Saeed Malik. Survey of nlos identification and error mitigation problems in uwb-based positioning algorithms for dense environments. *annals of telecommunications-annales des télécommunications*, 65(5-6):301–311, 2010.

[93] Genshiro Kitagawa. Non-gaussian state-space modeling of nonstationary time series. *Journal of the American statistical association*, 82(400):1032–1041, 1987.

[94] Genshiro Kitagawa. The two-filter formula for smoothing and an implementation of the gaussian-sum smoother. *Annals of the Institute of Statistical Mathematics*, 46(4):605–623, 1994.

[95] Lindsay Kleeman. Optimal estimation of position and heading for mobile robots using ultra-

sonic beacons and dead-reckoning. In *Robotics and Automation, 1992. Proceedings., 1992 IEEE International Conference on*, pages 2582–2587. IEEE, 1992.

[96] Daphne Koller and Raya Fratkina. Using learning for approximation in stochastic processes. In *ICML*, pages 287–295. Citeseer, 1998.

[97] Augustine Kong, Jun S Liu, and Wing Hung Wong. Sequential imputations and bayesian missing data problems. *Journal of the American statistical association*, 89(425):278–288, 1994.

[98] Jayesh H Kotecha and Petar M Djuric. Gaussian particle filtering. *Signal Processing, IEEE Transactions on*, 51(10):2592–2601, 2003.

[99] Hakan Koyuncu and Shuang Hua Yang. A survey of indoor positioning and object locating systems. *IJCSNS International Journal of Computer Science and Network Security*, 10(5):121–128, 2010.

[100] Stuart C Kramer and Harold W Sorenson. Recursive bayesian estimation using piece-wise constant approximations. *Automatica*, 24(6):789–801, 1988.

[101] Branislav Kusỳ. *Spatiotemporal coordination in wireless sensor networks*. PhD thesis, Vanderbilt University, 2007.

[102] S. Lanzisera, D.T. Lin, and K.S.J. Pister. "RF time of flight ranging for wireless sensor network localization. In *International Workshop on Intelligent Solutions in Embedded Systems*, pages 1–12. IEEE, 2006.

[103] L. Lazos and R. Poovendran. Serloc: Robust localization for wireless sensor networks. *ACM Transactions on Sensor Networks (TOSN)*, 1(1):73–100, 2005.

[104] Raskin Leonid, Rivlin Ehud, and Rudzsky Michael. Using gaussian process annealing particle filter for 3d human tracking. *EURASIP Journal on Advances in Signal Processing*, 2008, 2008.

[105] B. Li and H. Wang. A low complexity localization algorithm in wireless sensor network. In *Innovative Computing & Communication, Intl Conf on and Information Technology & Ocean Engineering, 2010 Asia-Pacific Conf on (CICC-ITOE)*, pages 217–220, 2010.

[106] Tiancheng Li, Shudong Sun, Tariq P Sattar, and Juan M Corchado. Fighting against sample degeneracy and impoverishment in particle filters: Particularly on intelligent choices. *arXiv preprint arXiv:1308.2443*, 2013.

[107] Xinrong Li. An iterative nlos mitigation algorithm for location estimation in sensor networks. *RN*, 4:1, 2006.

[108] Z. Li, W. Trappe, Y. Zhang, and B. Nath. Robust statistical methods for securing wireless localization in sensor networks. In *Fourth International Symposium on Information Processing*

in Sensor Networks, IPSN '05, pages 91–98, 2005.

[109] Tsung-Nan Lin and Po-Chiang Lin. Performance comparison of indoor positioning techniques based on location fingerprinting in wireless networks. In *Wireless Networks, Communications and Mobile Computing, 2005 International Conference on*, volume 2, pages 1569–1574. IEEE, 2005.

[110] Vern Lindberg. Uncertainties and error propagation. *Manual on Uncertainties, Graphing and the Vernier Caliper, Part I. Rochester Institute of Technology, New York, USA.(http://www. rit. edu/uphysics/uncertinities/Uncertinitiespart2. html# addsub)*, 2000.

[111] Y. Ling, S. Alexander, and R. Lau. On Quantification of Anchor Placement. In *INFOCOM, 2012 Proceedings IEEE*, pages 2192–2200. IEEE, 2012.

[112] H. Liu, H. Darabi, P. Banerjee, and J. Liu. Survey of wireless indoor positioning techniques and systems.

[113] Jane Liu and Mike West. Combined parameter and state estimation in simulation-based filtering. In *Sequential Monte Carlo methods in practice*, pages 197–223. Springer, 2001.

[114] Jun S Liu. *Monte Carlo strategies in scientific computing*. springer, 2008.

[115] Jun S Liu and Rong Chen. Blind deconvolution via sequential imputations. *Journal of the American Statistical Association*, 90(430):567–576, 1995.

[116] Xiwu Lv, Kaihua Liu, and Po Hu. Geometry influence on gdop in toa and aoa positioning systems. In *Networks Security Wireless Communications and Trusted Computing (NSWCTC), 2010 Second International Conference on*, volume 2, pages 58–61. IEEE, 2010.

[117] Stefano Marano, Wesley M Gifford, Henk Wymeersch, and Moe Z Win. Nlos identification and mitigation for localization based on uwb experimental data. *Selected Areas in Communications, IEEE Journal on*, 28(7):1026–1035, 2010.

[118] F Marchal, J Hackney, and Kay W Axhausen. Efficient map matching of large global positioning system data sets: Tests on speed-monitoring experiment in zürich. *Transportation Research Record: Journal of the Transportation Research Board*, 1935(1):93–100, 2005.

[119] Frank J Massey Jr. The kolmogorov-smirnov test for goodness of fit. *Journal of the American statistical Association*, 46(253):68–78, 1951.

[120] Rainer Mautz. Overview of current indoor positioning systems. *Geodezija ir kartografija*, 35(1):18–22, 2009.

[121] Santiago Mazuelas, Yuan Shen, and Moe Z Win. Belief condensation filtering. *Signal Processing, IEEE Transactions on*, 61(18):4403–4415, 2013.

[122] A.F. Molisch, K. Balakrishnan, C.C. Chong, S. Emami, A. Fort, J. Karedal, J. Kunisch, H. Schantz, U. Schuster, and K. Siwiak. Ieee 802.15.4a channel model-final report. *IEEE P*,

15(02), 2004.

[123] A.F. Molisch, J.R. Foerster, and M. Pendergrass. Channel models for ultrawideband personal area networks. *Wireless Communications, IEEE*, 10(6):14–21, 2003.

[124] Francesco Montorsi, Santiago Mazuelas, Giorgio Matteo Vitetta, and Moe Z Win. On the performance limits of map-aware localization. *Information Theory, IEEE Transactions on*, 59(8):5023–5038, 2013.

[125] David Munoz, Frantz Bouchereau Lara, Cesar Vargas, and Rogerio Enriquez-Caldera. *Position location techniques and applications*. Academic Press, 2009.

[126] Radford M Neal. Annealed importance sampling. *Statistics and Computing*, 11(2):125–139, 2001.

[127] Lionel M Ni, Yunhao Liu, Yiu Cho Lau, and Abhishek P Patil. Landmarc: indoor location sensing using active rfid. *Wireless networks*, 10(6):701–710, 2004.

[128] Dragos Niculescu and Badri Nath. Ad hoc positioning system (aps). In *Global Telecommunications Conference, 2001. GLOBECOM'01. IEEE*, volume 5, pages 2926–2931. IEEE, 2001.

[129] Dragoş Niculescu and Badri Nath. Dv based positioning in ad hoc networks. *Telecommunication Systems*, 22(1-4):267–280, 2003.

[130] Shuichi Obayashi and Jens Zander. A body-shadowing model for indoor radio communication environments. *Antennas and Propagation, IEEE Transactions on*, 46(6):920–927, 1998.

[131] Apostolia Papapostolou and Hakima Chaouchi. Exploiting multi-modality and diversity for localization enhancement: Wifi & rfid usecase. In *Personal, Indoor and Mobile Radio Communications, 2009 IEEE 20th International Symposium on*, pages 1903–1907. IEEE, 2009.

[132] Jun-geun Park, Dorothy Curtis, Seth Teller, and Jonathan Ledlie. Implications of device diversity for organic localization. In *INFOCOM, 2011 Proceedings IEEE*, pages 3182–3190. IEEE, 2011.

[133] Neal Patwari and Piyush Agrawal. Effects of correlated shadowing: Connectivity, localization, and rf tomography. In *Information Processing in Sensor Networks, 2008. IPSN'08. International Conference on*, pages 82–93. IEEE, 2008.

[134] L Perea, J How, L Breger, and P Elosegui. Nonlinearity in sensor fusion: Divergence issues in ekf, modified truncated sof, and ukf. In *Proceedings of the AIAA Guidance, Navigation and Control Conference and Exhibit*, pages 20–23, 2007.

[135] Henri Pesonen and Robert Piché. Numerical integration in bayesian positioning. In *Progress in Industrial Mathematics at ECMI 2006*, pages 908–912. Springer, 2008.

[136] Patrick Pfaff, Wolfram Burgard, and Dieter Fox. Robust monte-carlo localization using adap-

tive likelihood models. In *European robotics symposium 2006*, pages 181–194. Springer, 2006.

[137] Michael K Pitt and Neil Shephard. Filtering via simulation: Auxiliary particle filters. *Journal of the American statistical association*, 94(446):590–599, 1999.

[138] J Prieto, A Bahillo, S Mazuelas, RM Lorenzo, J Blas, and P Fernandez. Nlos mitigation based on range estimation error characterization in an rtt-based ieee 802.11, indoor location system. In *Intelligent Signal Processing, 2009. WISP 2009. IEEE International Symposium on*, pages 61–66. IEEE, 2009.

[139] Song S Qian, Craig A Stow, and Mark E Borsuk. On monte carlo methods for bayesian inference. *Ecological Modelling*, 159(2):269–277, 2003.

[140] Theodore S Rappaport et al. *Wireless communications: principles and practice*, volume 2. Prentice Hall PTR New Jersey, 1996.

[141] Jaume Riba and Andreu Urruela. A non-line-of-sight mitigation technique based on ml-detection. In *Acoustics, Speech, and Signal Processing, 2004. Proceedings.(ICASSP'04). IEEE International Conference on*, volume 2. IEEE, 2004.

[142] Richard Roberts, Praveen Gopalakrishnan, and Somya Rathi. Visible light positioning: Automotive use case. In *Vehicular Networking Conference (VNC), 2010 IEEE*, pages 309–314. IEEE, 2010.

[143] S Sarkka, Toni Tamminen, Aki Vehtari, and Jouko Lampinen. Probabilistic methods in multiple target tracking: review and bibliography. *Laboratory of Computational Engineering, Helsinki University of Technology, Tech. Rep. B*, 36, 2004.

[144] Simo Särkkä. *Bayesian filtering and smoothing*, volume 3. Cambridge University Press, 2013.

[145] Simo Särkkä et al. *Recursive Bayesian inference on stochastic differential equations*. Helsinki University of Technology, 2006.

[146] Simon Schmitt, Heiko Will, Benjamin Aschenbrenner, Thomas Hillebrandt, and Marcel Kyas. A reference system for indoor localization testbeds. In *Indoor Positioning and Indoor Navigation (IPIN), International Conference on*, pages 1–8. IEEE, 2012.

[147] Jens Schroeder, Stefan Galler, Kyandoghere Kyamakya, and Klaus Jobmann. Nlos detection algorithms for ultra-wideband localization. In *Positioning, Navigation and Communication, 2007. WPNC'07. 4th Workshop on*, pages 159–166. IEEE, 2007.

[148] Stephen Se, David Lowe, and Jim Little. Vision-based mobile robot localization and mapping using scale-invariant features. In *Robotics and Automation, 2001. Proceedings 2001 ICRA. IEEE International Conference on*, volume 2, pages 2051–2058. IEEE, 2001.

[149] Caifeng Shan, Tieniu Tan, and Yucheng Wei. Real-time hand tracking using a mean shift embedded particle filter. *Pattern Recognition*, 40(7):1958–1970, 2007.

[150] Yuan Shen, Santiago Mazuelas, and Moe Z Win. Network navigation: Theory and interpretation. *Selected Areas in Communications, IEEE Journal on*, 30(9):1823–1834, 2012.

[151] Yuan Shen and Moe Z Win. Fundamental limits of wideband localization part i: A general framework. *Information Theory, IEEE Transactions on*, 56(10):4956–4980, 2010.

[152] Harold W Sorenson and Daniel L Alspach. Recursive bayesian estimation using gaussian sums. *Automatica*, 7(4):465–479, 1971.

[153] Alvaro Soto. Self adaptive particle filter. In *IJCAI*, pages 1398–1406, 2005.

[154] Niklas Svenzen. *Real time implementation of map aided positioning using a Bayesian approach*. PhD thesis, Linköping, 2002.

[155] Sebastian Thrun, Wolfram Burgard, Dieter Fox, et al. *Probabilistic robotics*, volume 1. MIT press Cambridge, 2005.

[156] DJ TORRIERI. Statistical theory of passive location systems. *IEEE transactions on aerospace and electronic systems*, 20(2):183–198, 1984.

[157] S. Venkatesh and R.M. Buehrer. A linear programming approach to nlos error mitigation in sensor networks. In *Proc. 5th international conference on Information processing in sensor networks*, pages 301–308. ACM, 2006.

[158] Jaco Vermaak, Arnaud Doucet, and Patrick Pérez. Maintaining multimodality through mixture tracking. In *Computer Vision, 2003. Proceedings. Ninth IEEE International Conference on*, pages 1110–1116. IEEE, 2003.

[159] Eric A Wan and Rudolph Van Der Merwe. The unscented kalman filter for nonlinear estimation. In *Adaptive Systems for Signal Processing, Communications, and Control Symposium 2000. AS-SPCC. The IEEE 2000*, pages 153–158. IEEE, 2000.

[160] Tianheng Wang, Yuan Shen, Santiago Mazuelas, Hyundong Shin, and Moe Z Win. On ofdm ranging accuracy in multipath channels. 2014.

[161] W. Wang, T. Jost, C. Mensing, and A. Dammann. Toa and tdoa error models for nlos propagation based on outdoor to indoor channel measurement. In *Wireless Communications and Networking Conference, 2009. WCNC 2009. IEEE*, pages 1–6. IEEE, 2009.

[162] K. Whitehouse and D. Culler. A robustness analysis of multi-hop ranging-based localization approximations. In *Proc. 5th international conference on Information processing in sensor networks*, pages 317–325. ACM, 2006.

[163] K. Whitehouse, C. Karlof, and D. Culler. A practical evaluation of radio signal strength for ranging-based localization. *ACM SIGMOBILE Mobile Computing and Communications*

Review, 11(1):41–52, 2007.

[164] K. Whitehouse, C. Karlof, A. Woo, F. Jiang, and D. Culler. The effects of ranging noise on multihop localization: an empirical study. In *Proc. 4th international symposium on Information processing in sensor networks*, page 10. IEEE Press, 2005.

[165] Widyawan. *Learning Data Fusion for Indoor Localisation*. PhD thesis, Cork Institute of Technology, 2009.

[166] H. Will, T. Hillebrandt, Y. Yang, Y.B. Zhao, and M. Kyas. The membership degree min-max localization algorithm. In *Ubiquitous Positioning Indoor Navigation and Location Based Service (UPINLBS'12)*, pages 1–10. IEEE, 2012.

[167] Moe Z Win, Andrea Conti, Santiago Mazuelas, Yuan Shen, Wesley M Gifford, Davide Dardari, and Marco Chiani. Network localization and navigation via cooperation. *Communications Magazine, IEEE*, 49(5):56–62, 2011.

[168] Jürgen Wolf, Wolfram Burgard, and Hans Burkhardt. Robust vision-based localization by combining an image-retrieval system with monte carlo localization. *Robotics, IEEE Transactions on*, 21(2):208–216, 2005.

[169] Sung-Shik Woo, Heung-Ryeol You, and Jong-Seog Koh. The nlos mitigation technique for position location using is-95 cdma networks. In *Vehicular Technology Conference, 2000. IEEE-VTS Fall VTC 2000. 52nd*, volume 6, pages 2556–2560. IEEE, 2000.

[170] Marilynn P Wylie and Jack Holtzman. The non-line of sight problem in mobile location estimation. In *Universal Personal Communications, 1996. Record., 1996 5th IEEE International Conference on*, volume 2, pages 827–831. IEEE, 1996.

[171] Henk Wymeersch, Ulric Ferner, and Moe Z Win. Cooperative bayesian self-tracking for wireless networks. *Communications Letters, IEEE*, 12(7):505–507, 2008.

[172] Henk Wymeersch, Jaime Lien, and Moe Z Win. Cooperative localization in wireless networks. *Proceedings of the IEEE*, 97(2):427–450, 2009.

[173] Henk Wymeersch, Stefano Maranò, Wesley M Gifford, and Moe Z Win. A machine learning approach to ranging error mitigation for uwb localization. *Communications, IEEE Transactions on*, 60(6):1719–1728, 2012.

[174] Brian Yamauchi, Alan Schultz, and William Adams. Mobile robot exploration and map-building with continuous localization. In *Robotics and Automation, 1998. Proceedings. 1998 IEEE International Conference on*, volume 4, pages 3715–3720. IEEE, 1998.

[175] J. Yang and Y. Chen. Indoor localization using improved rss-based lateration methods. In *Proc. IEEE GLOBECOM '09*, pages 1–6, 2009.

[176] Yuan Yang, Yubin Zhao, and Marcel Kyas. A non-parametric modeling of time-of-flight rang-

ing error for indoor network localization. In *Global Communications Conference (GLOBECOM), 2013 IEEE*, pages 189–194. IEEE, 2013.

[177] Yuan Yang, Yubin Zhao, and Marcel Kyas. A statistics-based least squares (sls) method for non-line-of-sight error of indoor localization. In *Wireless Communications and Networking Conference (WCNC), 2013 IEEE*, pages 2299–2304. IEEE, 2013.

[178] Yuan Yang, Yubin Zhao, and Marcel Kyas. Weighted least-squares by bounding-box (b-wls) for nlos mitigation of indoor localization. In *Vehicular Technology Conference (VTC Spring), 2013 IEEE 77th*, pages 1–5. IEEE, 2013.

[179] Yuan Yang, Yubin Zhao, and Marcel Kyas. Geof: A geometric bayesian filter for indoor position tracking in mixed los/nlos conditions. In *Positioning, Navigation and Communication (WPNC), 2014 11th Workshop on*, pages 1–6. IEEE, 2014.

[180] Yuan Yang, Yubin Zhao, and Marcel Kyas. Rbgf: Recursively bounded grid-based filter for indoor position tracking using wireless networks. *IEEE Communications Letters*, 18(7):1234–1237, 2014.

[181] Jingang Yi, Junjie Zhang, Dezhen Song, and Suhada Jayasuriya. Imu-based localization and slip estimation for skid-steered mobile robots. In *Intelligent Robots and Systems, 2007. IROS 2007. IEEE/RSJ International Conference on*, pages 2845–2850. IEEE, 2007.

[182] Shigeng Zhang, Jiannong Cao, Chen Li-Jun, and Daoxu Chen. Accurate and energy-efficient range-free localization for mobile sensor networks. *Mobile Computing, IEEE Transactions on*, 9(6):897–910, 2010.